RIGA TECHNICAL UNIVERSITY

Darja Čirjuļina

# DESIGN AND PERFORMANCE EVALUATION OF CHAOS-BASED COMMUNICATION SYSTEMS UNDER NOISE AND MULTIPATH CONDITIONS

Doctoral Thesis

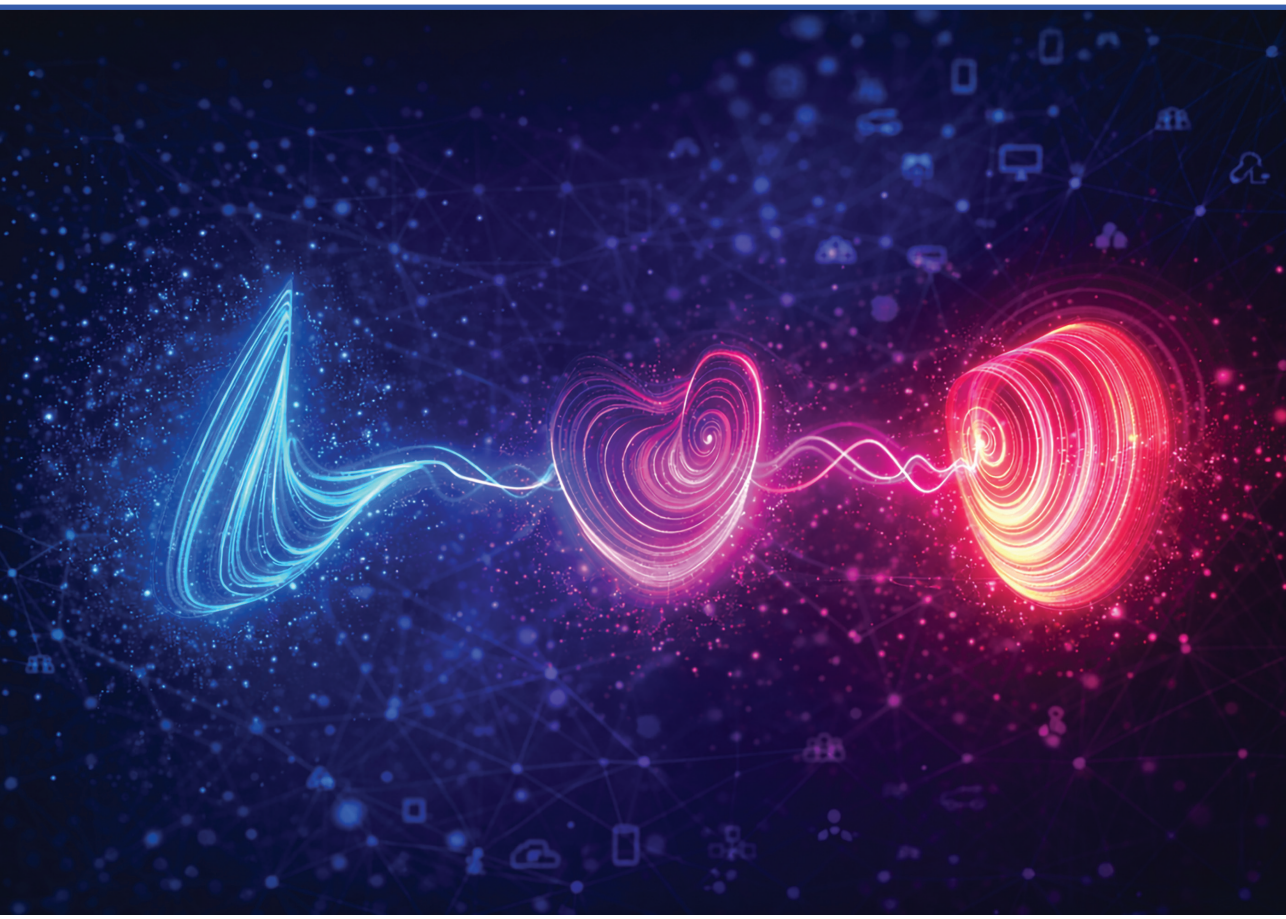

RTU Press
Riga 2026

**RIGA TECHNICAL UNIVERSITY**

Faculty of Computer Science, Information Technology and Energy

Institute of Photonics, Electronics and Telecommunications

**Darja Čirjuļina**

Doctoral Student of Study Programme "Electronics"

# DESIGN AND PERFORMANCE EVALUATION OF CHAOS-BASED COMMUNICATION SYSTEMS UNDER NOISE AND MULTIPATH CONDITIONS

**Doctoral Thesis**

Scientific supervisors:

Associate Professor Ph. D.

DENISS KOLOSOVS

Professor Dr. sc. ing.

DMITRIJS PIKUĻINS

Tenured Professor Ph. D.

XIAODAN PANG

RTU Press

Riga 2026

Čirjuļina, D. Design and Performance Evaluation of Chaos-Based Communication Systems under Noise and Multipath Conditions. Doctoral Thesis. — Riga: RTU Press, 2026. — 97 p.

Published in accordance with the decision of the Promotion Council "RTU P-08" of 2 February 2026, Minutes No. 47.


The research was partially supported by research and development grant No. RTU-PA-2024/1-0064 under the EU RRF project No. 5.2.1.1.i.0/2/24/I/CFLA/003.

**DOCTORAL THESIS PROPOSED TO RIGA TECHNICAL UNIVERSITY FOR THE PROMOTION TO THE SCIENTIFIC DEGREE OF DOCTOR OF SCIENCE**

To be granted the scientific degree of Doctor of Science (Ph. D.), the present Doctoral Thesis has been submitted for the defence at the open meeting of RTU Promotion Council on 24 April 2026 at 11:00 at the Faculty of Computer Science, Information Technology and Energy of Riga Technical University, 12 Āzenes Street, Room 201.

OFFICIAL REVIEWERS

Associate Professor, Dr. sc. ing. Aleksandrs Ipatovs
Riga Technical University

Professor, Dr. Christos Volos
Aristotle University of Thessaloniki, Greece

Assistant Professor, Ph. D. Lazaros Moysis
University of Nova Gorica, Slovenia

DECLARATION OF ACADEMIC INTEGRITY

I hereby declare that the Doctoral Thesis submitted for the review to Riga Technical University for the promotion to the scientific degree of Doctor of Science (Ph. D.) is my own. I confirm that this Doctoral Thesis had not been submitted to any other university for the promotion to a scientific degree.

Darja Čirjuļina _____

Date: _____

The Doctoral Thesis has been written in English. It consists of Introduction, four sections, Conclusions, 51 figures, eight tables, two appendices; the total number of pages is 97, not including appendices. The Bibliography contains 73 titles.

# ABSTRACT

The Doctoral Thesis “Design and Performance Evaluation of Chaos-Based Communication Systems under Noise and Multipath Conditions” summarizes the research conducted for the degree of Doctor of Science (Ph. D.). The work is devoted to the analysis, design, and experimental validation of chaos-based communication systems, with a particular emphasis on the influence of the fundamental frequency of chaotic oscillators, synchronization stability, and modulation techniques on system performance.

The thesis investigates the dynamics of analog chaotic oscillators and demonstrates that variation of the fundamental frequency provides a practical mechanism for adjusting the achievable data rate of chaos-based communication systems. The bit duration is determined using a lag-based analysis of cross-correlation functions. The approach is validated through simulations and experimental measurements for Colpitts and Vilnius chaotic oscillators.

A comprehensive study of chaotic synchronization under additive noise is presented, demonstrating that the synchronization quality is strongly dependent on the selected circuit node used for coupling the drive and response oscillators. Based on this study, a systematic methodology for selecting synchronization signals is developed. The results reveal that different signals of the same oscillator may exhibit unequal synchronization levels, which can introduce imbalance in correlation-based detection when chaos shift keying is applied.

The thesis proposes a compensation threshold for correlation-based detection that restores balance in symbol decision-making under conditions of unequal synchronization. The effectiveness of the proposed approach is demonstrated through experimental results, showing improved detection symmetry and communication reliability.

The work further investigates the integration of advanced modulation techniques with chaos-based communication. Quadrature amplitude modulation and frequency modulation are combined with chaos shift keying. The noise immunity of the resulting systems is evaluated in additive white Gaussian noise channels and in two-ray propagation channels. Comparative results show that chaos-based systems exhibit greater resilience to frequency-selective fading compared to conventional modulation schemes under identical bandwidth constraints.

All communication systems investigated in this thesis were implemented using a combined simulation and experimental framework, where chaotic oscillators were modeled at the circuit level and signal processing, detection, and performance evaluation were performed in MATLAB. Experimental prototypes were realized using discrete analog circuits and commercial modulation modules, and their performance was validated through measured bit error rate characteristics.

The Doctoral Thesis has been written in English. It consists of an Introduction, four sections, Conclusions, 51 figures, eigth tables, two appendices; the total number of pages is 97, not including appendices. The Bibliography contains 73 titles.

# ANOTĀCIJA

Promocijas darbā "Haosā balstītu sakaru sistēmu projektēšana un veiktspējas novērtēšana trokšņa un divstaru izplatīšanās kanālos" apkopoti pētījumi, kas veikti zinātņu doktora grāda (*Ph. D.*) iegūšanai. Darbs ir veltīts uz haosu balstītu sakaru sistēmu analīzei, projektēšanai un eksperimentālai validācijai, īpašu uzmanību pievēršot haotisko oscilatoru fundamentālās frekvences ietekmei, sinhronizācijas trokšņu noturībai un modulācijas metožu ietekmei uz sistēmas veiktspēju.

Promocijas darbā tiek pētīta analogo haotisko oscilatoru dinamika un parādīts, ka fundamentālās frekvences izmaiņas nodrošina praktisku mehānismu uz haosu balstītu sakaru sistēmu sasniedzamā datu pārraides ātruma pielāgošanai. Bita ilgums tiek noteikts, izmantojot savstarpējās korelācijas funkcijas laika nobīdes analīzi. Šī pieeja tiek apstiprināta ar simulāciju un eksperimentālo mērījumu rezultātiem Kolpica un Viļņas haotiskajiem oscilatoriem.

Darbā tiek veikts visaptverošs haotiskās sinhronizācijas pētījums trokšņa apstākļos, parādot, ka sinhronizācijas kvalitāte ir būtiski atkarīga no izvēlētā shēmas mezgla, kas tiek izmantots vadošā un vadāmā oscilatoru sinhronizēšanai. Balstoties uz šo pētījumu, ir izstrādāta sistemātiska sinhronizācijas signālu izvēles metodoloģija. Iegūtie rezultāti parāda, ka viena un tā paša oscilatora dažādi signāli var uzrādīt nevienlīdzīgus sinhronizācijas līmeņus, kas datu pārraides sistēmas gadījumā var radīt nelīdzsvarotību korelācijā balstītā detekcijā.

Lai novērstu šo problēmu, promocijas darbā tiek piedāvāts kompensācijas slieksnis korelācijā balstītai detekcijai, kas atjauno simbolu lēmumu pieņemšanas līdzsvaru nevienlīdzīgas sinhronizācijas apstākļos. Piedāvātās pieejas efektivitāte tiek demonstrēta ar eksperimentāliem rezultātiem, kas apliecina uzlabotu detekcijas simetriju un paaugstinātu sakaru uzticamību.

Darba turpinājumā tiek pētīta progresīvu modulācijas metožu integrācija ar uz haosu balstītām sakaru sistēmām. Kvadratūras amplitūdas modulācija un frekvences modulācija tiek apvienotas ar haotisko manipulāciju. Iegūto sistēmu trokšņu noturība tiek novērtēta piedevas baltā Gausa trokšņa kanālos un divstaru izplatīšanās kanālos. Iegūtie rezultāti liecina, ka uz haosu balstītas sakaru sistēmas uzrāda augstāku noturību pret frekvenču selektīvu slāpēšanu, salīdzinot ar konvencionālām modulācijas shēmām pie vienādiem joslas platuma ierobežojumiem.

Visas promocijas darbā pētītās sakaru sistēmas tika realizētas, izmantojot apvienotu modelēšanas un eksperimentālu metodoloģiju, kur haotiskie oscilatori tika modelēti shēmu līmenī, bet signālu apstrāde, detekcija un veiktspējas novērtēšana tika veikta programmvidē MATLAB. Eksperimentālie prototipi tika realizēti, izmantojot analogās shēmas un komerciālus modulācijas moduļus, un to veiktspēja tika validēta, balstoties uz izmērītām bitu kļūdu attiecību.

Promocijas darbs ir uzrakstīts angļu valodā, tajā ir ievads, četras nodaļas, secinājumi, literatūras saraksts, 51 attēli, astoņas tabulas, divi pielikumi; kopējais lappušu skaits 97, neieskaitot pielikumus. Literatūras sarakstā ir 73 avoti.

# CONTENTS


ACRONYMS . . . 12
LIST OF SYMBOLS . . . 13
INTRODUCTION . . . 14
Rationale . . . 14
The Objective Statement and the Tasks . . . 16
The Subject and the Object of the Research . . . 17
Research Methodology . . . 18
Scientific Novelty and Main Results . . . 19
Theses to be Defended . . . 20
Approbation and Practical Significance . . . 21
Structure of the Thesis . . . 25
1 CHAOTIC OSCILLATORS . . . 27
1.1 Colpitts Chaotic Oscillator . . . 28
Mathematical Model . . . 28
Fundamental Frequency . . . 30
Simulation Model . . . 30
Simulation Study . . . 32
Prototype . . . 37
Prototype Measurements . . . 38
1.2 Vilnius Chaotic Oscillator . . . 41
Mathematical Model . . . 42
Fundamental Frequency . . . 43
Simulation Model . . . 43
Simulation Study . . . 44
Prototype . . . 48
Prototype Measurements . . . 49
1.3 Discussion and Comparative Analysis . . . 52
2 CHAOTIC SYNCHRONIZATION . . . 55
2.1 Pecora–Carroll Synchronization . . . 55
2.2 Chaos Oscillator Synchronization Noise Immunity Study Methodology . . . 58
2.3 Chaos Oscillator Synchronization Noise Immunity Study Results . . . 59
2.4 Synchronization Signal Selection Methodology . . . 63
3 DESIGN AND SIGNAL PROCESSING IN CHAOS-BASED COMMUNICATION 65
3.1 System Architecture . . . 65
3.2 Chaos Shift Keying Implementation . . . 67
Simulation Implementation . . . 67

Prototype Implementation . . . . . 67
3.3 Detection and Threshold Determination under Imperfect Synchronization . 68
3.4 Impact of Threshold Selection on BER . . . . . 69
3.5 Discussion . . . . . 70
4 ADVANCED MODULATION TECHNIQUES FOR CHAOS-BASED COMMUNICATION . . . . . 72
4.1 Modulation Schemes . . . . . 73
Quadrature Amplitude Modulation . . . . . 73
Frequency Modulation . . . . . 74
4.2 Quadrature Amplitude Modulation-based Communication System . . . . . 76
Quadrature Chaos Shift Keying Communication System . . . . . 76
Communication System Noise Immunity . . . . . 77
4.3 Frequency Modulation-based Communication System . . . . . 79
Frequency-Modulated Chaos Shift Keying Communication System . . . . . 79
Communication System Noise Immunity . . . . . 80
4.4 Performance Analysis of the QCSK System under Different Synchronization Signal Configurations . . . . . 81
4.5 QAM- and FM-Based Communication System Performance in Selective Fading Conditions . . . . . 82
Study Setup . . . . . 83
Performance Analysis in the Selective Fading Conditions . . . . . 84
4.6 Discussion . . . . . 86
Bibliography . . . . . 90
APPENDICES . . . . . 98
A Chaotic oscillators . . . . . 98
A.1 Autocorrelation Function in Colpitts Chaotic Oscillator . . . . . 98
A.2 Autocorrelation Function in Vilnius Chaotic Oscillator . . . . . 100

# LIST OF FIGURES


1.1 Colpitts chaotic oscillator circuit diagram. . . . . 29
1.2 Colpitts chaotic oscillator model in the LTspice simulation environment. . . . . 31
1.3 Two-dimensional attractor projections of the Colpitts chaotic oscillator for the fundamental frequencies of (a) 96.86 kHz and (b) 968.59 kHz. . . . . 31
1.4 power spectral density (PSD) of $v_{C1}$, $v_{C2}$, and $i_L$ for the Colpitts chaotic oscillator at $f_0 = 96.86\,\text{kHz}$. . . . . 33
1.5 PSD of $v_{C1}$, $v_{C2}$, and $i_L$ for the Colpitts chaotic oscillator at $f_0 = 968.59\,\text{kHz}$. . . 33
1.6 Cross-correlation functions for $v_{C1}$ and $v_{C2}$, $v_{C1}$ and $i_L$, and $v_{C2}$ and $i_L$ in the Colpitts chaotic oscillator at $f_0 = 96.86\,\text{kHz}$. . . . . 34
1.7 Cross-correlation functions for $v_{C1}$ and $v_{C2}$, $v_{C1}$ and $i_L$, and $v_{C2}$ and $i_L$ in the Colpitts chaotic oscillator at $f_0 = 968.59\,\text{kHz}$. . . . . 35
1.8 Close-up view of the cross-correlation function between $v_{C1}$ and $v_{C2}$ (Fig. 1.6) in the Colpitts chaotic oscillator at $f_0 = 96.86\,\text{kHz}$, highlighting the dominant correlation peak at a nonzero time lag. . . . . 36
1.9 Fabricated Colpitts Chaotic Oscillator printed circuit board (PCB) Prototype. . . . . 37
1.10 Two-dimensional attractor projections from the Colpitts chaotic oscillator PCB for the fundamental frequencies of (a) 96.86 kHz and (b) 968.59 kHz. . . . . 38
1.11 PSD of $v_{C1}$, $v_{C2}$, and $v_{RL}$ for the Colpitts chaotic oscillator prototype at $f_0 = 96.86\,\text{kHz}$. . . . . 39
1.12 PSD of $v_{C1}$, $v_{C2}$, and $v_{RL}$ for the Colpitts chaotic oscillator prototype at $f_0 = 968.59\,\text{kHz}$. . . . . 39
1.13 Cross-correlation functions for $v_{C1}$ and $v_{C2}$, $v_{C1}$ and $v_{RL}$, and $v_{C2}$ and $v_{RL}$ in the Colpitts chaotic oscillator prototype at $f_0 = 96.86\,\text{kHz}$. . . . . 40
1.14 Cross-correlation functions for $v_{C1}$ and $v_{C2}$, $v_{C1}$ and $v_{RL}$, and $v_{C2}$ and $v_{RL}$ in the Colpitts chaotic oscillator prototype at $f_0 = 968.59\,\text{kHz}$. . . . . 40
1.15 Vilnius chaotic oscillator circuit diagram. . . . . 42
1.16 Vilnius Chaotic oscillator model in the LTspice simulation environment. . . . . 44
1.17 Two-dimensional attractor projections of the Vilnius chaotic oscillator for the fundamental frequencies of (a) 1.6 kHz and (b) 160 kHz. . . . . 45
1.18 PSD of key node voltages and inductor current for the Vilnius chaotic oscillator at $f_0 = 1.6\,\text{kHz}$. . . . . 45
1.19 PSD of key node voltages and inductor current for the Vilnius chaotic oscillator at $f_0 = 160\,\text{kHz}$. . . . . 46
1.20 Cross-correlation functions for $v_{C1}$ and $v_{C2}$, $v_{C1}$ and $i_L$, and $v_{C2}$ and $i_L$ in the Vilnius chaotic oscillator at $f_0 = 1.6\,\text{kHz}$. . . . . 46

1.21 Cross-correlation functions for $v_{C1}$ and $v_{C2}$, $v_{C1}$ and $i_L$, and $v_{C2}$ and $i_L$ in the Vilnius chaotic oscillator at $f_0 = 160\,\text{kHz}$. . . . . 47
1.22 Fabricated Vilnius Chaotic Oscillator PCB Prototype: (a) Top and (b) Bottom. . . . 48
1.23 Two-dimensional attractor projections from the Vilnius oscillator PCB for the fundamental frequencies of (a) 1.6 kHz and (b) 160 kHz. . . . . 49
1.24 PSD of $v_{C1}$, $v_{C2}$, and $v_{R1}$ for the Vilnius chaotic oscillator prototype at $f_0 = 1.6\,\text{kHz}$. 50
1.25 PSD of $v_{C1}$, $v_{C2}$, and $v_{R1}$ for the Vilnius chaotic oscillator prototype at $f_0 = 160\,\text{kHz}$. 50
1.26 Cross-correlation functions for $v_{C1}$ and $v_{C2}$, $v_{C1}$ and $v_{R1}$, and $v_{C2}$ and $v_{R1}$ in the Vilnius chaotic oscillator prototype at $f_0 = 1.6\,\text{kHz}$. . . . . 51
1.27 Cross-correlation functions for $v_{C1}$ and $v_{C2}$, $v_{C1}$ and $v_{R1}$, and $v_{C2}$ and $v_{R1}$ in the Vilnius chaotic oscillator prototype at $f_0 = 160\,\text{kHz}$. . . . . 51
2.1 Chaos oscillator synchronization block-scheme. . . . . 56
2.2 XY plot of drive-response system signals (a) without synchronization and (b) with chaotic synchronization applied. . . . . 57
2.3 Chaos oscillator synchronization noise immunity study block-scheme. . . . . 58
2.4 Colpitts chaos oscillator synchronization noise immunity. . . . . 59
2.5 Vilnius chaos oscillator synchronization noise immunity. . . . . 60
2.6 Results of the Colpitts chaos oscillator, showing the signal cross-correlation coefficients under different synchronization configurations. . . . . 61
2.7 Results of the Vilnius chaos oscillator, showing the signal cross-correlation coefficients for different synchronization signals. . . . . 62
3.1 Chaos-based communication system block scheme. . . . . 66
4.1 Block diagram of the quadrature amplitude modulation (QAM) transmitter and receiver used for chaos-based signal transmission. . . . . 73
4.2 Block diagram of the frequency modulation (FM) transmitter and receiver used for chaos-based signal transmission. . . . . 74
4.3 (a) Pre-emphasis and (b) de-emphasis filter configurations used in the FM system. . 75
4.4 amplitude–frequency response (AFR) of the pre-emphasis (red) and de-emphasis (blue) filters. . . . . 76
4.5 Block diagram of the quadrature chaos shift keying (QCSK) communication system combining chaos shift keying and quadrature modulation. . . . . 77
4.6 bit error rate (BER) performance of the QCSK communication system obtained from simulation (red) and experimental measurements (blue). . . . . 78
4.7 Block diagram of the frequency modulated chaos shift keying (FM-CSK) communication system combining chaos shift keying (CSK) with frequency modulation. . . 79
4.8 BER performance of the FM-CSK communication system obtained from simulation (red) and experimental measurements (blue). . . . . 80

4.9 BER versus $E_b/N_0$ curves of QCSK data transmission system. . . . . 82
4.10 The model of the emulated multipath channel. . . . . 83
4.11 The effect of a two-ray channel on 4-QAM (a) and QCSK (b). . . . . 84
4.12 The effect of a two-ray channel on frequency shift keying (FSK) (a) and FM-CSK (b). 84
4.13 QCSK communication system's performance for the two-ray channel. . . . . 85
4.14 QAM communication system's performance for the two-ray channel. . . . . 85
4.15 FM-CSK communication system's performance for the two-ray channel. . . . . 85
4.16 FSK communication system's performance for the two-ray channel. . . . . 86
A.1 Autocorrelation functions of $v_{C1}$, $v_{C2}$, and $i_L$ obtained from LTspice simulations of the Colpitts chaotic oscillator at $f_0 = 96.86\,\text{kHz}$. . . . . 98
A.2 Autocorrelation functions of $v_{C1}$, $v_{C2}$, and $i_L$ obtained from LTspice simulations of the Colpitts chaotic oscillator at $f_0 = 968.59\,\text{kHz}$. . . . . 98
A.3 Autocorrelation functions of $v_{C1}$, $v_{C2}$, and $v_{RL}$ obtained from prototype measurements of the Colpitts chaotic oscillator at $f_0 = 96.86\,\text{kHz}$. . . . . 99
A.4 Autocorrelation functions of $v_{C1}$, $v_{C2}$, and $v_{RL}$ obtained from prototype measurements of the Colpitts chaotic oscillator at $f_0 = 968.59\,\text{kHz}$. . . . . 99
A.5 Autocorrelation functions of $v_{C1}$, $v_{C2}$, and $i_L$ obtained from LTspice simulations of the Vilnius chaotic oscillator at $f_0 = 1.6\,\text{kHz}$. . . . . 100
A.6 Autocorrelation functions of $v_{C1}$, $v_{C2}$, and $i_L$ obtained from LTspice simulations of the Vilnius chaotic oscillator at $f_0 = 160\,\text{kHz}$. . . . . 100
A.7 Autocorrelation functions of $v_{C1}$, $v_{C2}$, and $v_{R1}$ obtained from prototype measurements of the Vilnius chaotic oscillator at $f_0 = 1.6\,\text{kHz}$. . . . . 101
A.8 Autocorrelation functions of $v_{C1}$, $v_{C2}$, and $v_{R1}$ obtained from prototype measurements of the Vilnius chaotic oscillator at $f_0 = 160\,\text{kHz}$. . . . . 101

# LIST OF TABLES


1.1 Colpitts oscillator LTspice cross-correlation parameters . . . . . 35
1.2 Colpitts oscillator prototype cross-correlation parameters . . . . . 40
1.3 Vilnius oscillator LTspice cross-correlation parameters . . . . . 47
1.4 Vilnius oscillator prototype cross-correlation parameters . . . . . 52
1.5 Achievable data rates summary of the Colpitts chaotic oscillator . . . . . 53
1.6 Achievable data rates summary of the Vilnius chaotic oscillator . . . . . 53
2.1 Colpitts and Vilnius chaos oscillators configurations . . . . . 59
3.1 Error count without and with the detection threshold in a system based on the Vilnius chaos oscillator using $v_{R1}$ as the synchronization signal . . . . . 70

# ACRONYMS

**ADP3450** Digilent's Analog Discovery Pro

**AFR** amplitude–frequency response

**AWGN** additive white Gaussian noise

**BER** bit error rate

**BJT** bipolar junction transistor

**BPF** band-pass filter

**CSK** chaos shift keying

**DC** direct current

**DCSK** differential chaos shift keying

**ETSI** European Telecommunications Standards Institute

**FM** frequency modulation

**FM-CSK** frequency modulated chaos shift keying

**FSK** frequency shift keying

**HPF** high-pass filter

**IF** intermediate frequency

**IoT** Internet-of-Things

**LPF** low-pass filter

**MSE** mean square error

**NB-IoT** narrowband Internet of Things

**PCB** printed circuit board

**PLS** physical layer security

**PSD** power spectral density

**QAM** quadrature amplitude modulation

**QCSK** quadrature chaos shift keying

**RF** radio frequency

**SNR** signal-to-noise ratio

**WSN** wireless sensor network

**Z1TEST** 0–1 test for chaos

# LIST OF SYMBOLS

**Operations**

| | |
|---|---|
| $\frac{\mathrm{d}x}{\mathrm{d}t}$ | the derivative of $x$ with respect to $t$ |
| $\bar{x}$ | the mean value of $x$ |

**Variables**

| | |
|---|---|
| $\beta$ | correlation coefficient |
| $\beta_F$ | transistor's forward current gain |
| $C$ | capacitor |
| $c$ | rotation parameter |
| $C_{eq}$ | equivalent capacitance |
| $f_0$ | fundamental frequency |
| $i_0$ | current of the resistor $R_0$ |
| $i_B$ | transistor base current |
| $i_C$ | transistor collector current |
| $i_D$ | diode current |
| $i_L$ | inductor current |
| $i_S$ | saturation current of the diode |
| $k$ | gain of the operational amplifier |
| $K(f)$ | channel's estimated transfer function |
| $L$ | inductor |
| $M_c(n)$ | mean square displacement |
| $N$ | number of samples |
| $n$ | sample |
| $N_c$ | number of $c$ samples |
| $R$ | resistor |
| $R_{ON}$ | small-signal on-resistance of the base-emitter |
| $v_n'$ | voltage over component $n$ in response circuit |
| $v_{C1}$ | capacitor $C_1$ voltage |
| $v_{C2}$ | capacitor $C_2$ voltage |
| $v_D$ | voltage across the diode |
| $v_n$ | voltage over component $n$ in drive circuit |
| $v_{R1}$ | resistance $R_1$ voltage |
| $v_{RL}$ | resistance $R_L$ voltage |
| $V_{TH}$ | threshold voltage |
| $v_T$ | the thermal voltage of the diode |
| $x$ | signal from the drive oscillator |
| $y$ | signal from the response circuit |

# INTRODUCTION

## Rationale

The rapid expansion of Internet-of-Things (IoT) infrastructures is transforming conventional environments into interconnected smart ecosystems, enabling applications in healthcare, smart cities, industrial automation, and environmental monitoring. According to the Ericsson Mobility Report [1], the number of IoT-connected devices is expected to grow sharply in the coming years, driven by advances in 5G and beyond. This growth significantly increases the amount of sensitive data transmitted over wireless channels, heightening the importance of secure, reliable, and resource-efficient communication mechanisms.

Security in IoT networks is predominantly handled through cryptographic mechanisms operating at higher protocol layers, including link-, network-, and application-layer encryption and authentication techniques [2], [3]. These methods provide strong protection for data confidentiality and integrity once a communication link has been established; however, they often introduce considerable computational and energy overhead, which is problematic for resource-constrained IoT devices [4], [5]. Complementary architectural approaches, such as fog computing and software-defined networking, enable localized processing and centralized traffic control, potentially reducing latency and improving manageability, but at the cost of increased system complexity and new security challenges related to control-plane vulnerabilities and heterogeneous network architectures [6], [7]. Importantly, security mechanisms operating at higher protocol layers are inherently limited in mitigating attacks that exploit the wireless transmission medium itself, such as jamming, passive eavesdropping, or man-in-the-middle interference during signal propagation [8].

To address these limitations, physical layer security (PLS) has emerged as a complementary security measure that exploits inherent properties of the communication medium and device-specific characteristics rather than replacing cryptographic protection [8]–[10]. By leveraging hardware imperfections and signal-level features, PLS enhances confidentiality and resilience without relying on computationally intensive cryptographic operations, making it particularly attractive for low-power and resource-constrained IoT devices. Techniques including artificial noise injection and radio-frequency fingerprinting further strengthen PLS by degrading an eavesdropper's reception quality or enabling device authentication at the signal level [11], [12].

Among the promising developments within PLS is the integration of chaos theory, which enhances security by exploiting the inherent unpredictability of chaotic signals. Chaos-based communication techniques offer a compelling solution for secure data transmission, particularly in IoT sensor networks where devices are constrained in terms of computational complexity and energy consumption. The reason is that these systems rely on relatively simple analog chaos oscillators rather than conventional encryption-based security mechanisms [8]. Chaotic systems such as the Lorenz and Chua circuits have been effectively utilized in chaos-based communication schemes to secure

data transmission [13]–[15]. These systems generate wide-band, noise-like waveforms, being sensitive at the same time to initial conditions, which makes them well-suited for enhancing information security. In coherent chaos-based implementations, accurate data recovery requires precise synchronization between the transmitter and receiver chaotic oscillators, thereby introducing an additional security layer, since any disruption of synchronization renders the intercepted signal unreadable and significantly complicates unauthorized access [16], [17].

A variety of chaos-based modulation techniques have been proposed to exploit these properties, including CSK, differential chaos shift keying (DCSK), and their extensions [17]–[20]. These schemes benefit from the inherent decorrelation and wide-band nature of chaotic signals, which enhance resilience against interception and narrowband interference. Recent studies have also explored the integration of chaos-based signaling with multi-carrier and multiple-input multiple-output configurations to improve spectral efficiency and robustness while preserving security properties [18], [21].

Researchers are developing advanced chaotic models to overcome limitations of existing systems, such as high complexity and limited resilience to noise. Innovations such as the exponential chaotic model have introduced the concept of robust chaos, defined as a dynamical regime in which chaotic behavior persists over a continuous range of system parameters without the emergence of periodic windows or coexisting stable attractors. Therefore, small parameter perturbations do not suppress the chaotic attractor, which is particularly advantageous for secure communication systems operating under component tolerances and channel noise [22]–[24]. Beyond communication, chaos has found applications in multimedia security and the generation of random numbers [25]–[27]. Advanced image encryption algorithms based on dynamic chaotic systems provide resilience against statistical and differential attacks and ensure data integrity in IoT environments [12], [28]–[31].

Chaotic signals are generally wide-band, but they can be characterized by the fundamental (basic) frequency value. This frequency primarily depends on the nominal values of components chosen during circuit design [32]. Alternatively, in some cases, the frequency can be controlled by adjusting the operational amplifier gain value [33]. Most implementations of chaotic analog oscillators using discrete circuit components have a sub-MHz fundamental frequency, the increase of which is limited due to the use of an operational amplifier (if present) [32]. Some reports on chaotic oscillator implementations in ultrahigh-frequency ranges [34]–[36] are available, but they require more advanced high-frequency technologies, such as resonant tunneling diodes and integrated chaotic circuits. Changing the chaotic oscillator frequency can be beneficial in chaotic communication systems to increase the data transmission rate, differentiate between multiple user channels, or implement frequency-hopping modulation schemes.

Another critical aspect of chaos-based communication systems is synchronization, which enables reliable data transmission and receiving in IoT and wireless sensor network (WSN). At its core, chaotic synchronization ensures that the state variables of a receiver's chaotic oscillator replicate

those of the transmitter's oscillator, enabling precise signal decoding. Techniques like the Pecora–Carroll method [37] and adaptive control [38], [39] are commonly used to achieve synchronization by coupling specific state variables between drive and response oscillators.

Research on the topic has consistently emphasized the critical role of synchronization stability in the performance of chaos-based systems [40]–[42]. For instance, studies on systems such as the Vilnius chaos oscillator emphasize the importance of stable synchronization methods to overcome noise, parameter deviations, and environmental variability [43]. This is particularly crucial in applications of chaos-based communication, where synchronization directly impacts the system's ability to securely and accurately transmit data [44]–[47].

In practical wireless deployments, chaos-based signaling must also be compatible with radio frequency (RF) transmission and resilient to multipath propagation. The integration of chaotic waveforms with conventional modulation techniques, such as QAM and FM, enables operation within regulated frequency bands and compatibility with existing transceiver hardware. At the same time, multipath-induced frequency-selective fading remains a dominant impairment in wireless sensor networks, motivating comparative studies between chaos-based and conventional communication schemes under realistic propagation conditions [48].

## The Objective Statement and the Tasks

The **objective** of this Doctoral Thesis is to investigate the dynamical and synchronization properties of chaotic oscillators from a chaos-based communication system design perspective. The Thesis examines the impact of the oscillator's fundamental frequency on data rate and formulates a systematic methodology for developing chaos-based communication architectures that ensure stable and noise-resilient transmission in additive white Gaussian noise (AWGN) and two-ray propagation channels.

The fulfillment of the objective is established through quantitative analysis of chaotic dynamics, synchronization quality, correlation properties, and BER performance in both simulation and experimental implementations.

The following **tasks** are stated to achieve the previously defined objective:

- To analyze the influence of the fundamental frequency on the dynamical properties of chaotic oscillators, including spectral characteristics, oscillator signals cross-correlation, and aperiodicity, using LTspice simulations and hardware prototypes.
- To investigate the noise immunity of chaotic oscillator synchronization when different oscillator state variables are used as synchronization signals, and to quantify synchronization quality using correlation-based metrics.
- To study the impact of unequal correlation levels between received and synchronized oscillator's regenerated signals among state variables on CSK-based communication systems, and

to estimate the resulting error probability imbalance in correlation-based data detection.

- To develop a technique for optimal decision-making threshold calculation that ensures balanced symbol detection and error probability minimization in CSK-based communication systems.
- To design and implement chaos-based communication systems that employ advanced modulation techniques, including QAM and FM, enabling the radio-frequency transmission.
- To evaluate the noise immunity of the proposed chaos-based communication systems under AWGN and multipath propagation conditions, and to compare their performance with conventional modulation schemes.

The effectiveness of the proposed approaches is demonstrated through comparative simulation and experimental studies, focusing on synchronization quality, achievable data rates, and bit error rate metrics under various channel conditions.

## The Subject and the Object of the Research

This Doctoral Thesis investigates chaos-based communication systems employing analog chaotic oscillators. The study follows a structured progression, beginning with the analysis of chaotic oscillator dynamics and concluding with system-level performance evaluation under different propagation conditions.

The **object** of this research is a chaos-based communication system, evaluated at different levels ranging from the chaotic oscillator and its synchronization to the complete data transmission system operating over noisy and multipath channels. The object includes:

- Analog chaotic oscillators operating at different fundamental frequencies.
- Drive–response synchronization of chaotic oscillators using different circuit nodes.
- Chaos shift keying–based data transmission schemes.
- Communication channels affected by additive noise and multipath propagation.
- Receiver-side correlation-based detection and bit error rate evaluation.

The **subject** of this research is the set of methods and principles that define the performance of chaos-based communication systems, with particular emphasis on:

- The influence of the chaotic oscillator fundamental frequency on signal dynamics, correlation time, and achievable bit duration.
- Noise immunity of chaotic synchronization when different oscillator signals are used as synchronization signals.
- The impact of unequal synchronization levels among oscillator state variables and their impact on correlation-based data detection.
- The development and validation of a decision threshold to compensate for detection imbalance caused by unequal synchronization.

- The evaluation of chaos-based communication systems' performance under additive white Gaussian noise and two-ray multipath propagation.

By systematically addressing these aspects, the Thesis establishes a direct connection between chaotic oscillator dynamics, synchronization behavior, detection, and communication performance.

## Research Methodology

The research presented in this Doctoral Thesis follows a systematic methodology based primarily on numerical simulations and hardware measurements aimed at investigating chaotic oscillator dynamics, synchronization behavior, and their application in chaos-based communication systems. The work combines theoretical modeling and experimental validation to ensure consistency and reproducibility of the obtained results.

At the initial stage, an extensive review of the scientific literature on chaotic oscillators, chaotic synchronization, and chaos-based data transmission techniques was conducted. This review provided the background required to identify open research questions related to oscillator parameter variation, synchronization stability, and system-level performance in practical communication environments.

Accurate modeling is essential when analyzing nonlinear and chaotic systems. Therefore, the research begins with the development and validation of circuit-level models of chaotic oscillators. Two structurally distinct oscillators—the Colpitts and Vilnius chaotic oscillators—are selected to ensure generality of the observations. Their behavior is examined under variations of the fundamental frequency to analyze changes in spectral characteristics, the cross-correlation properties of generated signals, and time-lag behavior relevant to symbol duration selection.

The methodology is based on a structured research framework that integrates both sequential and parallel stages:

- Development and validation of chaotic oscillator models using circuit simulations and experimental prototypes.
- Analysis of oscillator dynamics under fundamental frequency variation, including spectral properties and generated signals' cross-correlation behavior.
- Investigation of chaotic synchronization properties in drive–response configurations under additive noise conditions.
- Evaluation of multiple circuit nodes as potential synchronization signals using correlation-based metrics.
- Identification of synchronization quality when different state variables are used as synchronization signals and estimation of the impact of synchronization quality on correlation-based data detection.
- Expression of the optimal detection threshold to compensate for error probability imbalance and restore balanced symbol detection.

- Integration of chaotic baseband transmission with advanced modulation techniques, including QAM and FM.
- Performance evaluation of chaos-based communication systems in AWGN and two-ray propagation channels using simulation and experimental measurements.

Simulations are carried out using LTspice for chaotic oscillator modeling and MATLAB for signal processing, synchronization analysis, and bit error rate evaluation. Experimental validation is performed using custom-built hardware prototypes and commercially available modulation and measurement equipment. This combined approach ensures that both simulation and experimental proof support the conclusions drawn in this Thesis.

## Scientific Novelty and Main Results

The scientific contributions of this Doctoral Thesis are based on original system-level analysis and design methodology, circuit-level simulations, and experimental investigations of chaos-based communication systems. Several of the proposed methods and observations are either introduced for the first time or represent a novel application of nonlinear dynamics and synchronization theory to practical communication system design. The main elements of scientific novelty are summarized as follows:

- For the first time, the relationship between the fundamental frequency of an analog chaotic oscillator and the achievable data rate of a chaos-based communication system is quantitatively established using a lag-based analysis of cross-correlation functions applied to simulated and experimentally measured signals.
- For the first time, it is experimentally demonstrated that different state variables of the same chaotic oscillator can exhibit significantly different correlation levels under identical coupling conditions, despite the use of the same synchronization signal.
- It is shown that unequal correlation levels between data-carrying chaotic signals lead to systematic imbalance in correlation-based detection, resulting in asymmetric symbol decision errors in chaos-based communication systems.
- For the first time, an error-probability-optimal compensation-based decision threshold formulation is derived for correlation-based detection with correlated chaotic carriers, restoring decision symmetry without modifying the synchronization mechanism.
- The influence of synchronization signal selection on the bit error rate performance of chaos-based communication systems is experimentally demonstrated and quantified under additive noise and multipath propagation conditions.

In addition to the scientific contributions, this Thesis provides several important practical and methodological results that support the design and evaluation of chaos-based communication systems:

- A reusable evaluation workflow for chaos-based communication systems is established, combining LTspice circuit-level simulations, MATLAB-based signal processing, and hardware prototype measurements, enabling consistent analysis of chaotic oscillator dynamics, synchronization behavior, and communication performance. The developed simulation and signal processing codes are publicly available on GitHub.
- A systematic methodology for selecting synchronization signals in chaos-based communication systems is established, providing a structured workflow based on noise immunity, correlation properties, and practical signal accessibility to ensure balanced chaotic synchronization.
- A practical approach for integrating chaos shift keying with quadrature and frequency modulation is demonstrated, enabling chaotic baseband signals generated by analog oscillators to be upconverted to arbitrary carrier frequencies compatible with conventional RF transmission systems.
- An experimental procedure for assessing the noise immunity of QCSK and FM-CSK communication systems under AWGN conditions is provided, including detection, bit error rate estimation, and post-processing performed in MATLAB.
- A simulation-based methodology for evaluating the performance of chaos-based communication systems in multipath environments is presented using a two-ray propagation channel model, allowing direct and fair comparison with conventional modulation schemes under identical bandwidth and channel conditions.

Together, these results advance the understanding of how chaotic oscillator properties, synchronization signal selection, and modulation techniques influence the performance and reliability of chaos-based communication systems, providing a structured foundation for their application in practical wireless environments.

## Theses to be Defended

1. In chaos shift keying communication systems based on chaotic oscillators, the symbol rate adjustment for Vilnius oscillator up to 55 kb/s and for Colpitts oscillator up to 166 kb/s can be established through modification of the fundamental frequency of the oscillator.

2. In chaos shift keying communication system with non-equal correlation levels $\beta_X$, $\beta_Y$ for the corresponding pairs of the received and synchronized oscillator's regenerated chaotic signals, the error probability minimizing optimal detection is achieved with threshold defined as:

$$\beta_{X'} \geq \beta_{Y'} + \frac{1}{2}\left(\beta_X - \beta_Y\right),$$

   where $\beta_{X'}$ and $\beta_{Y'}$ are the correlation levels of the symbol-carrying chaotic pulses.

3. QCSK and FM-CSK communication systems based on Vilnius chaotic oscillator outperform

correspondingly 4-QAM and 2-FSK communication systems in a two-ray multipath channel with 3.25 dB notch at the carrier frequency, ensuring error probability of $3.29 \times 10^{-3}$ and $1.52 \times 10^{-3}$, respectively.

## Approbation and Practical Significance

The results presented in this Doctoral Thesis were obtained within the framework of applied research and experimental development activities carried out by the author during doctoral studies at Riga Technical University. The research evolved in close connection with ongoing academic, industrial, and applied research projects, ensuring both scientific relevance and practical applicability of the proposed chaos-based communication methods.

The scientific results of this Thesis have been published in peer-reviewed international journals and conference proceedings. The most significant publications directly reflecting the core contributions of this work are listed below. Publications in which the author is the first author are highlighted in **bold**. In one publication, the contribution was shared equally with the listed first author.


**[46]** D. Cirjulina et al. "Experimental Study on Frequency Modulated Chaos Shift Keying Communication System." In: *2022 Workshop on Microwave Theory and Techniques in Wireless Communications (MTTW)*. Riga, Latvia: IEEE, Oct. 2022, pp. 1–4. ISBN: 978-1-6654-6439-0. DOI: 10.1109/MTTW56973.2022.9942593

[48] R. Babajans et al. "Performance Analysis of Vilnius Chaos Oscillator-Based Digital Data Transmission Systems for IoT." en. In: *Electronics* 12.3 (Jan. 2023). Number: 3, p. 709. ISSN: 2079-9292. DOI: 10.3390/electronics12030709

**[49]** D. Cirjulina et al. "Fundamental Frequency Impact on Colpitts Chaos Oscillator Dynamics." In: *2023 Workshop on Microwave Theory and Technology in Wireless Communications (MTTW)*. Riga, Latvia: IEEE, Oct. 2023, pp. 19–23. ISBN: 9798350393491. DOI: 10.1109/MTTW59774.2023.10320021

**[50]** D. Cirjulina et al. "Experimental Study on Colpitts Chaotic Oscillator-Based Communication System Application for the Internet of Things." en. In: *Applied Sciences* 14.3 (Jan. 2024), p. 1180. ISSN: 2076-3417. DOI: 10.3390/app14031180

**[51]** D. Cirjulina, R. Babajans, and D. Kolosovs. "Experimental Study on Quadrature Chaos Shift Keying Communication System." In: *2024 IEEE Workshop on Microwave Theory and Technology in Wireless Communications (MTTW)*. Riga, Latvia: IEEE, Oct. 2024, pp. 29–32. ISBN: 979-8-3315-3317-5. DOI: 10.1109/MTTW64344.2024.10742187

**[52]** D. Cirjulina et al. "Fundamental Frequency Impact on Vilnius Chaos Oscillator Dynamics." en. In: *16th Chaotic Modeling and Simulation International Conference*. Ed. by C. H. Skiadas and Y. Dimotikalis. Series Title: Springer Proceedings in Complexity. Cham: Springer Nature Switzerland, 2024, pp. 87–101. ISBN: 978-3-031-60906-0 978-3-031-60907-7. DOI:

10.1007/978-3-031-60907-7_8

**[47]** D. Cirjulina, R. Babajans, and D. Kolosovs. "Design Particularities of Quadrature Chaos Shift Keying Communication System with Enhanced Noise Immunity for IoT Applications." en. In: *Entropy* 27.3 (Mar. 2025), p. 296. ISSN: 1099-4300. DOI: 10.3390/e27030296

The research results of this Thesis were also presented at international scientific conferences, workshops, and symposia, providing peer feedback and dissemination within the research community. The author presented the results of this Doctoral Thesis at the following international scientific conferences:

1. D. Cirjulina. "QCSK Communication System Performance in Multipath Propagation Channel," Days of Applied Nonlinearity and Complexity (DANOC 2026), Aristotle University of Thessaloniki, Thessaloniki, Greece, 23–25 January 2026.
2. D. Cirjulina. "Nonlinear Dynamics of the Colpitts Chaotic Oscillator Under Bias Voltage Tuning," RTU 66th International Scientific Conference, Riga Technical University, Riga, Latvia, 27 November 2025.
3. D. Cirjulina. "Synchronization Noise Immunity in the Vilnius Chaos Oscillator for Secure Communications in IoT," RTU 66th Student Scientific and Technical Conference, Riga Technical University, Riga, Latvia, 25 April 2025.
4. D. Cirjulina. "Experimental Study of a Quadrature Modulation Chaos Shift Keying-Based Data Transmission System," RTU 65th International Scientific Conference, Riga Technical University, Riga, Latvia, 11 October 2024.
5. D. Cirjulina. "Experimental Study on Quadrature Chaos Shift Keying Communication System," IEEE Workshop on Microwave Theory and Technology in Wireless Communications (MTTW 2024), IEEE Latvia COM/MTT/AP Joint Chapter, Riga, Latvia, 2–4 October 2024.
6. D. Cirjulina. "Experimental Study on Colpitts Chaotic Oscillator-Based Communication System Application for the Internet of Things," RTU 65th Student Scientific and Technical Conference, Riga Technical University, Riga, Latvia, 29 April 2024.
7. D. Cirjulina. "Experimental Study on Quadrature Chaos Shift Keying Communication System," Days of Applied Nonlinearity and Complexity (DANOC 2024), Aristotle University of Thessaloniki, Thessaloniki, Greece, 12–14 January 2024.
8. D. Cirjulina. "Fundamental Frequency Impact on Colpitts Chaos Oscillator Dynamics," RTU 64th International Scientific Conference, Riga Technical University, Riga, Latvia, 6 October 2023.
9. D. Cirjulina. "Fundamental Frequency Impact on Colpitts Chaos Oscillator Dynamics," IEEE Workshop on Microwave Theory and Technology in Wireless Communications (MTTW 2023), IEEE Latvia COM/MTT/AP Joint Chapter, Riga Technical University, Riga, Latvia, 4–6 October 2023.
10. D. Cirjulina. "Fundamental Frequency Impact on Vilnius Chaos Oscillator Dynamics," The

16th CHAOS 2023 International Conference, Technical University of Crete, Crete, Greece, 13–17 June 2023.

11. D. Cirjulina. "Experimental Study on Frequency Modulated Chaos Shift Keying Communication System," IEEE Workshop on Microwave Theory and Techniques in Wireless Communications (MTTW 2022), IEEE Latvia COM/MTT/AP Joint Chapter, Riga, Latvia, 5–7 October 2022.

The research was conducted in parallel with participation in several national and institutional research projects, which supported the experimental validation, prototype development, and applied investigations addressed in this Thesis:

1. Digital Europe Programme (DIGITAL) "Microchip Competence Centre of the Republic of Latvia" 0B000-3.5.2-e/3 | 101217976 (01.10.2025–28.02.2027)
2. "Implementation of consolidation and management changes at RTU, LiepU, Rēzekne Academy of Technology and Latvian Maritime Academy and Liepāja Maritime College for progress towards excellence in higher education, science and innovation." Grant No RTU-PA-2024/1-0064 under the EU RRF project No 5.2.1.1.i.0/2/24/I/CFLA/003 (01.01.2024–31.01.2026)
3. Internal funding of RTU "Exploring cyber-secure IoT data-driven agricultural management" 04000-1.3-e/24 | ZI-2024/7 (02.01.2024–31.12.2024)
4. Internal funding of RTU "Exploring the Next Generation IoT Network" 003000-3.1.2.1-e/14 | ZI-2023/3 (02.01.2023–31.12.2023)
5. SAM 8.2.2. "Strengthening of Ph. D. students and academic personnel of Riga Technical University and BA School of Business and Finance in the strategic fields of specialization" of the Specific Objective 8.2.2 "To Strengthen Academic Staff of Higher Education Institutions in Strategic Specialization Areas" of the Operational Program "Growth and Employment" and the RTU doctoral grant program. Project 03000-3.1.2.1-e/177 | 8.2.2.0/20/I/008. (01.12.2022–30.11.2023)
6. Internal funding of RTU "Frequency Modulated Chaos Manipulated Data Transmission System" 03000-3.1.1.1-e/145-1 | AM-2021/2 (07.06.2022–30.11.2022)
7. LZP fundamental and applied research project "Advanced wireless power transmission techniques" 03000-3.1.2.1-e/4 | lzp-2021/1-0170 (03.01.2022–30.12.2024)

An essential practical outcome of the present Doctoral Thesis is the development and application of an integrated simulation and experimental framework for chaos-based communication systems. The framework combines circuit-level modeling of chaotic oscillators in LTspice with signal processing, synchronization analysis, modulation, and detection implemented in MathWorks ® MATLAB. This approach enables the consistent evaluation of chaotic dynamics, synchronization stability, and communication performance under conditions of additive noise and multipath propagation.

The developed models and analysis procedures were utilized for both research purposes and practical validation through experimental measurements. The gained scientific and engineering ex-

perience was directly applied in the author's teaching activities at Riga Technical University. In particular, the results and methodologies developed during the PhD studies were incorporated into study courses related to signal processing, communication systems, and electronics, contributing to the improvement of course content and practical assignments.

During the Doctoral studies, the author has been involved in teaching the following study courses at Riga Technical University:

- DE0848 — Digital Optical Communication Systems (6 ECTS).
- RDE713 — Digital Optical Communication Systems (6 ECTS).
- SDD701 — Innovative Product Development and Entrepreneurship (4 ECTS).
- RR713 — Digital Signal Processing (study project) (3 ECTS).
- RTR825 — Fundamentals of Smart Radio (study project) (3 ECTS).
- ERA708 — Research Seminars in the Field of Electronics (3 ECTS).
- RRI324 — Digital Signal Processing (3 ECTS).

The development of this Doctoral Thesis was further supported by international academic and research mobility, enabling collaboration with external research institutions and access to advanced experimental infrastructure. During the doctoral studies, the author remained employed at Riga Technical University while completing the following mobility periods:

- KTH Royal Institute of Technology, Sweden (01.05.2023–31.05.2023).
- Infineon Technologies Austria (18.09.2023–22.09.2023).
- Central European Student and Young Professionals Congress, Cracow University of Technology (30.11.2023–03.12.2023).
- Keysight Technologies GmbH, Germany (13.08.2024–21.08.2024).
- Politecnico di Torino, Italy (18.11.2024–22.11.2024).
- Keysight Technologies GmbH, Germany (18.02.2025–27.02.2025).
- Keysight Technologies GmbH, Germany (13.06.2025–20.06.2025).
- Keysight Technologies GmbH, Germany (26.08.2025–04.09.2025).
- Aristotle University of Thessaloniki, Greece (30.11.2025–05.12.2025).

The scientific and academic contributions of the author during doctoral studies were recognized by the following awards:

- IEEE Student & Young Professional (SYP) Travel Grant, 19.08.2025.
- Best Presentation Award for Students, Days of Applied Nonlinearity and Complexity (DANOC'24), 14.01.2024.
- Gratitude from RTU Children and Youth University, 24.05.2024.

Overall, the results presented in this Doctoral Thesis were validated through peer-reviewed publications, international conference presentations, experimental prototypes, and applied research projects. The combination of simulation-based analysis, experimental measurements, and system-level validation confirms the scientific relevance and practical applicability of the proposed chaos-

based communication methods.

## Structure of the Thesis

This Doctoral Thesis follows an incremental research structure, where each section builds upon the results and conclusions obtained in the prior stages. While certain well-established concepts related to chaotic oscillators and communication systems are introduced where necessary, the focus is placed on the development, analysis, and experimental validation of original research contributions. Background material is included only to the extent required to support subsequent analysis and discussion.

The organization of the Thesis reflects the logical progression from the study of individual chaotic oscillators to the evaluation of complete chaos-based communication systems under different channel conditions. The content of each section is summarized as follows.

The first section investigates the properties of chaotic oscillators with an emphasis on the influence of the fundamental frequency. Two structurally different oscillators—the Colpitts and Vilnius chaotic oscillators—are analyzed using simulations and experimental prototypes. The section examines spectral characteristics, cross-correlation behavior, and time-lag properties relevant to symbol duration selection in chaos-based communication systems.

The second section focuses on chaotic synchronization in drive–response chaotic oscillator configurations. The noise immunity of synchronization is studied using different circuit nodes as synchronization signals. Correlation-based metrics are employed to quantify synchronization quality under additive noise, enabling a systematic comparison of potential synchronization signals for both chaotic oscillators.

The third section addresses the impact of unequal synchronization on correlation-based data detection. It demonstrates that imbalanced synchronization between different signals leads to biased symbol decisions. To compensate for this effect, a detection threshold is introduced to restore balanced decision-making in chaos shift-keying systems.

The fourth section focuses on the integration of advanced modulation techniques with chaos-based communication systems. It first introduces the use of QAM and FM for transmitting chaotic signals at a specified carrier frequency, describing the corresponding system architectures and signal processing chains. The noise immunity of the resulting chaos-based communication systems is then evaluated through both simulation and experimental prototype measurements, with performance assessed in terms of bit error rate under AWGN conditions. Subsequently, the impact of synchronization signal selection and chaotic oscillator topology on system performance is investigated. The section concludes with an analysis of system performance in a two-ray propagation channel, where QCSK and FM-CSK systems are evaluated under frequency-selective fading and compared with conventional modulation schemes to assess their performance in practical wireless environments.

The fifth section concludes the Thesis by summarizing the main research findings, discussing their implications for chaos-based communication system design, and outlining directions for future work.

Together, these sections provide a coherent framework that connects chaotic oscillator dynamics, synchronization behavior, detection strategy design, and system-level communication performance. The structure ensures a clear transition from circuit-level analysis to practical communication scenarios, supporting the overall objectives of the Thesis.

# 1 CHAOTIC OSCILLATORS

This section introduces and analyzes two representative continuous-time chaotic oscillators—the Colpitts and Vilnius circuits—through simulation and hardware prototype studies. The mathematical model, tunability, spectral and temporal characteristics are presented for each oscillator, using the PSD, the 0–1 test for chaos (Z1TEST), and cross-correlation analysis. Both low- and high-frequency configurations are investigated to expose frequency-scaling effects (Colpitts at $f_0 \approx 96.86\,\text{kHz}$ and $968.59\,\text{kHz}$; Vilnius at $f_0 \approx 1.6\,\text{kHz}$ and $160\,\text{kHz}$).

The choice of the Colpitts and Vilnius chaotic oscillators in this Thesis is motivated by their complementary circuit structures and their suitability for communication-oriented applications. The Colpitts oscillator represents one of the simplest realizations of a chaotic circuit, consisting of a transistor-driven RLC resonant tank where the transistor simultaneously provides gain and introduces the required nonlinearity. In contrast, the Vilnius oscillator employs an operational amplifier as the active element to sustain oscillations and a diode as the nonlinear element, providing an alternative and equally fundamental route to chaos generation. Together, these two circuits capture the two most common approaches to chaotic oscillator design—using a transistor as the active nonlinear component or separating the roles of amplification and nonlinearity into distinct devices. Beyond their structural simplicity, both oscillators offer frequency tunability through component selection, making them highly relevant for communication systems with adaptable bandwidth and data rates. Although more advanced chaotic circuits, such as those incorporating memristors, exist in the literature [53]–[56], they are typically limited to low-frequency operation and remain less practical for broadband communication. For these reasons, the Colpitts and Vilnius oscillators provide a representative and practical foundation for analyzing the trade-offs between circuit simplicity, tunability, and communication performance in chaos-based systems [49], [52].

Although chaotic signals are inherently broadband, they can be associated with a *fundamental* frequency corresponding to the natural oscillation frequency in a non-chaotic, period-1 mode. This frequency is typically near the center frequency of oscillations under chaotic conditions and is determined by component selection in circuit design [32]. In certain designs, the operating frequency can also be tuned by adjusting parameters such as the gain of an operational amplifier [33]. Most discrete-component chaotic oscillators exhibit sub-MHz operating frequencies, with performance limitations primarily determined by the bandwidth and dynamic response of active elements such as operational amplifiers [32]. Nonetheless, high-frequency implementations of chaotic oscillators—spanning ultrahigh-frequency ranges—have been demonstrated using advanced technologies such as resonant tunneling diodes and integrated circuit platforms [34]–[36]. Tunable or frequency-scalable chaotic oscillators are particularly advantageous in communication systems, as they enable higher data rates, frequency-hopping schemes, and multi-user separation through frequency diversity.

The main thesis of this section is that the fundamental frequency of a chaotic oscillator directly influences the achievable data rate of chaos-based communication systems. In this section, the bit

length is determined using the cross-correlation function of the chaotic signals. Specifically, the bit duration is selected based on the settling point of the cross-correlation function amplitude, defined as the time lag beyond which the correlation values decay from their dominant central peak and fluctuate around small values [46]. This lag-based criterion ensures that bits are transmitted using sufficiently decorrelated chaotic waveforms, and improves symbol distinguishability. As the fundamental frequency increases, the extent of the high-correlation lag region decreases, allowing for shorter bit durations and, consequently, higher achievable data rates. This frequency-dependent behavior is confirmed through both simulation and prototype measurements.

The section is organized as follows. Section 1.1 details the Colpitts oscillator, including its model, frequency tunability, simulation setup, and hardware prototype measurements. Section 1.2 presents the Vilnius oscillator using the same structure, with both simulation and experimental results discussed within the section. Finally, Section 1.3 provides a comparative discussion, illustrating how fundamental-frequency tuning can be used as a practical design parameter to adjust the extent of the high-correlation lag region and the achievable data rate for different application requirements.

## 1.1 Colpitts Chaotic Oscillator

This subsection introduces the nonlinear dynamics of the Colpitts chaotic oscillator. The Colpitts chaotic oscillator was chosen for this study because of its simple design and ability to adjust the fundamental frequency, as well as the sharp cross-correlation function of its generated signals. The primary objective is to evaluate the dynamics of a Colpitts chaotic oscillator in simulation and prototype.

*Mathematical Model*

The oscillator examined in this work operates as a nonlinear dynamical system capable of producing chaotic signals. The circuit diagram of the Colpitts oscillator is shown in Fig. 1.1, comprising standard passive components—resistors, capacitors, and an inductor—as well as an active nonlinear element—a bipolar junction transistor (BJT). The system exhibits chaotic behavior under specific operating conditions and component values provided in [57].

The Colpitts oscillator, originally designed for single-tone RF signal generation, enters a chaotic regime when driven into nonlinear operation. Its topology includes a BJT, an inductive element $L_1$, and a capacitive voltage divider formed by $C_1$ and $C_2$, which provides the necessary feedback for sustained oscillation. The resonant characteristics of the circuit are determined by the LC circuit formed by the inductor $L_1$ and the capacitive divider $C_1$–$C_2$, whose equivalent capacitance sets the fundamental oscillation frequency. Biasing is provided by voltage sources $V_1$ and $V_2$ to ensure proper transistor operation.

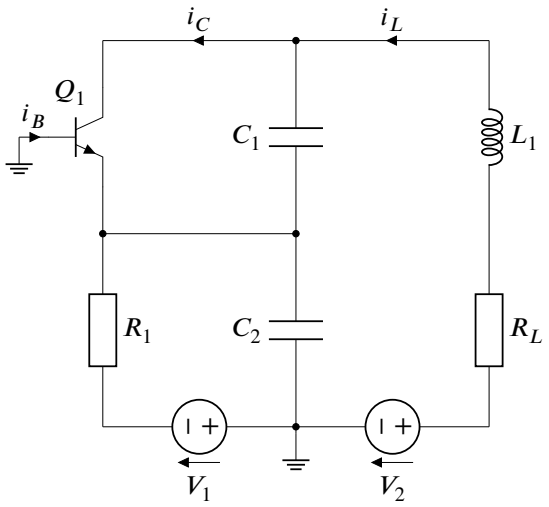


Fig. 1.1. Colpitts chaotic oscillator circuit diagram.

The dynamics of the Colpitts chaotic oscillator is described by a set of nonlinear differential equations derived from Kirchhoff's laws [58]:

$$\begin{cases} C_1 \dfrac{\mathrm{d}v_{C1}}{\mathrm{d}t} = i_L - i_C \\ C_2 \dfrac{\mathrm{d}v_{C2}}{\mathrm{d}t} = \dfrac{V_1 - v_{C2}}{R_1} - i_L - i_B \\ L_1 \dfrac{\mathrm{d}i_L}{\mathrm{d}t} = V_2 - v_{C1} - v_{C2} - i_L \cdot R_L \end{cases}, \tag{1.1}$$

where $v_{C1}$ and $v_{C2}$ are the voltages across capacitors $C_1$ and $C_2$, respectively; $i_L$ is the inductor current; and $i_B$ and $i_C$ are the base and collector currents, respectively.

The oscillator's chaotic behavior depends on its nonlinear element. The nonlinear voltage-controlled resistance of the transistor in the Colpitts oscillator can be approximated by a piecewise-linear function:

$$i_B = \begin{cases} 0, & \text{if } -v_{C2} \le V_{TH} \\ -\dfrac{v_{C2} + V_{TH}}{R_{ON}}, & \text{if } -v_{C2} > V_{TH} \end{cases}, \tag{1.2}$$

$$i_C = \beta_F \cdot i_B, \tag{1.3}$$

where $V_{TH}$ denotes the threshold voltage, $R_{ON}$ represents the small-signal on-resistance of the base-emitter, and $\beta_F$ indicates the transistor's forward current gain.

*Fundamental Frequency*

The Colpitts chaotic oscillator includes a series RLC resonance circuit. The fundamental frequency $f_0$ refers to the natural oscillation frequency of this resonant circuit, that is, the frequency at which the energy exchange between the inductor and the equivalent capacitance occurs most efficiently. At this frequency, the reactive components ideally cancel each other, resulting in the highest amplitude steady-state oscillation. Thomson's formula defines the fundamental frequency $f_0$ of the circuit:

$$f_0 = \frac{1}{2\pi\sqrt{L_1 \cdot C_{eq}}}, \tag{1.4}$$

where $C_{eq}$ is equivalent capacitance calculated from the series connection of capacitors $C_1$ and $C_2$:

$$C_{eq} = \frac{C_1 \cdot C_2}{C_1 + C_2}. \tag{1.5}$$

The original study [58] introduced the Colpitts chaotic oscillator with the following parameter values: $R_L = 35\,\Omega$, $L_1 = 98.5\,\mu\text{H}$, $C_1 = 54\,\text{nF}$, $C_2 = 54\,\text{nF}$, $R_1 = 40\,\Omega$, $V_1 = 5\,\text{V}$, $V_2 = 5\,\text{V}$, and transistor 2N2222. However, due to the limited availability of an inductance value of 98.5 µH, it was approximated to 100 µH. These specified parameter values resulted in a fundamental frequency of 96.86 kHz. In order to maintain the oscillator's chaotic behavior for different fundamental frequencies, it is necessary to adjust the nominal values of the reactive components while maintaining the same ratios between $C_1$, $C_2$, and $L_1$.

A tenfold increase in the fundamental frequency was achieved when the nominal values of the reactive components were reduced by a factor of ten: $L_1 = 10\,\mu\text{H}$, $C_1 = 5.4\,\text{nF}$, $C_2 = 5.4\,\text{nF}$. This modification resulted in a fundamental frequency of 968.59 kHz. Furthermore, by utilizing reactive elements values of $L_1 = 1\,\mu\text{H}$, $C_1 = 540\,\text{pF}$, $C_2 = 540\,\text{pF}$, chaotic behavior was successfully observed in the Colpitts chaotic oscillator, achieving a fundamental frequency of 9.69 MHz [49].

Although this proportional scaling does not provide real-time tunability, it demonstrates that the Colpitts oscillator can be implemented over a broad frequency range by appropriate selection of reactive component values, which is beneficial for applications requiring different carrier frequencies in chaos-based communication systems.

*Simulation Model*

A model of the Colpitts chaotic oscillator was constructed in the LTspice simulation environment, with simulated signals exported as text files and subsequently processed in MATLAB for analysis (Fig. 1.2). The simulation was configured to run for 5 ms with a maximum timestep of 0.1 µs for the fundamental frequency of 96.86 kHz. These parameters were chosen to ensure a sufficiently long signal duration for MATLAB post-processing and provide satisfactory temporal resolution for

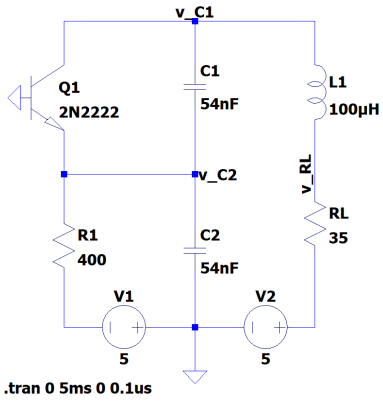


Fig. 1.2. Colpitts chaotic oscillator model in the LTspice simulation environment.

accurately capturing the oscillator's chaotic behavior. Although LTspice dynamically adjusts the timestep based on the rate of change of voltages and currents, specifying a maximum timestep helps maintain numerical stability. It ensures that the rapid state transitions characteristic of chaotic systems are properly resolved.

For the oscillator configuration with a higher fundamental frequency of 968.59 kHz, the total

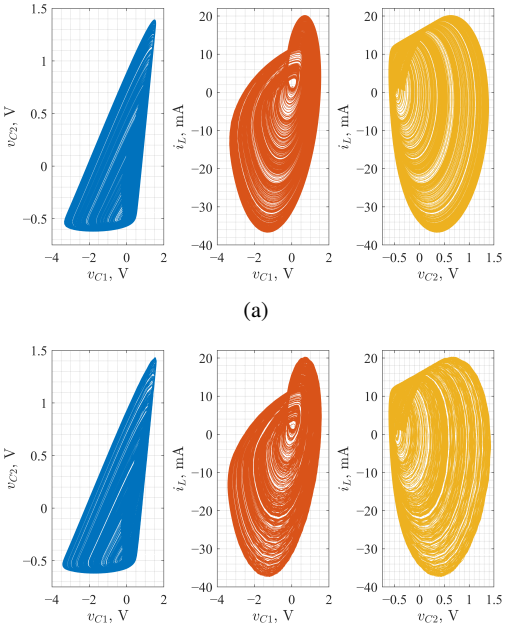


(a)

(b)

Fig. 1.3. Two-dimensional attractor projections of the Colpitts chaotic oscillator for the fundamental frequencies of (a) 96.86 kHz and (b) 968.59 kHz.

simulation time was reduced to 500 µs with a maximum timestep of 0.01 µs. After completing the simulations, the time-domain signals were exported from LTspice in text format and processed in MATLAB. This post-processing enabled further analysis. The simulation model is verified by plotting two-dimensional attractor projections, which are unique for each chaotic oscillator.

Fig. 1.3 (a) and (b) shows the attractor projections for both oscillator configurations. The geometrical structures of the attractors appear similar across the fundamental frequencies of 96.86 kHz and 968.59 kHz, indicating that the chaotic behavior is preserved despite the change in the fundamental frequency. Additionally, the attractor shapes are consistent with those reported in the original study [58], validating the accuracy of the simulation models.

*Simulation Study*

The dynamics of the Colpitts chaotic oscillator were analyzed using simulations conducted in the LTspice environment, with subsequent data processing and analysis performed in MATLAB. To quantitatively verify the chaotic nature of the generated signals, the 0–1 test for chaos (Z1TEST) [59] was applied to the simulated waveforms.

The Z1TEST produces a numerical value between 0 and 1, where values close to 0 indicate periodic behavior, while values close to 1 indicate chaos. The method is based on four key steps:

1. Constructing translation variables from the input signal $x(n)$ using a fixed parameter $c$, where $c \in (0, \pi)$ is a rotation parameter that determines how the scalar signal is mapped into a two-dimensional representation and is independent of the underlying system dynamics;
2. Computing the mean square displacement $M_c(n)$ of the translation variables, where $M_c(n)$ remains constant for periodic dynamics and increases with $n$ for chaotic dynamic
3. Evaluating the correlation coefficient $\beta$ between $M_c(n)$ and a linearly increasing sequence to quantify whether the observed behavior corresponds to periodic or chaotic dynamics
4. Repeating steps 1–3 for $N_c$ values of the parameter $c$ chosen randomly from the interval $(0, \pi)$, where in practice $N_c = 100$ is sufficient, and defining the final Z1TEST value as the median of the corresponding $\beta$ values, such that values close to 0 indicate periodic dynamics and values close to 1 indicate chaotic dynamics.

Both oscillator configurations yielded Z1TEST values exceeding 0.95, validating chaotic behavior. This result is particularly relevant for chaos-based communication systems, where chaotic dynamics significantly enhance physical-layer security.

The impact of the fundamental frequency on the bandwidth and statistical characteristics of the generated chaotic signals was evaluated using two oscillator configurations with fundamental frequencies of 96.86 kHz and 968.59 kHz. Figs. 1.4 and 1.5 show the PSD of the simulated signals $v_{C1}$, $v_{C2}$, and $i_L$ for both frequency configurations.

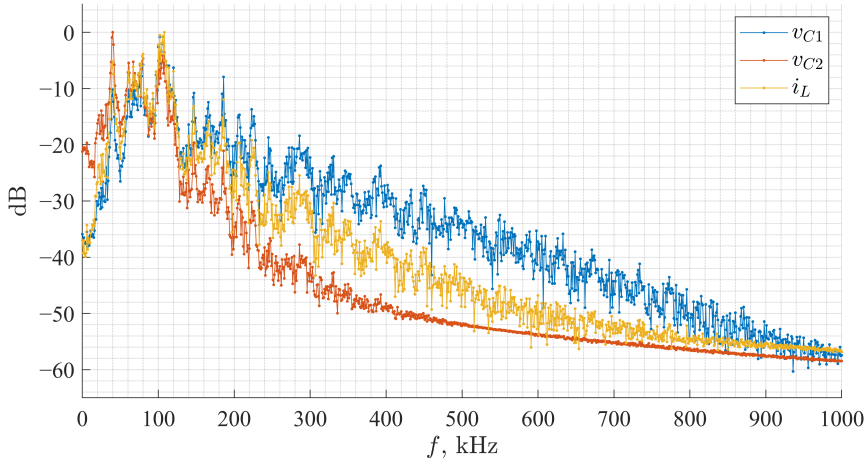


Fig. 1.4. PSD of $v_{C1}$, $v_{C2}$, and $i_L$ for the Colpitts chaotic oscillator at $f_0 = 96.86\,\text{kHz}$.

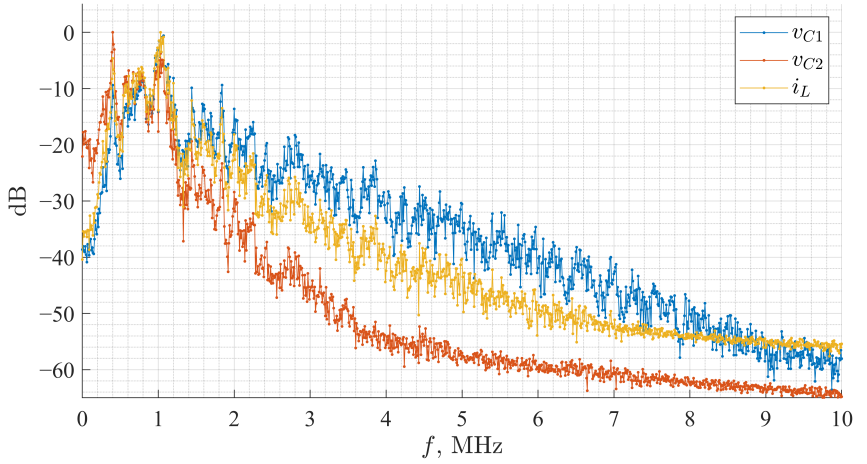


Fig. 1.5. PSD of $v_{C1}$, $v_{C2}$, and $i_L$ for the Colpitts chaotic oscillator at $f_0 = 968.59\,\text{kHz}$.

As shown in Figs. 1.4 and 1.5, the PSD of the main oscillator variables ($v_{C1}$, $v_{C2}$, and $i_L$) is broadly distributed and centered around the fundamental frequency for each case. When comparing the two cases, it is evident that increasing the fundamental frequency from 96.86 kHz to 968.59 kHz leads to a clear expansion of the signal bandwidth, while the overall shape of the PSD remains similar. This demonstrates that the bandwidth of the signals obtained from Colpitts chaotic oscillator can be controlled by adjusting the fundamental frequency, enabling the system to be adapted for applications requiring signals with different spectral properties. The observed wideband spectral distribution is advantageous for chaos-based communication systems, offering inherent resilience to narrowband

interference and supporting spread-spectrum operation. It is also worth noting that the signals exhibit a wideband spectrum with gradually decreasing amplitude.

The cross-correlation function was computed between signals within a single Colpitts chaotic oscillator to evaluate the temporal relationship between different signals and to estimate the minimum bit length [46]. The cross-correlation of periodic signals is itself periodic; however, when a finite time interval is observed, the envelope of the cross-correlation function decreases with increasing time shift between signals due to the progressively reduced number of overlapping samples. For periodic signals, this decay is gradual. In contrast, for aperiodic and chaotic signals, the cross-correlation amplitude decreases rapidly with time shift and does not exhibit regular repetition, reflecting the absence of long-term temporal periodicity.

Based on this approach, the cross-correlation properties of the Colpitts chaotic oscillator were analyzed for two fundamental frequency configurations using signals obtained from LTspice simulations. The cross-correlation functions between the signals $v_{C1}$ and $v_{C2}$, $v_{C1}$ and $i_L$, and $v_{C2}$ and $i_L$ are shown in Figs. 1.6 and 1.7 for fundamental frequencies of 96.86 kHz and 968.59 kHz, respectively. The corresponding numerical cross-correlation parameters are summarized in Table 1.1.

Figs. 1.6 and 1.7 show that, for all analyzed signal pairs and both fundamental frequencies, the cross-correlation functions exhibit a pronounced peak at a lag close to zero, followed by a rapid reduction in amplitude as the time shift increases, confirming chaotic behavior. However, the maximum correlation does not exactly coincide with zero lag in most cases, as confirmed by the numerical values in Table 1.1 and illustrated by the close-up view in Fig. 1.8. Autocorrelation functions in Appendix A.1 show a distinct peak at zero lag followed by rapid decay, confirming the non-periodic nature of the Colpitts chaotic oscillator under different parameter conditions.

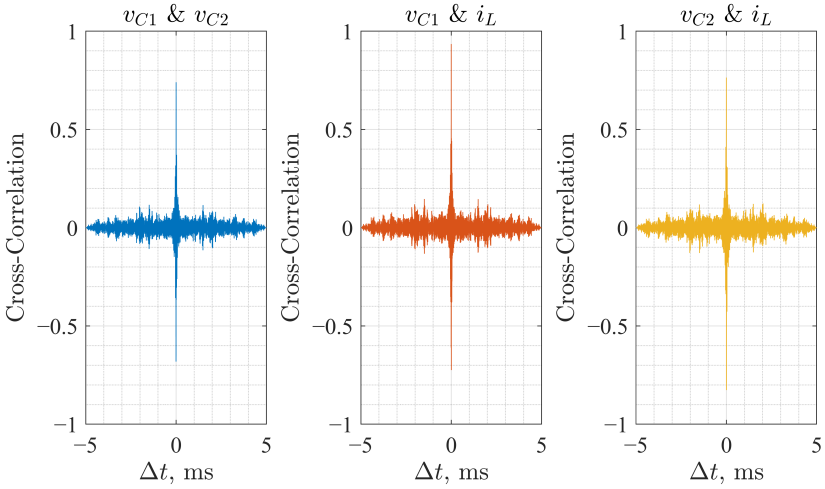


Fig. 1.6. Cross-correlation functions for $v_{C1}$ and $v_{C2}$, $v_{C1}$ and $i_L$, and $v_{C2}$ and $i_L$ in the Colpitts chaotic oscillator at $f_0 = 96.86$ kHz.

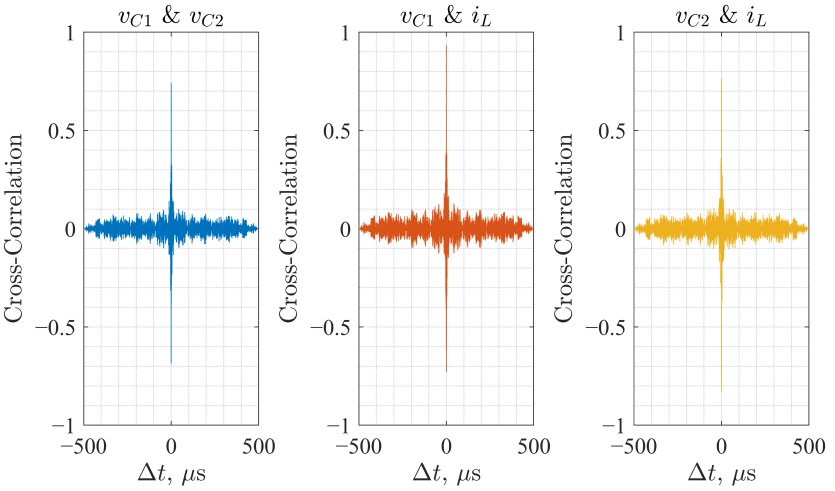


Fig. 1.7. Cross-correlation functions for $v_{C1}$ and $v_{C2}$, $v_{C1}$ and $i_L$, and $v_{C2}$ and $i_L$ in the Colpitts chaotic oscillator at $f_0 = 968.59$ kHz.

Table 1.1 reports three key parameters for each signal pair: the correlation coefficient at zero lag $\beta(0)$, the lag corresponding to the maximum cross-correlation value ($\text{Lag}_{\beta_{\max}}$), and the maximum cross-correlation function value $\beta_{\max}$. For both fundamental frequencies, the maximum correlation values occur at nonzero lags for all signal pairs. The sign of the lag indicates whether one signal leads or lags the other in time, while the magnitude reflects the relative temporal offset between the signals. A magnified view of the cross-correlation function for a representative signal pair is shown in Fig. 1.8. The zoomed representation makes it evident that the maximum of the cross-correlation function occurs at a small but nonzero time lag, rather than exactly at zero. This observation directly corresponds to the numerical values of $\text{Lag}_{\beta_{\max}}$ reported in Table 1.1 and confirms that the dominant correlation peak is shifted due to phase relationships between the oscillator state variables.

The values of $\beta(0)$ remain significantly lower than the corresponding $\beta_{\max}$ values in all cases. For example, at $f_0 = 96.86$ kHz, $\beta(0)$ ranges from $-0.11$ to 0.60, whereas $\beta_{\max}$ reaches values between 0.74 and 0.93. Similar trends are observed at $f_0 = 968.59$ kHz. This indicates that the strongest correlation between signals is achieved only when an appropriate time shift is applied,

Table 1.1.
Cross-correlation parameters for different signal pairs and fundamental frequencies in the Colpitts oscillator obtained from LTspice simulations

| Signal pair | $f_0 = 96.86$ kHz | | | $f_0 = 968.59$ kHz | | |
|---|---|---|---|---|---|---|
| | $\beta(0)$ | $\text{Lag}_{\beta_{\max}}$, µs | $\beta_{\max}$ | $\beta(0)$ | $\text{Lag}_{\beta_{\max}}$, µs | $\beta_{\max}$ |
| $v_{C1}$ & $v_{C2}$ | 0.60 | 1.00 | 0.74 | 0.60 | 0.1 | 0.74 |
| $v_{C1}$ & $i_L$ | 0.48 | −1.50 | 0.93 | 0.49 | −0.15 | 0.94 |
| $v_{C2}$ & $i_L$ | −0.11 | −2.90 | 0.76 | −0.11 | −0.29 | 0.77 |

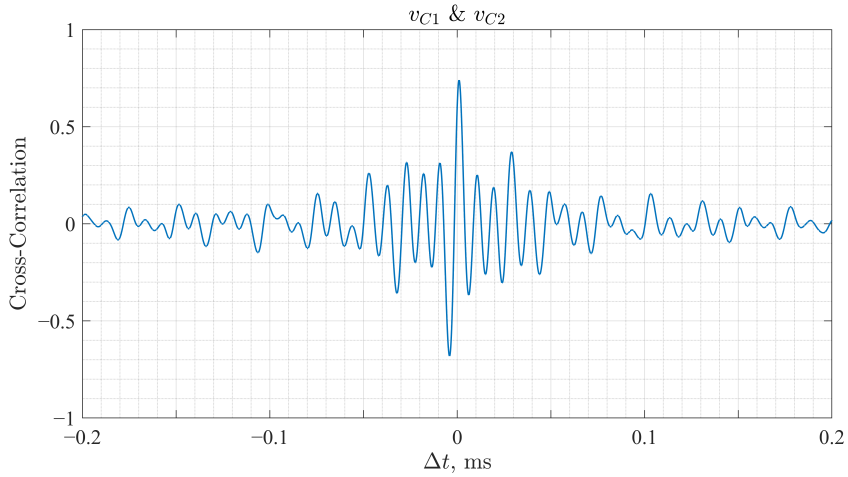


Fig. 1.8. Close-up view of the cross-correlation function between $v_{C1}$ and $v_{C2}$ (Fig. 1.6) in the Colpitts chaotic oscillator at $f_0 = 96.86$ kHz, highlighting the dominant correlation peak at a nonzero time lag.

rather than at zero lag.

The occurrence of nonzero correlation lags is a direct consequence of the physical nature of the oscillator state variables. Voltages across capacitors and the current through the inductor are related through differential equations, resulting in inherent phase shifts between signals measured at different circuit nodes. As a result, the signals are not phase-aligned; moreover, due to the chaotic behavior, they cannot be considered delayed replicas of one another, even when high correlation values are observed.

The cross-correlation characteristics discussed above also provide insight into the feasibility of employing the investigated Colpitts chaotic oscillator as a signal source in a chaos-based communication system. In such systems, information is transmitted using distinct chaotic waveforms and recovered through correlation-based processing; therefore, the symbol duration must exceed the inherent correlation time of the chaotic signals to prevent inter-symbol correlation that would degrade reliable detection. The cross-correlation functions were used to determine this limit by identifying the lag at which the correlation amplitude decays from its dominant peak and falls below a threshold of 0.4, indicating sufficient decorrelation for reliable symbol discrimination [46]. This lag corresponds to the correlation time of the chaotic signal, beyond which the normalized cross-correlation becomes sufficiently small so that residual statistical dependence does not significantly influence the correlation-based decision. At a fundamental frequency of 96.86 kHz, this characteristic lag is approximately 60 µs, corresponding to an achievable data rate of 16.7 kb/s. Increasing the fundamental frequency to 968.59 kHz reduces the extent of the high-correlation lag region to approximately 6 µs, enabling data rates up to 166.7 kb/s.

These results demonstrate that increasing the fundamental frequency reduces the cross-correlation decay time interval, thereby allowing for shorter bit durations and an increase in the maximum achievable data rate. The numerical values obtained from the cross-correlation analysis provide a quantitative basis for selecting communication parameters when using the Colpitts chaotic oscillator in chaos-based transmission systems.

*Prototype*

A hardware prototype was developed to experimentally validate the Colpitts oscillator's chaotic behavior. The PCB layout was designed using the KiCad PCB design software. The same PCB layout was used for both oscillator configurations—96.86 kHz and 968.59 kHz—since the primary difference lies in the values of the reactive components. The circuit topology and component packages remained unchanged, with only the inductors and capacitors replaced by components of different nominal values to achieve the desired fundamental frequency. A photograph of the fabricated Colpitts chaotic oscillator PCB is shown in Fig. 1.9. This physical implementation replaces the simulation model and is the basis for experimental signal acquisition and validation.

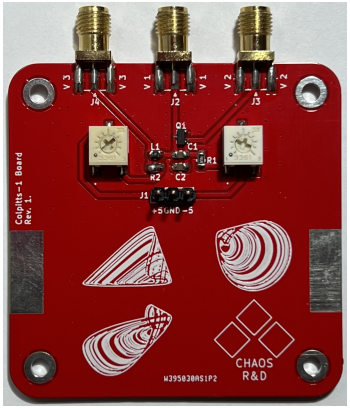


Fig. 1.9. Fabricated Colpitts Chaotic Oscillator PCB Prototype.

The Digilent's Analog Discovery Pro (ADP3450) portable high-resolution mixed-signal oscilloscope measured the voltage signals from selected circuit nodes. Acquired signals were exported and further processed in MATLAB to enable visualization and analysis of the circuit dynamics. Two-dimensional attractor projections were generated from the recorded signals to assess the chaotic behavior. Fig. 1.10 shows the attractor projections obtained from the prototype for both frequency configurations. The attractor geometries are similar to those observed in simulation and correspond to the shapes reported in previous studies [58], indicating consistent and repeatable chaotic behavior.

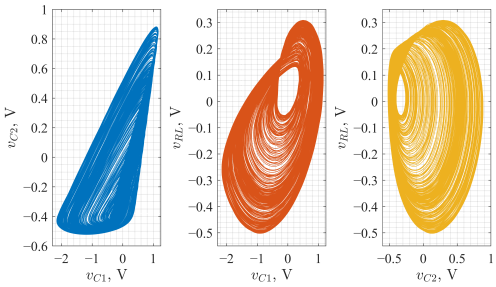


(a)

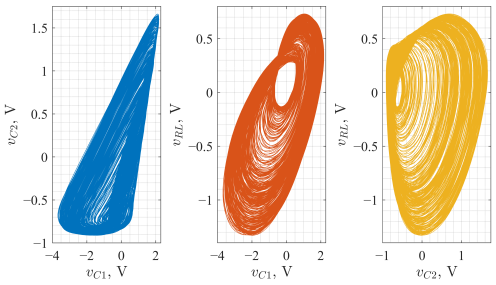


(b)

Fig. 1.10. Two-dimensional attractor projections from the Colpitts chaotic oscillator PCB for the fundamental frequencies of (a) 96.86 kHz and (b) 968.59 kHz.

*Prototype Measurements*

Both prototype configurations were measured using the ADP3450, with data analyzed in MATLAB. For both fundamental frequencies, the Z1TEST values reached 0.95, indicating that the physical implementation successfully reproduced chaotic behavior. This consistency with simulation demonstrates the persistence of the chaotic dynamics in the physical Colpitts oscillator, even under real-world conditions with parasitic effects.

Figs. 1.11 and 1.12 present the measured PSD of the prototype signals $v_{C1}$, $v_{C2}$, and $v_{RL}$. The spectra are centered around the fundamental frequency, and bandwidth scales with $f_0$, consistent with the simulation. However, the measured spectra exhibit slightly narrower central regions, which can be attributed to PCB parasitics and component tolerances.

As shown in Figs. 1.11 and 1.12, the estimated PSD for both fundamental frequency configurations is centered around their respective fundamental frequencies. When the fundamental frequency is increased from 96.86 kHz to 968.59 kHz, the signal bandwidth expands accordingly. At the same time, the overall spectral shape remains consistent with the chaotic behavior observed in simulations. However, the measured PSD exhibit slightly narrower central regions compared to the simulated results due to the parasitic effects introduced by the physical PCB layout and real component nominal tolerances.

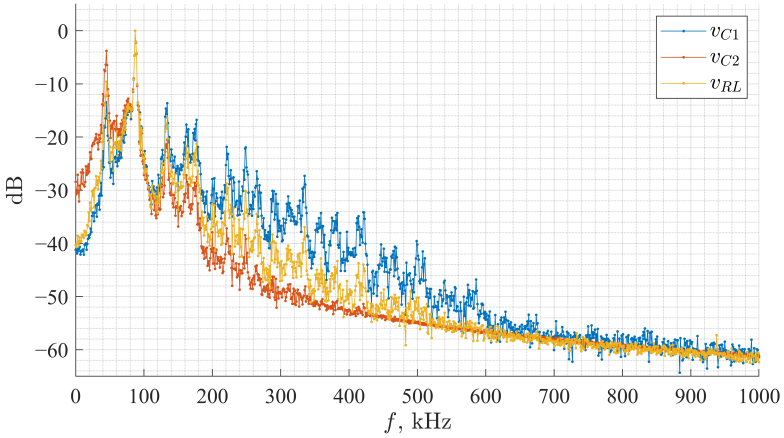


Fig. 1.11. PSD of $v_{C1}$, $v_{C2}$, and $v_{RL}$ for the Colpitts chaotic oscillator prototype at $f_0 = 96.86$ kHz.

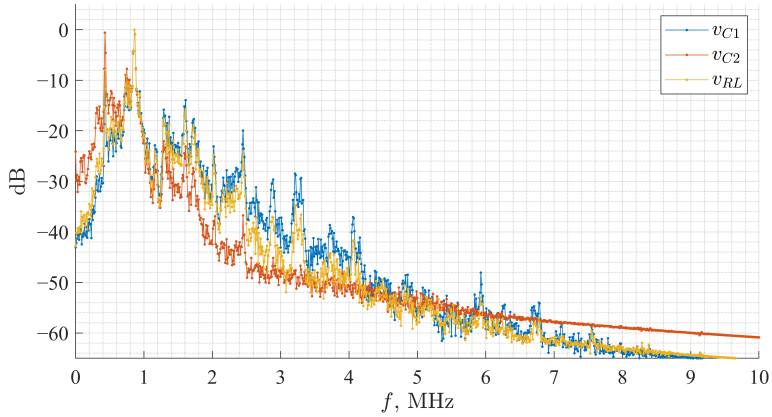


Fig. 1.12. PSD of $v_{C1}$, $v_{C2}$, and $v_{RL}$ for the Colpitts chaotic oscillator prototype at $f_0 = 968.59$ kHz.

The cross-correlation functions of the Colpitts chaotic oscillator prototype were analyzed for two fundamental frequency configurations using experimentally measured signals. The cross-correlation functions between $v_{C1}$ and $v_{C2}$, $v_{C1}$ and $v_{RL}$, and $v_{C2}$ and $v_{RL}$ are shown in Figs. 1.13 and 1.14 for fundamental frequencies of 96.86 kHz and 968.59 kHz, respectively. The corresponding numerical cross-correlation parameters are summarized in Table 1.2. Additional signal dynamics validation data in the form of autocorrelation functions are provided in Appendix A.1.

Figs. 1.13 and 1.14 show that, for all analyzed signal pairs for both fundamental frequencies, the cross-correlation amplitude decreases as the time shift increases, which is consistent with aperiodic and chaotic dynamics.

Table 1.2 presents the cross-correlation coefficient value at zero lag $\beta(0)$, the lag corresponding

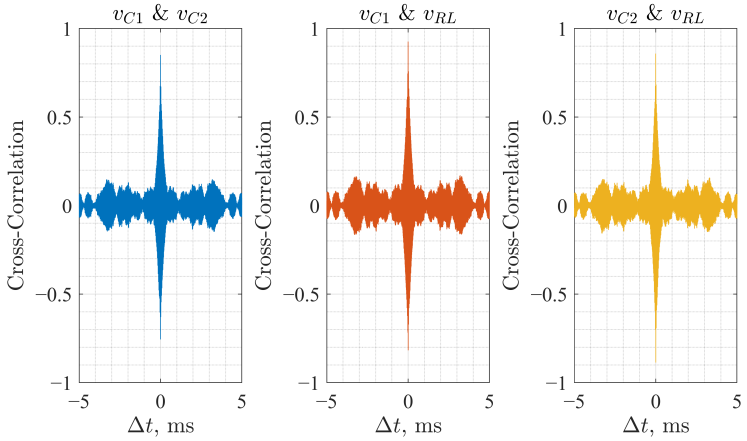


Fig. 1.13. Cross-correlation functions for $v_{C1}$ and $v_{C2}$, $v_{C1}$ and $v_{RL}$, and $v_{C2}$ and $v_{RL}$ in the Colpitts chaotic oscillator prototype at $f_0 = 96.86$ kHz.

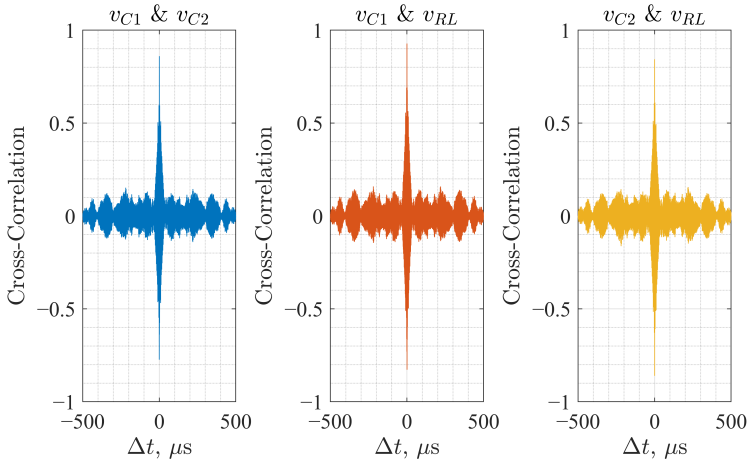


Fig. 1.14. Cross-correlation functions for $v_{C1}$ and $v_{C2}$, $v_{C1}$ and $v_{RL}$, and $v_{C2}$ and $v_{RL}$ in the Colpitts chaotic oscillator prototype at $f_0 = 968.59$ kHz.

Table 1.2.
Cross-correlation parameters for different signal pairs and fundamental frequencies in the Colpitts oscillator prototype

| Signal pair | $f_0 = 96.86$ kHz | | | $f_0 = 968.59$ kHz | | |
|---|---|---|---|---|---|---|
| | $\beta(0)$ | $\mathrm{Lag}_{\beta_{\max}}$, µs | $\beta_{\max}$ | $\beta(0)$ | $\mathrm{Lag}_{\beta_{\max}}$, µs | $\beta_{\max}$ |
| $v_{C1}$ & $v_{C2}$ | 0.71 | 1.00 | 0.85 | 0.75 | 0.10 | 0.86 |
| $v_{C1}$ & $v_{RL}$ | 0.51 | −2.00 | 0.93 | 0.62 | −0.10 | 0.93 |
| $v_{C2}$ & $v_{RL}$ | −0.05 | −3.00 | 0.86 | −0.13 | −0.30 | 0.84 |

to the maximum correlation value ($\mathrm{Lag}_{\beta_{\max}}$), and the maximum cross-correlation coefficient $\beta_{\max}$ for each signal pair. For both fundamental frequencies, the maximum correlation occurs at nonzero

lags for all signal pairs. The sign of $\mathrm{Lag}_{\beta_{\max}}$ quantifies the relative temporal offsets between signals measured at different circuit nodes.

At a fundamental frequency of 96.86 kHz, the values of $\beta(0)$ range from $-0.05$ to 0.71, while the corresponding $\beta_{\max}$ values range between 0.85 and 0.93. At the higher fundamental frequency of 968.59 kHz, $\beta(0)$ ranges from $-0.13$ to 0.75, with $\beta_{\max}$ values between 0.84 and 0.93. In all cases, the strongest correlation between signals is observed only after applying a nonzero time shift, as listed in Table 1.2.

The maximum value of the cross-correlation function occurs at a nonzero time lag because the signals measured at different circuit nodes are time-shifted relative to each other. This time shift is introduced by the reactive elements of the circuit: capacitors and the inductor introduce a phase shift between the voltage and current waveforms. As a result, the strongest similarity between two signals is observed only when one signal is shifted in time with respect to the other, leading to a nonzero lag at which the cross-correlation reaches its maximum.

Since the investigated oscillator is intended to serve as a signal source in a chaos-based communication system, the cross-correlation functions obtained for the prototype signals were used to determine the minimum bit duration. The bit length was selected based on the time lag at which the absolute value of the cross-correlation function decays from its initial maximum and settles into small fluctuations, indicating sufficient decorrelation between consecutive symbols. For the prototype operating at a fundamental frequency of 96.86 kHz, this characteristic lag is approximately 78 µs, corresponding to a maximum achievable data rate of 12.82 kb/s. Increasing the fundamental frequency to 968.59 kHz reduces the period of the high-correlation lag region to approximately 7.5 µs, enabling data rates up to 133.3 kb/s.

These numerical results provide a quantitative basis for selecting the bit duration and achievable data rate when using the Colpitts chaotic oscillator prototype in chaos-based communication systems.

## 1.2 Vilnius Chaotic Oscillator

The Vilnius chaotic oscillator [60] is a simple, nonlinear circuit widely used in studies of chaotic dynamics due to its ease of implementation and reliable operation. Its well-established behavior has made it a common choice in both research and educational contexts [43], [52], [61], [62]. This oscillator was selected for the present work because its straightforward structure and stable performance enable good agreement between simulations and experimental measurements. The chosen chaotic oscillator can generate signals at different frequency ranges by adjusting the nominal values of its reactive elements. This frequency scalability is particularly relevant for chaos-based communication systems, where carrier frequency selection must align with channel bandwidth and system requirements.

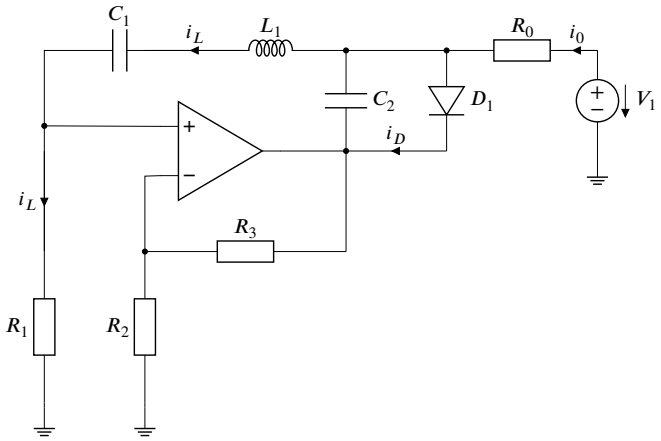


Fig. 1.15. Vilnius chaotic oscillator circuit diagram.

*Mathematical Model*

The circuit of the Vilnius oscillator, shown in Fig. 1.15, consists of an operational amplifier, an RLC resonance circuit in a positive feedback loop, an additional capacitor, and a diode functioning as the nonlinear element. This configuration ensures chaotic dynamics with minimal components.

The behavior of the Vilnius chaotic oscillator is described by a system of differential equations combining the states of three variables: $v_{C1}$, the voltage across the capacitor $C_1$; $i_L$, the current through inductor $L_1$; and $v_{C2}$, the voltage across the supplementary capacitor $C_2$. The system is derived using Kirchhoff's circuit laws:

$$\begin{cases} C_1 \dfrac{\mathrm{d}v_{C1}}{\mathrm{d}t} = i_L \\ C_2 \dfrac{\mathrm{d}v_{C2}}{\mathrm{d}t} = i_0 + i_L - i_D \\ L_1 \dfrac{\mathrm{d}i_L}{\mathrm{d}t} = (k-1) \cdot R_1 \cdot i_L - v_{C_1} - v_{C_2} \end{cases}, \tag{1.6}$$

where $i_D$ is the current of the diode $D_1$, $i_0$ is the current of the resistor $R_0$, and $k$ is the closed-loop gain of the non-inverting operational amplifier, determined by the surrounding resistor network:

$$k = 1 + \frac{R_3}{R_2} \tag{1.7}$$

The oscillator's nonlinearity is introduced by the diode's current-voltage characteristic, represented by the following equation:

$$i_D = i_S \cdot \left( e^{\frac{v_D}{v_T}} - 1 \right), \tag{1.8}$$

where $v_D$ is the voltage across the diode (due to parallel connection $v_D = v_{C2}$), $i_S$ is the diode saturation current (approximately $2 \times 10^{-14}$ A for a standard 1N4148 diode), and $v_T$ is the thermal voltage (about 25.8 mV at room temperature, 298 K).

This nonlinear characteristic, combined with the circuit design, facilitates the onset of chaotic oscillations. The system exhibits a universal period-doubling route to chaos, as demonstrated through bifurcation diagrams and positive Lyapunov exponents, verifying its chaotic nature under suitable parameter conditions [61].

*Fundamental Frequency*

The Vilnius chaotic oscillator, first introduced in [60], is based on an RLC resonant circuit topology. In its original configuration, the component values are: $C_1 = 100\,\text{nF}$, $C_2 = 15\,\text{nF}$, $L_1 = 100\,\text{mH}$, $R_1 = 1\,\text{k}\Omega$, $R_2 = 10\,\text{k}\Omega$, $R_3 = 6\,\text{k}\Omega$, $R_0 = 20\,\text{k}\Omega$, $V_1 = 5\,\text{V}$, $k = 1.6$. The fundamental frequency $f_0$ of the oscillator can be estimated using the standard RLC resonance formula:

$$f_0 = \frac{1}{2\pi\sqrt{L_1 \cdot C_1}}. \tag{1.9}$$

With these component values, the fundamental frequency is approximately 1.6 kHz.

The fundamental frequency can be increased by proportionally decreasing the values of the reactive elements. For instance, reducing $C_1$, $C_2$, and $L_1$ by a factor of 100—to $C_1 = 1\,\text{nF}$, $C_2 = 150\,\text{pF}$, and $L_1 = 1\,\text{mH}$—results in a fundamental frequency of approximately 160 kHz. Importantly, maintaining the same proportional relationship among these elements preserves the oscillator's chaotic behavior.

*Simulation Model*

A model of the Vilnius chaotic oscillator was constructed in the LTspice simulation environment to evaluate its dynamic behavior (Fig. 1.16). For the low-frequency configuration with a fundamental frequency of 1.6 kHz, the simulation was set to run for 100 ms. For the higher frequency case at 160 kHz, the simulation time was reduced to 1 ms. In both cases, the maximum timestep was fixed at 1 µs. These settings provided sufficiently long and well-sampled time-domain signals for post-processing in MATLAB.

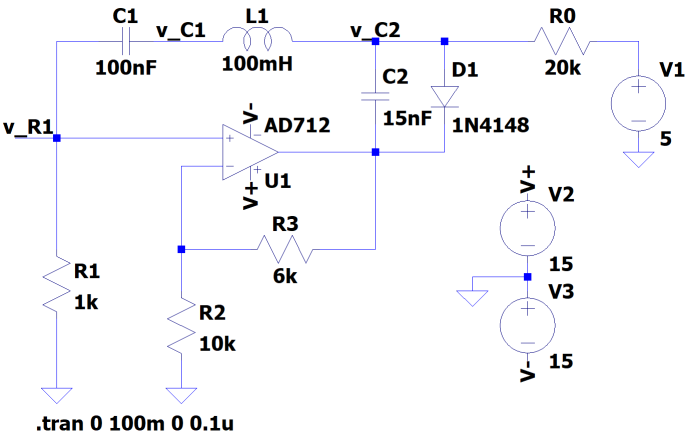


Fig. 1.16. Vilnius Chaotic oscillator model in the LTspice simulation environment.

The simulated signals were exported as text files and processed in MATLAB. Two-dimensional attractor projections were generated to visualize the oscillator dynamics under both frequency configurations. As shown in Fig. 1.17, the attractor shapes are consistent across the two cases, indicating chaotic behavior. The two-dimensional projections also agree with those reported in the original study [60].

*Simulation Study*

The influence of oscillator frequency on signal bandwidth was explored by simulating the system with fundamental frequencies of 1.6 kHz and 160 kHz. Figs. 1.18 and 1.19 illustrate the PSD of the simulated signals $v_{C1}$, $v_{C2}$, and $i_L$ for both frequency configurations.

In both cases, the PSD of the oscillator variables is widely distributed, centered on the respective fundamental frequencies. An increase in $f_0$ from 1.6 kHz to 160 kHz leads to a notable widening of the spectral envelope, although the overall broadband nature is preserved. This tunable spectral width offers a practical pathway for matching oscillator output to the bandwidth requirements of different communication systems. The Vilnius oscillator's broadband spectrum inherently supports resistance to narrowband jamming and enables implementation of spread-spectrum signaling. As with other chaotic sources, the gradual decay of spectral amplitude across frequency suggests that careful filter selection remains crucial in system integration.

The temporal properties of the Vilnius chaotic oscillator were analyzed using cross-correlation functions to characterize the time relationships between different signals and to estimate the minimum bit length. The cross-correlation functions were calculated for all three signal pairs within a single oscillator, $v_{C1}$ and $v_{C2}$, $v_{C1}$ and $i_L$, and $v_{C2}$ and $i_L$. The oscillator signals were obtained from LTspice simulations, while the cross-correlation functions were computed and plotted in MATLAB. The resulting cross-correlation functions for two fundamental frequency configurations are shown

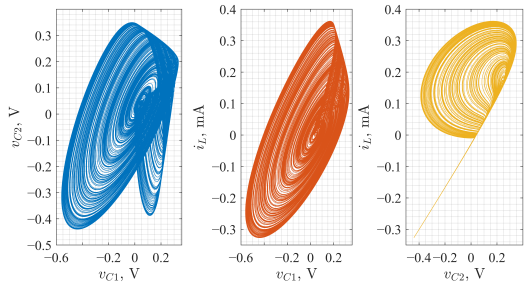


(a)

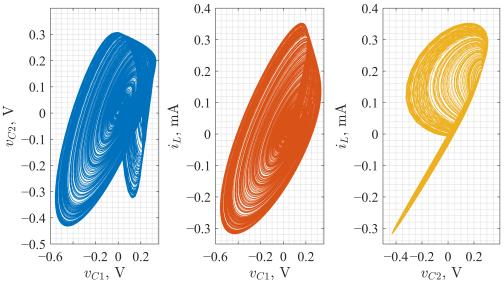


(b)

Fig. 1.17. Two-dimensional attractor projections of the Vilnius chaotic oscillator for the fundamental frequencies of (a) 1.6 kHz and (b) 160 kHz.

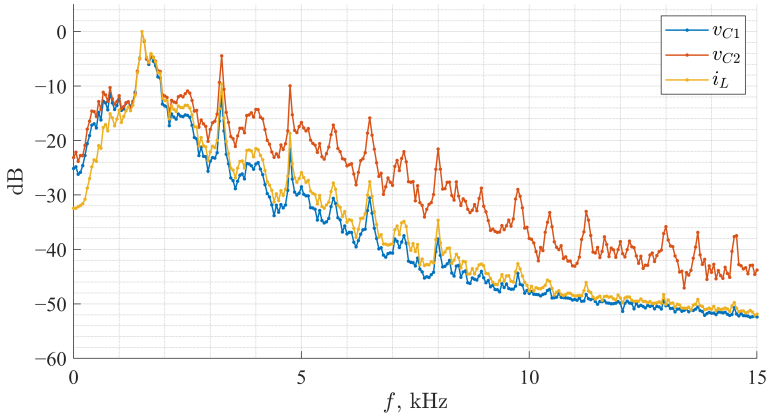


Fig. 1.18. PSD of key node voltages and inductor current for the Vilnius chaotic oscillator at $f_0 = 1.6$ kHz.

in Figs. 1.20 and 1.21.

For both fundamental frequencies and all analyzed signal pairs, the cross-correlation functions exhibit a dominant peak at a lag close to zero, followed by a rapid decrease in amplitude as the

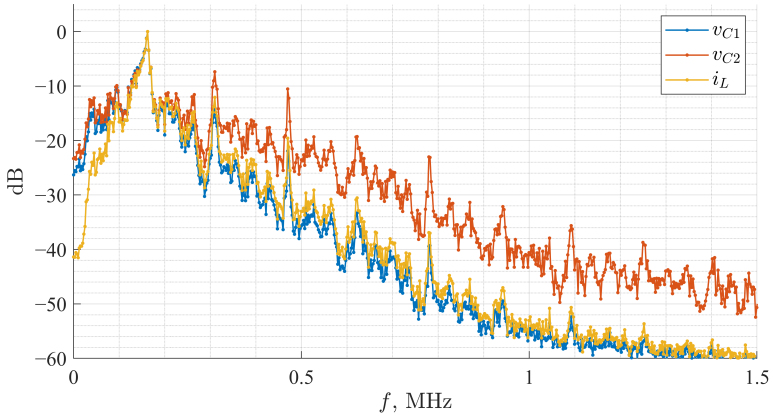


Fig. 1.19. PSD of key node voltages and inductor current for the Vilnius chaotic oscillator at $f_0 = 160\,\text{kHz}$.

time shift increases. This behavior indicates that the signals exhibit short-term correlation at close to zero lag, but lack long-term periodic alignment, indicating a chaotic behavior of the analyzed signals. The autocorrelation functions provide additional confirmation of the aperiodic nature of the signals in Appendix A.2, which show a distinct peak at zero lag followed by rapid decay for all analyzed signals. Quantitative cross-correlation parameters are summarized in Table 1.3, including the correlation coefficient at zero lag $\beta(0)$, the lag corresponding to the maximum correlation value ($\text{Lag}_{\beta_{\max}}$), and the maximum correlation coefficient $\beta_{\max}$, for both fundamental frequencies.

As shown in Table 1.3, the maximum cross-correlation values occur at nonzero time lags for

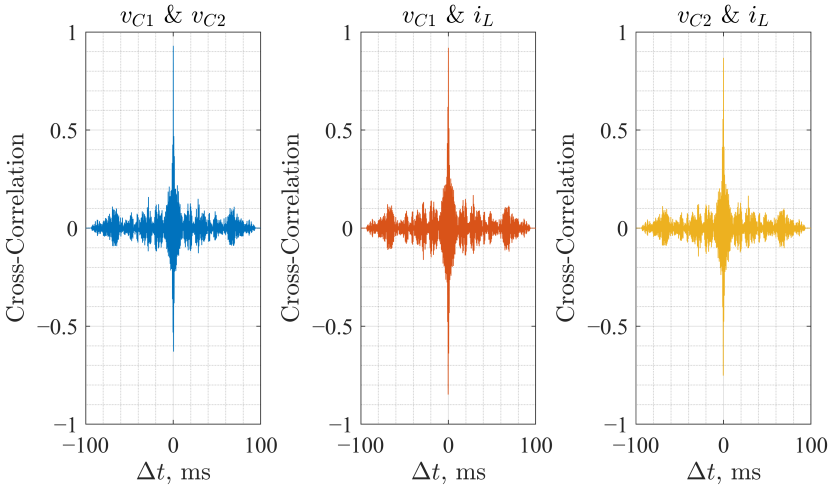


Fig. 1.20. Cross-correlation functions for $v_{C1}$ and $v_{C2}$, $v_{C1}$ and $i_L$, and $v_{C2}$ and $i_L$ in the Vilnius chaotic oscillator at $f_0 = 1.6\,\text{kHz}$.

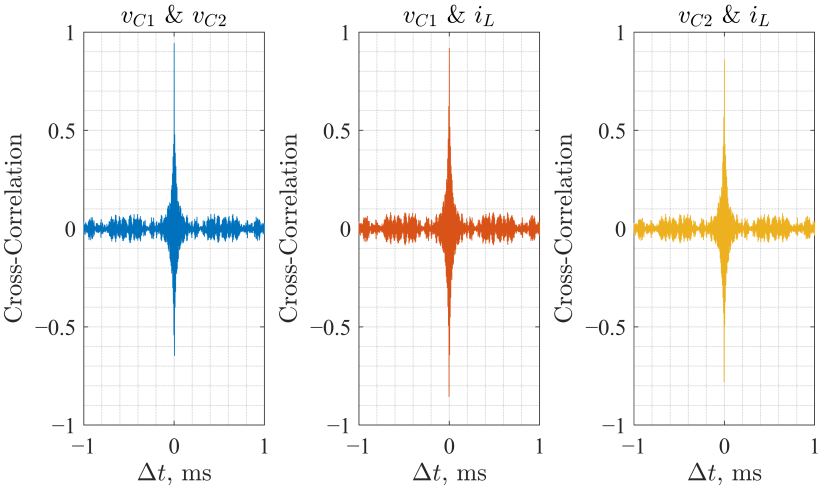


Fig. 1.21. Cross-correlation functions for $v_{C1}$ and $v_{C2}$, $v_{C1}$ and $i_L$, and $v_{C2}$ and $i_L$ in the Vilnius chaotic oscillator at $f_0 = 160\,\text{kHz}$.

all signal pairs and both operating frequencies. At $f_0 = 1.6\,\text{kHz}$, the lag corresponding to the maximum correlation ranges from $-20\,\mu\text{s}$ to $70\,\mu\text{s}$, depending on the selected signal pair, while at $f_0 = 160\,\text{kHz}$ the corresponding lags are reduced to the range of $-0.20\,\mu\text{s}$ to $0.70\,\mu\text{s}$. The sign of the lag indicates which signal foregoes the other in time.

These nonzero lag values arise from time delays introduced by the reactive elements of the oscillator circuit. In the Vilnius chaotic oscillator, voltages across capacitors and the current through the inductive element oscillate at different times due to energy storage and release in the reactive components. As a result, signals measured at different circuit nodes are not temporally aligned, and the maximum of the cross-correlation function appears at a nonzero time lag corresponding to this delay.

The correlation coefficients at zero lag $\beta(0)$ are consistently lower than the corresponding maximum correlation values $\beta_{\text{max}}$. For example, at $f_0 = 1.6\,\text{kHz}$, $\beta(0)$ varies between 0.61 and 0.83, whereas $\beta_{\text{max}}$ ranges from 0.87 to 0.93. A similar relationship is observed at $f_0 = 160\,\text{kHz}$, where $\beta(0)$ lies between 0.65 and 0.84 and $\beta_{\text{max}}$ between 0.86 and 0.94. This confirms that the correlation

Table 1.3.
Cross-correlation parameters for different signal pairs and fundamental frequencies in the Vilnius oscillator obtained from LTspice simulations

| Signal pair | $f_0 = 1.6\,\text{kHz}$ | | | $f_0 = 160\,\text{kHz}$ | | |
|---|---|---|---|---|---|---|
| | $\beta(0)$ | $\text{Lag}_{\beta_{\text{max}}}$, µs | $\beta_{\text{max}}$ | $\beta(0)$ | $\text{Lag}_{\beta_{\text{max}}}$, µs | $\beta_{\text{max}}$ |
| $v_{C1}$ & $v_{C2}$ | 0.61 | 70 | 0.93 | 0.65 | 0.70 | 0.94 |
| $v_{C1}$ & $i_L$ | 0.69 | 60 | 0.92 | 0.68 | 0.70 | 0.92 |
| $v_{C2}$ & $i_L$ | 0.83 | −20 | 0.87 | 0.84 | −0.20 | 0.86 |

between signals is achieved only after applying a nonzero time shift.

Since the Vilnius chaotic oscillator is considered as a potential signal source for a chaos-based communication system, the cross-correlation functions were used to estimate the minimum supported bit duration by identifying the time lag at which the correlation amplitude decays from its dominant central peak and settles into small fluctuations [46]. This lag defines the minimum symbol interval required to ensure adequate decorrelation between adjacent symbol intervals. For the Vilnius chaotic oscillator operating at $f_0 = 1.6$ kHz, the identified lag is approximately 1.87 ms, corresponding to an achievable data rate of about 535 b/s. When the fundamental frequency is increased to 160 kHz, the duration of the high-correlation lag region is reduced to approximately 18.1 µs, enabling data rates up to 55.2 kb/s.

The cross-correlation results indicate that increasing the fundamental frequency of the Vilnius chaotic oscillator reduces the duration of the high-correlation period, thereby allowing shorter bit durations and higher achievable data rates. These simulation results provide a quantitative basis for selecting the operating frequency and bit length in chaos-based communication systems employing the Vilnius chaotic oscillator.

*Prototype*

A Vilnius chaotic oscillator hardware prototype was developed to validate the simulation results experimentally. The PCB was designed in KiCad, and the same board was used for both frequency configurations—1.6 kHz and 160 kHz—since only the reactive component values were changed to set $f_0$, while the topology and packages remained unchanged. Photographs of the assembled board are shown in Fig. 1.22; this prototype served as the basis for signal acquisition and analysis.

Voltage signals were captured at key nodes using the ADP3450 portable mixed-signal oscilloscope, exported as text, and processed in MATLAB. Two-dimensional attractor projections for both configurations are shown in Fig. 1.23; the geometries closely match the simulated attractors and

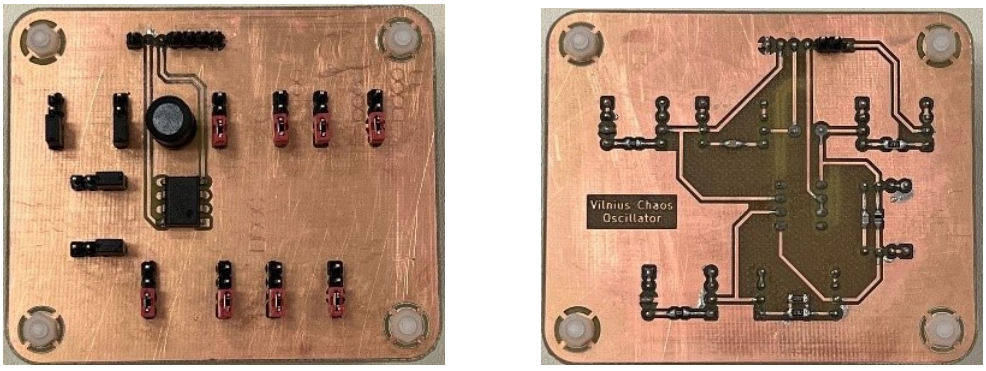


(a) (b)

Fig. 1.22. Fabricated Vilnius Chaotic Oscillator PCB Prototype: (a) Top and (b) Bottom.

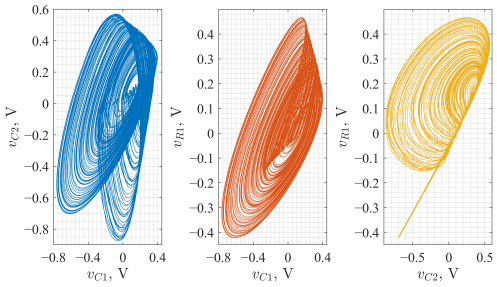


(a)

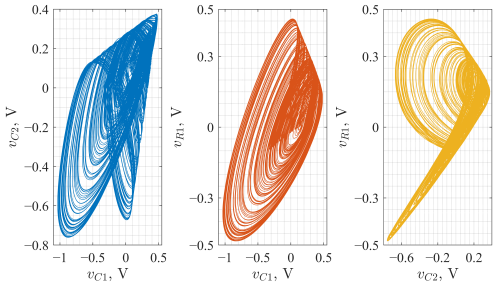


(b)

Fig. 1.23. Two-dimensional attractor projections from the Vilnius oscillator PCB for the fundamental frequencies of (a) 1.6 kHz and (b) 160 kHz.

those reported in prior work [60], indicating consistent and repeatable chaotic behavior.

*Prototype Measurements*

Both prototype configurations were measured using the ADP3450, and the data were analyzed in MATLAB. For both $f_0$ values, the Z1TEST results approached 0.9, indicating that the hardware Vilnius oscillator operated in the chaotic regime, consistent with simulation despite the presence of parasitic effects in the real world.

The frequency-domain properties of the prototype were then evaluated by examining the PSD of the measured voltages $v_{C1}$, $v_{C2}$, and $v_{R1}$. Figs. 1.24 and 1.25 present the spectra for both fundamental frequency cases.

In both configurations, the measured PSD reveals energy concentration around the respective fundamental frequencies, and the signal bandwidth expands with increasing $f_0$, consistent with simulation results. The prototype PSD exhibit modest narrowing in the central region compared to the simulated data, reflecting the influence of real-world parasitic effects and component tolerances. Despite these non-idealities, the underlying broadband chaotic behavior is preserved.

The time-domain characteristics of the Vilnius chaotic oscillator prototype were analyzed using cross-correlation functions to characterize the relationships between different circuit signals and to

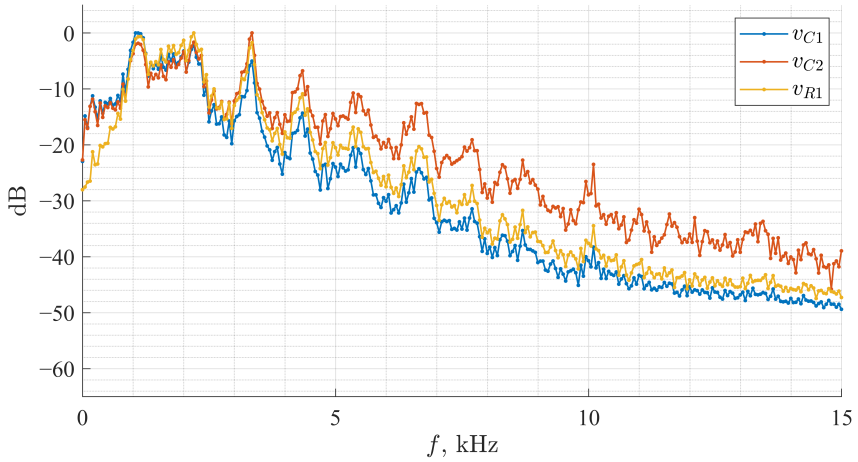


Fig. 1.24. PSD of $v_{C1}$, $v_{C2}$, and $v_{R1}$ for the Vilnius chaotic oscillator prototype at $f_0 = 1.6\,\text{kHz}$.

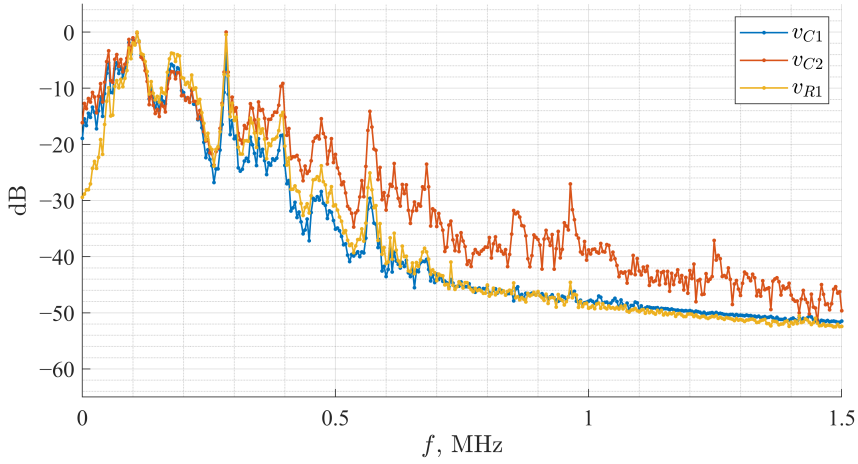


Fig. 1.25. PSD of $v_{C1}$, $v_{C2}$, and $v_{R1}$ for the Vilnius chaotic oscillator prototype at $f_0 = 160\,\text{kHz}$.

estimate the minimum bit length. Cross-correlation functions were calculated for all three signal pairs within a single oscillator, $v_{C1}$ and $v_{C2}$, $v_{C1}$ and $v_{R1}$, and $v_{C2}$ and $v_{R1}$. The results for two fundamental frequency configurations are shown in Figs. 1.26 and 1.27.

For both operating frequencies and all analyzed signal pairs, the cross-correlation functions exhibit a maximum at a lag close to zero, followed by a decrease in amplitude as the time shift increases. The rapid decay of the cross-correlation amplitude with increasing lag indicates that the signals lose correlation over time, which is consistent with aperiodic and chaotic signal behavior. Autocorrelation functions corresponding to the prototype measurements are provided in Appendix A.2 for

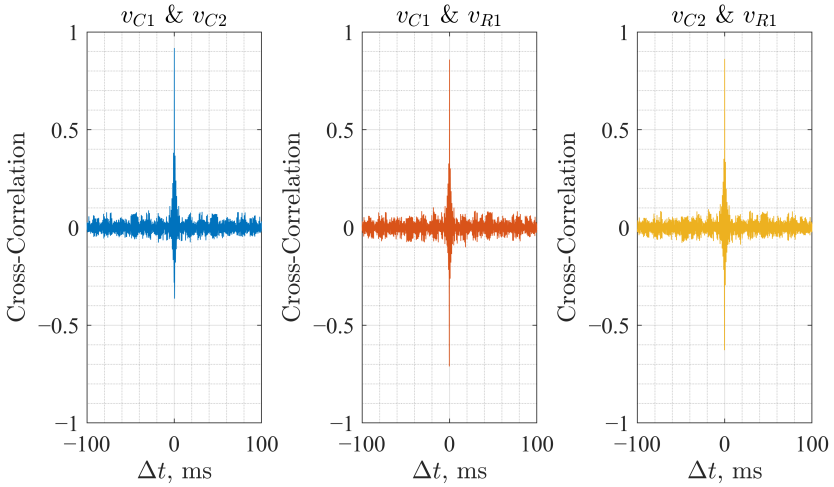


Fig. 1.26. Cross-correlation functions for $v_{C1}$ and $v_{C2}$, $v_{C1}$ and $v_{R1}$, and $v_{C2}$ and $v_{R1}$ in the Vilnius chaotic oscillator prototype at $f_0 = 1.6\,\text{kHz}$.

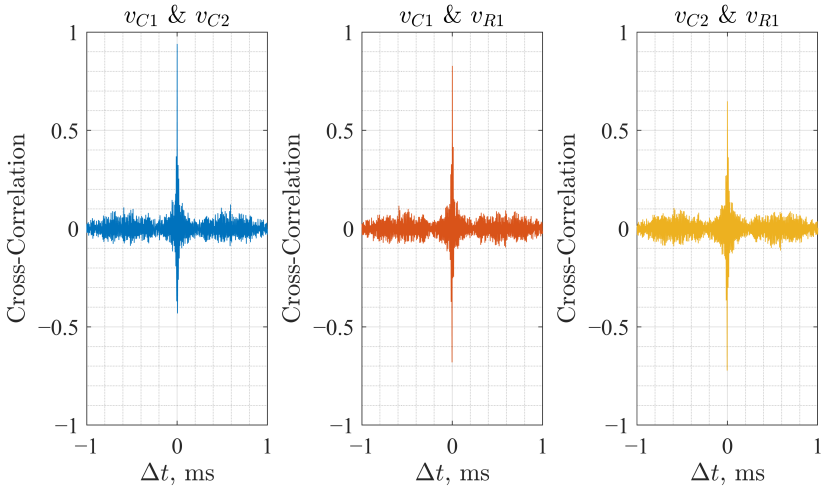


Fig. 1.27. Cross-correlation functions for $v_{C1}$ and $v_{C2}$, $v_{C1}$ and $v_{R1}$, and $v_{C2}$ and $v_{R1}$ in the Vilnius chaotic oscillator prototype at $f_0 = 160\,\text{kHz}$.

further confirmation of the aperiodic nature of the Vilnius chaotic oscillator signals.

Quantitative cross-correlation values are summarized in Table 1.4, including the correlation coefficient at zero lag $\beta(0)$, the lag corresponding to the maximum correlation value ($\text{Lag}_{\beta_{\max}}$), and the maximum correlation coefficient $\beta_{\max}$.

As shown in Table 1.4, the maximum cross-correlation values occur at nonzero time lags for all signal pairs and both operating frequencies. At $f_0 = 1.6\,\text{kHz}$, the lag corresponding to the maximum correlation ranges from $-30\,\mu\text{s}$ to $65\,\mu\text{s}$, while at $f_0 = 160\,\text{kHz}$ the corresponding lags lie between

Table 1.4.
Cross-correlation parameters for different signal pairs and fundamental frequencies in the Vilnius oscillator prototype

| Signal pair | $f_0 = 1.6\,\text{kHz}$ | | | $f_0 = 160\,\text{kHz}$ | | |
|---|---|---|---|---|---|---|
| | $\beta(0)$ | $\text{Lag}_{\beta_{\max}}$, µs | $\beta_{\max}$ | $\beta(0)$ | $\text{Lag}_{\beta_{\max}}$, µs | $\beta_{\max}$ |
| $v_{C1}$ & $v_{C2}$ | 0.58 | 65 | 0.92 | 0.71 | 0.77 | 0.94 |
| $v_{C1}$ & $v_{R1}$ | 0.69 | 50 | 0.86 | 0.64 | 0.66 | 0.83 |
| $v_{C2}$ & $v_{R1}$ | 0.77 | −30 | 0.86 | 0.61 | −0.30 | 0.65 |

−0.30 µs and 0.77 µs.

These nonzero lag values arise from time delays introduced by the reactive elements of the oscillator circuit. Capacitive and inductive components store and release energy at different times, causing voltages and currents measured at different circuit nodes to be time-shifted relative to one another. Consequently, the maximum of the cross-correlation function appears at a nonzero time lag corresponding to this delay.

To estimate the minimum symbol duration supported by the prototype implementation, the cross-correlation functions of the measured signals were analyzed to determine the time shift at which the correlation magnitude decreases from its principal peak and transitions into low-amplitude fluctuations. This characteristic delay defines the minimum symbol interval required to ensure sufficient decorrelation between adjacent symbol intervals. For $f_0 = 1.6\,\text{kHz}$, the obtained lag is approximately 1.89 ms, corresponding to an achievable data rate of 529.1 b/s. Increasing the fundamental frequency to 160 kHz reduces the duration of the high-correlation region to approximately 18.81 µs, enabling data rates up to 53.2 kb/s. These numerical results provide a quantitative basis for selecting bit duration and achievable data rate when using the Vilnius chaotic oscillator prototype in chaos-based communication systems.

## 1.3 Discussion and Comparative Analysis

The Colpitts chaotic oscillator demonstrated strong and reproducible chaotic dynamics in simulation and prototype experiments. Across the explored frequency range, Z1TEST values consistently exceeded 0.90, indicating stable chaotic dynamics. PSD analysis revealed that the bandwidth increased proportionally with the fundamental frequency, and cross-correlation results showed a short time shift for the correlation peak and aperiodicity—key characteristics for secure communications. The measured bit length and achievable data rate increased at higher frequencies. However, minor data rate decay was observed in hardware due to non-idealities.

The estimation of bit length in this thesis is based on the time lag obtained from cross-correlation functions. Specifically, the minimal bit duration is defined as the time interval over which the cross-correlation amplitude decays from its sharp peak at zero lag and settles to small fluctuations around zero. This settling interval indicates when the chaotic signals become effectively decorrelated, ensur-

ing that consecutive bits do not interfere. Such a method provides a physically meaningful criterion for determining bit duration in chaos-based communication systems.

A summary of the main results for the Colpitts oscillator, including the fundamental frequency, minimum bit length, and data rate for both simulation and prototype, is presented in Table 1.5.

Table 1.5.
Achievable data rates summary of the Colpitts chaotic oscillator

| $f_0$, kHz | Simulation | | Prototype | |
|---|---|---|---|---|
| | Bit length (μs) | Data rate (kb/s) | Bit length (μs) | Data rate (kb/s) |
| 96.86 | 60 | 16.7 | 78 | 12.82 |
| 968.59 | 6 | 166.7 | 7.5 | 133.3 |

These results show that increasing the fundamental frequency reduces the period of the high-correlation lag region, thereby shortening the required bit duration and enabling higher communication throughput. At the lower fundamental frequency of 96.86 kHz, the system supports a data rate of 16.7 kb/s, which is suitable for low-rate, power-efficient applications. In contrast, increasing the fundamental frequency to 968.59 kHz significantly reduces the characteristic lag extracted from the cross-correlation function, allowing data rates up to 166.7 kb/s and supporting more demanding communication scenarios. This demonstrates that the Colpitts oscillator provides a scalable mechanism for adapting chaos-based communication systems to diverse application requirements.

The Vilnius chaotic oscillator also exhibited stable chaotic operation over a wide frequency range in both simulations and hardware. Z1TEST values remained above 0.90, indicating a strong presence of chaos. The frequency-domain results revealed wide-band spectral characteristics, and cross-correlation analysis supported the existence of rapid decorrelation. As with the Colpitts oscillator, increasing the fundamental frequency caused substantial bit length reductions and corresponding data rate increases. Hardware measurements showed similar trends, albeit with minor decreases in data rate attributed to physical parasitics.

As with the Colpitts case, the bit length was estimated using the time lag derived from cross-correlation analysis, ensuring that consecutive bits were located outside the high-correlation region. Table 1.6 summarizes the achievable data rates for the Vilnius oscillator, listing simulation and prototype measurements results.

Table 1.6.
Achievable data rates summary of the Vilnius chaotic oscillator

| $f_0$ (kHz) | Simulation | | Prototype | |
|---|---|---|---|---|
| | Bit length | Data rate (kb/s) | Bit length | Data rate (kb/s) |
| 1.6 | 1.87 ms | 0.535 | 1.89 ms | 0.529 |
| 160 | 18.1 μs | 55.2 | 18.81 μs | 53.16 |

At the lower fundamental frequency of 1.6 kHz, the Vilnius oscillator enables transmission at

rates around 0.5 kb/s. Increasing the fundamental frequency to 160 kHz significantly reduces the period of the high-correlation lag region extracted from the cross-correlation function, increasing the maximum achievable data rate to more than 50 kb/s. As with the Colpitts oscillator, this scalability arises directly from the dependence of the bit length on the characteristic cross-correlation lag, demonstrating a tunable mechanism for adjusting data rate and system complexity.

A direct comparison between the two oscillators highlights both similarities and important distinctions. The Colpitts oscillator achieves shorter bit lengths and higher maximum data rates at comparable frequencies, which may be attributed to differences in circuit topology and inherent bandwidth. While achieving lower absolute data rates, the Vilnius oscillator confirms the same frequency-scaling trend across two orders of magnitude in its fundamental frequency. In both designs, the bit length derived from cross-correlation analysis scaled predictably with the fundamental frequency, validating the proposed method for defining symbol duration in chaos-based systems.

From a practical perspective, the achieved data rates align with the operational regimes of several established IoT communication standards. For example, LoRaWAN in the 868 MHz ISM band supports data rates from approximately 0.3 kb/s up to 50 kb/s under configurations defined by the LoRa Alliance [63], and the Zigbee built on the IEEE 802.15.4 standard [64] at 868 MHz and 915 MHz supports up to approximately 20 kb/s and 40 kb/s, respectively. Cellular narrowband Internet of Things (NB-IoT) uplink can deliver on the order of 20 kb/s in single-tone modes and up to approximately 250 kb/s in multi-tone configurations under 3GPP specifications [65], while Sigfox systems operate near 100 bit/s in the 868 MHz band under European Telecommunications Standards Institute (ETSI) EN 300 220-2 regulations [66]. These comparisons indicate that chaos-based communication systems can be configured to operate within data-rate regimes required by current IoT networks.

In conclusion, the results of this section confirm the thesis that adjusting the fundamental frequency of a chaotic oscillator provides a direct, quantitative means of controlling the achievable data rate in chaos shift keying communication systems. The analysis shows that variations in the oscillator fundamental frequency alter the characteristic time lag obtained from the cross-correlation function, thereby determining the minimum bit duration and limiting the transmission rate. For the investigated implementations, this mechanism enabled symbol rates up to approximately 55 kb/s for the Vilnius oscillator and up to approximately 166 kb/s for the Colpitts oscillator. These findings were experimentally validated using two structurally distinct chaotic oscillators in both circuit-level simulations and hardware prototypes. The results demonstrate that the oscillator fundamental frequency serves as a physically meaningful tuning parameter for symbol-rate scaling, allowing a single topology to operate across a broad range of transmission speeds. Overall, the section establishes an experimentally verified relationship between chaotic oscillator dynamics and achievable data rates, thereby supporting the proposed thesis and providing a foundation for subsequent investigations.

# 2 CHAOTIC SYNCHRONIZATION

Synchronization of chaotic oscillators is critical for the practical realization of secure chaos-based communication systems. By aligning the states of two or more chaotic systems, synchronization enables the reliable transmission and retrieval of information, even in the presence of channel noise and hardware imperfections. Among the various synchronization schemes, the Pecora-Carroll [67] method is notable for its conceptual simplicity and broad applicability to both analog and digital chaotic circuits [47], [68].

This section focuses on the synchronization of the Colpitts and Vilnius chaotic oscillators introduced in the first section. Specifically, the analysis is performed using the Colpitts oscillator with a fundamental frequency of 968.59 kHz and the Vilnius oscillator operating at 160 kHz. In the context of communication system design, the selection of the synchronization configuration and the resilience of synchronization to noise and circuit non-idealities directly impact the reliability of secure data transmission.

The following sections present the theoretical background and practical implementation of chaotic synchronization, followed by a detailed experimental analysis of noise immunity for both oscillators. Through systematic evaluation of various synchronization signals and configurations, the section provides key insights into optimal synchronization strategies for secure communication based on chaotic systems.

This section is organized as follows. Section 2.1 introduces the Pecora–Carroll (state-substitution) synchronization principle and its practical implementation. Section 2.2 then describes the noise-immunity study methodology, including the drive–response setup, the AWGN channel model, and the correlation metrics used for evaluation. The corresponding synchronization noise-immunity results are reported in Section 2.3. Finally, Section 2.4 formulates a synchronization-signal selection methodology and summarizes the key guidelines used in the subsequent communication-system analysis.

## 2.1 Pecora–Carroll Synchronization

Chaotic synchronization is fundamental for utilizing chaotic oscillators in secure communication systems [69]. It enables secure transmission of information by ensuring that only synchronized systems can accurately extract data from received signals. Among the various synchronization methods, the substitution method, also known as Pecora-Carroll synchronization [70], is particularly noteworthy for its simplicity and effectiveness in both analog and discrete chaotic systems.

The substitution method replaces one of the state variables in the response chaotic oscillator with its corresponding variable from the drive oscillator. In this approach, the response oscillator is driven by a signal from the drive circuit to align their chaotic trajectories. Pearson's correlation coefficient is often employed to evaluate the quality of synchronization. This metric quantifies the

similarity between the signals from the drive and response oscillators. The coefficient, denoted as $\beta$, is calculated using the equation:

$$\beta = \frac{\sum_{i=1}^{n}(x_i - \bar{x})(y_i - \bar{y})}{\sqrt{\sum_{i=1}^{n}(x_i - \bar{x})^2 \sum_{i=1}^{n}(y_i - \bar{y})^2}}, \tag{2.1}$$

where $x$ represents the signal from the drive oscillator and $y$ denotes the signal from the response oscillator. The coefficient $\beta$ takes values in the interval $[-1, 1]$ and quantifies the linear similarity between the two signals. A value of $\beta = 1$ indicates perfect in-phase synchronization, whereas $\beta = -1$ corresponds to complete anti-phase synchronization. Values of $\beta$ close to zero indicate the absence of linear correlation and therefore the lack of synchronization. In practical synchronization analysis, values of $\beta$ in the range of approximately 0.8 to 1 are typically considered indicative of established synchronization, with values closer to unity corresponding to stronger trajectory alignment between the drive and response systems. Conversely, values below approximately 0.5 suggest that synchronization is not achieved, as the statistical similarity between the signals becomes weak.

The same circuit's node is selected for synchronization in both the drive and response chaos oscillators to implement the state-substitution (Pecora-Carroll) method, which is presented in Fig. 2.1. A unity-gain operational amplifier buffer (voltage follower) is commonly used to isolate the drive oscillator from the response oscillator and to deliver the synchronization signal without loading the drive circuit [71]–[73]. This configuration determines the direction of synchronization and allows the signal in the response circuit to be substituted with the corresponding signal from the drive oscillator. Since chaotic oscillators typically have multiple nodes, synchronization can be achieved in various configurations by selecting different nodes for substitution.

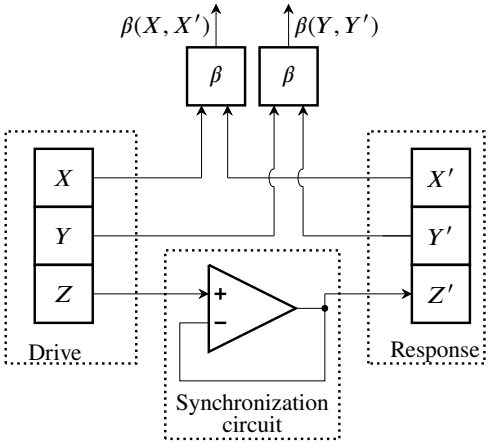


Fig. 2.1. Chaos oscillator synchronization block-scheme.

An example illustration of synchronized and unsynchronized behavior of chaotic oscillators is presented in Fig. 2.2. The plots were obtained by simulating the drive–response configuration of

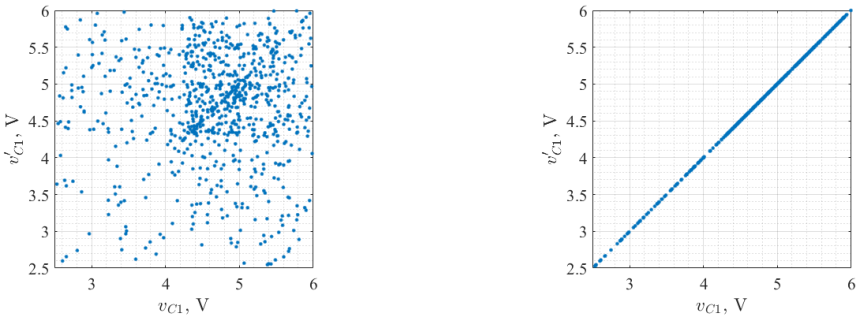


Fig. 2.2. XY plot of drive-response system signals (a) without synchronization and (b) with chaotic synchronization applied.

identical chaotic oscillators with and without synchronization. The voltages from the same circuit node in the drive and response oscillators were sampled at identical time steps, and the resulting values were plotted in an XY format, where the x-axis represents the drive oscillator voltage, and the y-axis the corresponding response oscillator voltage. The voltages are displayed as discrete points to emphasize their instantaneous correspondence at each sampled moment.

Fig. 2.2 (a) shows the unsynchronized case, where the data points are randomly scattered, indicating a lack of correlation between the oscillators. In contrast, Fig. 2.2 (b) illustrates the synchronized state. Here, the data points align closely along a diagonal line, demonstrating that the voltages in the response oscillator accurately follow those of the drive oscillator. This relationship confirms the successful synchronization between the chaotic systems.

In the Colpitts chaos oscillator (Fig. 1.1), synchronization can be established using configurations: $v_{C1}$, $v_{C2}$ or $v_{RL}$ as synchronization signals [50]. For instance, if $v_{C1}$ is chosen for synchronization, the drive oscillator generates all three state variables ($v_{C1}$, $v_{C2}$, and $i_{L1}$), while the response oscillator generates $v_{C2}$ and $i_{L1}$, with $v_{C1}$ being substituted by the corresponding signal from the drive oscillator. In the Vilnius chaos oscillator (Fig. 1.15), synchronization can be achieved using $v_{C1}$, $v_{C2}$, or $v_{R1}$ (representing the current $i_L$) as a synchronization signal. These multiple synchronization points offer flexibility for future applications.

As synchronization in chaotic oscillators forms the basis for their integration into communication systems, it is essential to assess the noise resilience of synchronization across various configurations. Understanding how synchronization performance varies in noisy environments is critical to ensuring reliable communication. These experiments and their results will be discussed in the following section.

## 2.2 Chaos Oscillator Synchronization Noise Immunity Study Methodology

The study methodology follows the block diagram presented in Fig. 2.3. In this figure, $X$, $Y$, and $Z$ represent the state variables in the drive chaos oscillator, while $X'$, $Y'$, and $Z'$ denote the corresponding state variables in the response chaos oscillator.

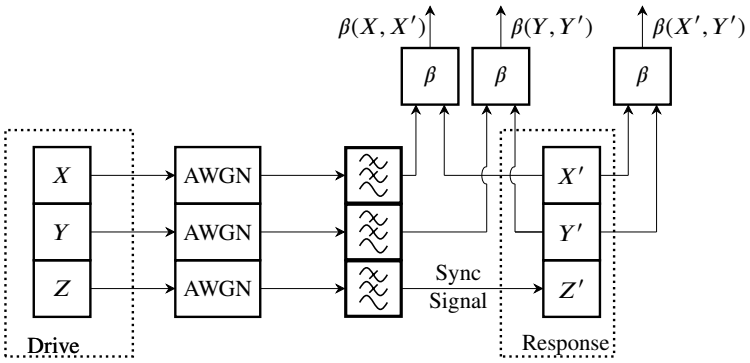


Fig. 2.3. Chaos oscillator synchronization noise immunity study block-scheme.

In this setup, $Z$ is selected as the synchronization signal, replacing $Z'$ in the response oscillator. The $X$ and $Y$ signals generated by the drive oscillator will be used in the final data transmission system for CSK. Once the drive oscillator generates the signals, they are transmitted through an AWGN channel, where the noise level is controlled between $-20$ dB and 30 dB in terms of the signal-to-noise ratio (SNR).

On the receiver side, the signals pass through a low-pass filter (LPF), which is specifically tuned to preserve the main spectral components of the chaotic signal. The LPF bandwidth is determined by comparing the original chaotic signal (before noise addition and filtering) with the filtered version (without noise). The bandwidth is selected when mean square error (MSE) reaches $-25$ dB, ensuring that the signal maintains its chaotic properties. After filtering, the synchronization signal substitutes the variable in the drive-response chaotic system to ensure the oscillators are in the same state. Once synchronization is achieved, the Pearson correlation coefficient is calculated for the corresponding state variables: $X$ and $X'$, $Y$ and $Y'$, and $X'$ and $Y'$. This analysis provides insights into the effect of noise on chaotic synchronization in the transmission channel.

The study is conducted for both the Colpitts and Vilnius chaos oscillators. Since each chaotic oscillator has three state variable signals, all of them are tested for synchronization capability. Table 2.1 summarizes the different configurations tested. For the Colpitts chaos oscillator (Fig. 1.1), synchronization is tested using $v_{C1}$, $v_{C2}$, and $v_{RL}$, while for the Vilnius chaos oscillator (Fig. 1.15), synchronization is evaluated using $v_{C1}$, $v_{C2}$, and $v_{R1}$. The remaining signals are analyzed to assess synchronization quality across different configurations.

Table 2.1.

Colpitts and Vilnius chaos oscillators configurations

| **Colpitts chaos oscillator** | | | **Vilnius chaos oscillator** | | |
|---|---|---|---|---|---|
| ***X*** | ***Y*** | ***Z*** | ***X*** | ***Y*** | ***Z*** |
| $v_{C1}$ | $v_{C2}$ | $v_{RL}$ | $v_{C1}$ | $v_{C2}$ | $v_{R1}$ |
| $v_{RL}$ | $v_{C1}$ | $v_{C2}$ | $v_{R1}$ | $v_{C1}$ | $v_{C2}$ |
| $v_{C2}$ | $v_{RL}$ | $v_{C1}$ | $v_{C2}$ | $v_{R1}$ | $v_{C1}$ |

## 2.3 Chaos Oscillator Synchronization Noise Immunity Study Results

This study analyzes the performance of Colpitts and Vilnius chaos oscillators in different drive-response system configurations within a noisy channel. The goal is to evaluate synchronization performance across configurations and identify the configuration exhibiting the highest noise immunity.

Fig. 2.4 presents the study results for the Colpitts chaos oscillator. The $x$-axis represents the SNR levels but is flipped to encourage a more convenient interpretation. The $y$-axis represents the correlation coefficient, which quantifies the synchronization quality. The figure contains six curves, each pair corresponding to a specific configuration, as summarized in Table 2.1. Each pair represents the correlation between $X$ and $X'$ and $Y$ and $Y'$, illustrating how synchronization is maintained under different noise conditions.

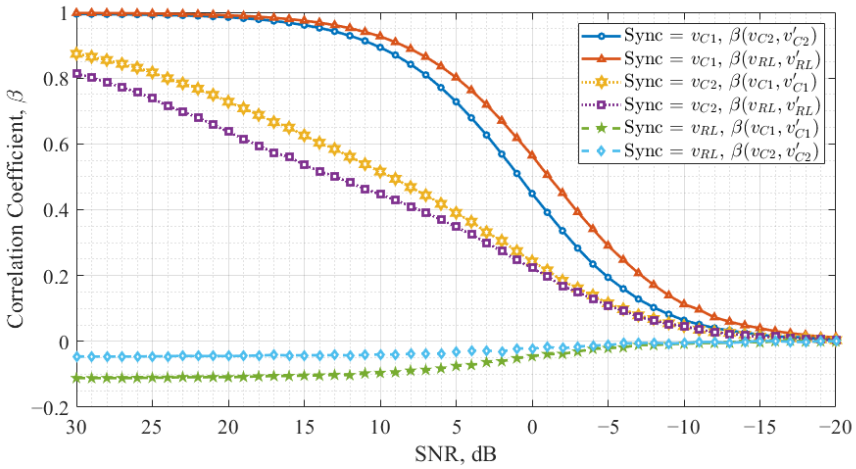


Fig. 2.4. Colpitts chaos oscillator synchronization noise immunity.

Examining Fig. 2.4, it can be observed that $X'$ and $Y'$ signals synchronize differently for each SNR level. When $v_{RL}$ is used as the synchronization signal, the system fails to achieve synchronization in the drive-response configuration. When $v_{C1}$ is used, $X'$ and $Y'$ (corresponding to $v_{C2}$

and $v_{RL}$) synchronize at different levels for the same SNR values. A similar trend is observed when $v_{C2}$ is used as the synchronization signal; however, $X'$ and $Y'$ synchronize at different levels and show smaller correlation coefficients in this configuration.

Fig. 2.5 illustrates the synchronization noise immunity across all three configurations for the Vilnius chaos oscillator. Like Fig. 2.4, it consists of six curves, where each pair represents the correlation between $X$ and $X'$ and $Y$ and $Y'$, corresponding to a specific configuration described in Table 2.1.

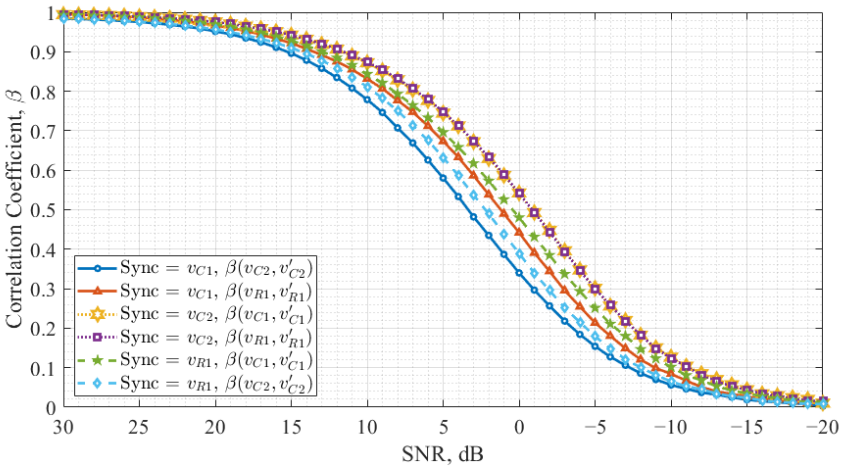


Fig. 2.5. Vilnius chaos oscillator synchronization noise immunity.

When $v_{C1}$ is used for synchronization, the response oscillator signals $v_{C2}$ and $v_{R1}$ do not synchronize at the same level for a given SNR value. In contrast, when $v_{C2}$ is the synchronization signal, $v_{C1}$ and $v_{R1}$ synchronize at the same level, as the two curves overlap entirely. Additionally, this configuration achieves synchronization at lower SNR values than others. When $v_{R1}$ is selected as the synchronization signal, an imbalance in synchronization levels is observed, similar to the case of $v_{C1}$.

Comparing the results for Colpitts and Vilnius oscillators, it is evident that for the Vilnius chaos oscillator, all three configurations achieve synchronization once the noise level is sufficiently low. In contrast, the Colpitts oscillator demonstrates reliable synchronization only in one configuration when $v_{C1}$ is used as the synchronization signal. The synchronization with the considerably lower correlation level occurs in the $v_{C2}$ configuration. Additionally, one configuration exists for the Colpitts oscillator in which synchronization is never achieved.

The results suggest that the Colpitts oscillator exhibits a more restrictive synchronization behavior due to its circuit topology, nonlinear characteristics, and strong variable coupling, which limit the effectiveness of synchronization in some configurations. In contrast, the Vilnius chaos oscillator

provides more flexible synchronization possibilities, allowing multiple high-correlation configurations.

Another important observation is the presence of synchronization imbalances across different configurations for oscillators at the same SNR level. This imbalance can negatively impact data transmission, as one signal may be more likely to be detected correctly, leading to an increased error rate for specific bits. For example, an imbalance in synchronization levels may result in a scenario where more '0' s are incorrectly detected compared to '1' s. It is a point to improve the chaos-based communication system so that each bit is detected with equal probability, ensuring a balanced transmission process.

The next part of this study examines the cross-correlation of response chaos oscillator signals as a function of the synchronization channel SNR. This analysis extends the findings from the previous part by evaluating how the relationship between $X'$ and $Y'$ signals evolves across different configurations. The cross-correlation value between these signals is crucial for maintaining balance in a data transmission system, as imbalances can lead to an increased number of errors.

Fig. 2.6 presents the study results for the Colpitts chaos oscillator, illustrating the cross-correlation coefficients under different synchronization configurations.

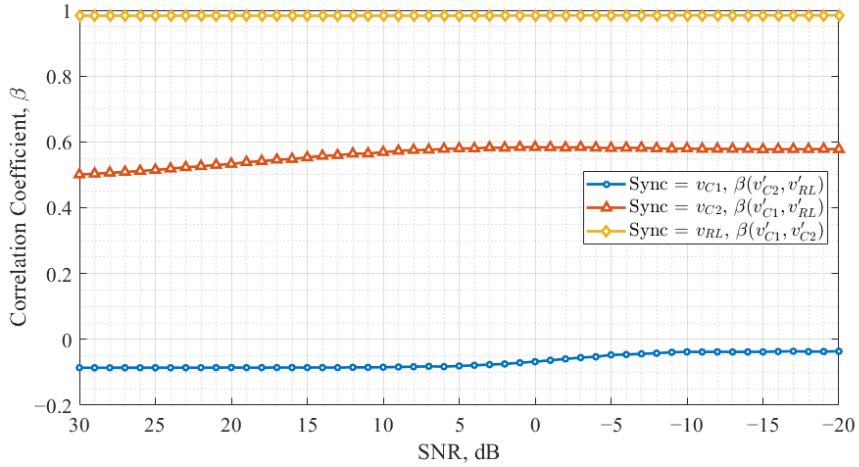


Fig. 2.6. Results of the Colpitts chaos oscillator, showing the signal cross-correlation coefficients under different synchronization configurations.

The results indicate that when $v_{RL}$ is used as the synchronization signal, the cross-correlation coefficient remains close to one, meaning the response chaos oscillator signals exhibit similar dynamics. However, in this configuration, the Colpitts chaos oscillator correlation coefficient of data-carrying signals was nearly zero in the drive-response system, leading the response oscillator to enter a periodic mode instead of remaining chaotic. For the other two synchronization signals, $v_{C1}$ and $v_{C2}$, the cross-correlation between response oscillator signals decreases as the noise level decreases.

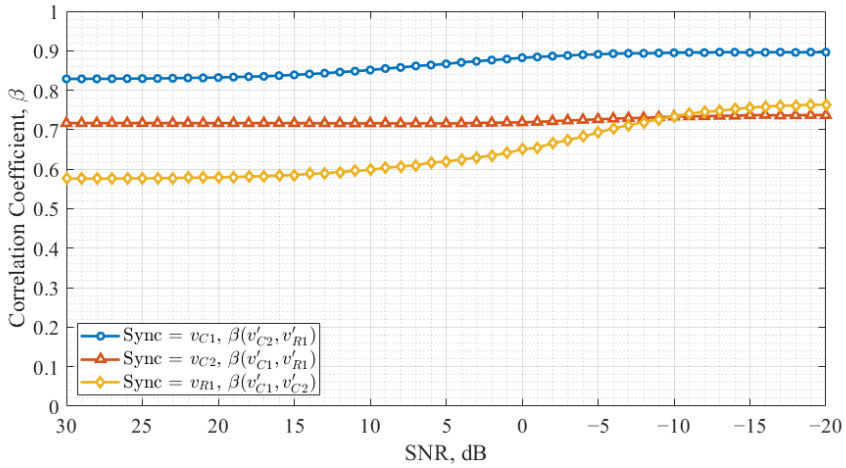


Fig. 2.7. Results of the Vilnius chaos oscillator, showing the signal cross-correlation coefficients for different synchronization signals.

Additionally, it can be observed that when $v_{C1}$ is used as the synchronization signal, the absolute value of the cross-correlation coefficient is lower compared to the $v_{C2}$ configuration.

Fig. 2.7 illustrates the cross-correlation coefficients as a function of the SNR in the Vilnius chaos oscillator for different synchronization signals.

In Fig. 2.7, the cross-correlation coefficient between $X'$ and $Y'$ decreases as the noise level decreases in configurations where $v_{C1}$ and $v_{R1}$ are used as synchronization signals. A more significant variation in the cross-correlation coefficient is observed when $v_{R1}$ is used, suggesting that synchronization in this configuration is more affected by noise. Conversely, when $v_{C2}$ is used as the synchronization signal, the cross-correlation coefficient remains nearly constant, indicating a strong and noise-resistant synchronization.

Comparing Fig. 2.6 and 2.7 with previous results (Fig. 2.4 and 2.5), it is evident that the Vilnius chaos oscillator demonstrates the most stable synchronization when $v_{C2}$ is employed as the synchronization signal. In this case, the correlation between $X$ and $X'$ and between $Y$ and $Y'$ is balanced, while the cross-correlation between $X'$ and $Y'$ remains stable, regardless of the noise level. However, a high cross-correlation level between data-carrying signals complicates signal discrimination in the receiver in this configuration.

On the other hand, in the Colpitts chaos oscillator, $v_{C1}$ appears to be the most suitable synchronization signal for communication system applications. In this configuration, the absolute value of the cross-correlation coefficient is the lowest among the observed values, and its dependence on the noise level is minimal. Additionally, the correlation curves between $X$ and $X'$ and between $Y$ and $Y'$ achieve synchronization as rapidly as in the Vilnius chaos oscillator when $v_{C2}$ is used as the synchronization signal.

## 2.4 Synchronization Signal Selection Methodology

The results of the noise immunity study highlight that the choice of synchronization signal is crucial for achieving reliable synchronization in chaos-based communication systems. Given the differences observed between the Colpitts and Vilnius oscillators, a systematic approach is necessary for selecting the optimal synchronization signal for a given application.

For each oscillator, the preferred synchronization signal should be determined by evaluating several key criteria:

- The correlation coefficient between corresponding drive and response signals should remain high across a wide range of noise conditions. Signals that consistently achieve strong synchronization—demonstrated by high Pearson correlation coefficients even at low SNR—are generally the most suitable.
- All data-carrying signals in the response oscillator should exhibit comparable synchronization quality to ensure balanced behavior across signal channels. Significant differences in correlation coefficients lead to suboptimal synchronization performance, thereby affecting symbol-detection reliability, as discussed in Section 3.
- The optimal synchronization signal should demonstrate minimal degradation in synchronization performance as the noise level increases. Signals that are highly sensitive to noise, showing rapid drops in correlation, are less suitable for practical systems.
- Low cross-correlation between data-carrying signals in the response oscillator facilitates better discrimination at the receiver, supporting more accurate and balanced detection.
- Practical considerations, such as circuit node accessibility, signal amplitude, and sensitivity to external disturbances, may also influence the selection of the synchronization signal.

Applying these criteria to the results obtained for the Colpitts and Vilnius oscillators, the following guidelines can be established:

- For the Colpitts chaotic oscillator, the $v_{C1}$ node emerges as the most favorable synchronization signal, providing high synchronization quality, relatively low sensitivity to noise, and minimal cross-correlation between data-carrying signals. This configuration supports both stable synchronization and balanced communication.
- For the Vilnius chaotic oscillator, the $v_{C2}$ node is the optimal choice, as it achieves strong synchronization with the lowest sensitivity to noise and maintains stable, balanced performance across varying channel conditions.

In practice, the synchronization signal should be selected based on a comprehensive evaluation of these criteria, as the optimal choice may vary with oscillator topology, channel conditions, and specific application requirements. To translate this methodology into a practical procedure suitable for system implementation, the following structured approach can be applied when developing chaos-based communication systems:

1. Identify several potential circuit nodes that can serve as synchronization points. These nodes

should correspond to distinct state variables of the chaotic oscillator and be accessible for coupling or measurement.

2. Configure the oscillator pair in a drive-response setup and evaluate synchronization for each candidate signal under noise-free conditions. The quality of synchronization can be quantified by calculating the correlation coefficient between the corresponding drive and response signals.
3. Introduce AWGN into the communication channel to test noise-immunity. Recalculate the correlation coefficient for each candidate signal across a range of SNRs to determine which maintains the most stable synchronization under noisy conditions.
4. Verify that all response oscillator state variables used for data detection achieve similar synchronization levels. Significant discrepancies between correlation coefficients indicate detection imbalance and can result in increased bit error rates. In such cases, compensation during the detection process is required to restore balance and ensure reliable system operation.
5. Evaluate the cross-correlation between the response oscillator's data-carrying signals. A low cross-correlation value improves symbol discrimination and enhances detection reliability.
6. When multiple synchronization nodes exhibit similar performance, select the one offering the best practical characteristics, such as higher signal amplitude, easier circuit access, and lower susceptibility to parasitic effects or external interference.

The synchronization signal selection methodology established in this section forms the basis for the subsequent stages of the study. In the following section, the observed differences in correlation levels across oscillator signals are used to motivate and develop a detection threshold that compensates for imbalances in correlation-based decision-making. Building on this formulation, the impact of synchronization signal selection on the overall performance of chaos-based communication systems is then examined in 3rd and 4th Sections.

# 3 DESIGN AND SIGNAL PROCESSING IN CHAOS-BASED COMMUNICATION

The development of chaos-based communication systems has attracted significant attention due to the unique properties of chaotic signals, including broad spectral content, inherent unpredictability, and potential for enhanced security [13]–[15], [22], [23]. This section outlines the foundational aspects of designing such systems, focusing on the architectural choices, key signal processing steps, and the implementation of CSK as the primary modulation scheme. Both simulation and hardware considerations are discussed to highlight the practical challenges and solutions encountered during system development. Particular emphasis is placed on synchronization, signal processing, and threshold-based detection, which are essential for achieving reliable data transmission in chaos-based architectures.

Specifically, the following subsections detail the general system architecture, describe the practical realization of CSK modulation in both simulation and prototype environments, and address the importance of adaptive threshold determination for accurate bit detection under imperfect synchronization conditions. The section concludes with a discussion of the performance benefits achieved through these signal processing strategies.

This section is organized as follows. Section 3.1 introduces the overall architecture of the chaos-based communication system and outlines the signal flow between the transmitter and receiver. Section 3.2 describes the practical realization of chaos shift keying, including both simulation-based and hardware prototype implementations. Section 3.3 addresses correlation-based detection under imperfect synchronization and derives an adaptive decision threshold to compensate for synchronization imbalances. The impact of threshold selection on system performance is then analyzed in Section 3.4. Finally, Section 3.5 summarizes the key findings and discusses their implications for chaos-based communication design.

## 3.1 System Architecture

This subsection introduces the fundamental concept of a chaos-based communication system, where chaotic signals are employed for information encoding and synchronization. Fig. 3.1 presents the general block diagram of such a system, illustrating the main components and signal flow.

At the core of the transmitter is an analog chaos oscillator operating in a drive-response configuration, enabling the implementation of coherent chaos-based communication. The drive oscillator generates three state variables—denoted as $X$, $Y$, and $Z$—which correspond to voltages across capacitors and currents through inductors in the oscillator circuit. These state variables possess chaotic dynamics, resulting in broadband, noise-like signals that are well-suited for secure communication.

One of the drive oscillator's state variables (e.g., $Z$) is typically selected as the synchroniza-

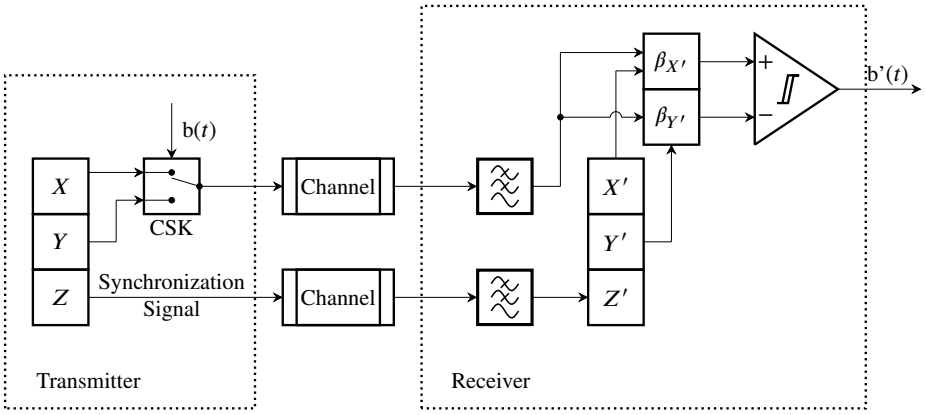


Fig. 3.1. Chaos-based communication system block scheme.

tion signal. The remaining state variables ($X$ and $Y$) are utilized for information transmission. The information-carrying signal is formed by a binary information-signal-controlled switch that alternates between the $X$ and $Y$ signals, mapping bit '1' to $X$ and bit '0' to $Y$. This binary selection process is known as CSK, where the binary data stream modulates which chaotic signal is transmitted. To ensure matched amplitudes and to remove baseline offsets, the direct current (DC) components of all signals are eliminated before further processing.

Depending on the requirements of the application or the nature of the communication channel, the information-carrying and synchronization signals can be transmitted directly or further processed using an additional modulation scheme, such as FM or QAM. This modular architecture provides flexibility, allowing the chaos-based communication system to adapt to various scenarios and channel conditions.

The signals propagate through a communication channel between the transmitter and receiver, which may introduce various distortions and impairments. In the most basic case, this channel can be modeled as an AWGN channel; however, more complex channel models can also be considered, including those with phase noise, multipath propagation, or other real-world impairments. The analysis and design of the system can be adapted according to the specific channel conditions of the intended application.

At the receiver, the response chaos oscillator synchronizes with the drive oscillator, generating its own state variables $X'$ and $Y'$. The synchronization signal $Z$ received from the transmitter is directly injected into the response oscillator, replacing its corresponding state variable $Z'$. This substitution forces the response oscillator to align its dynamics with those of the transmitter, achieving synchronization between the two chaotic systems. Accurate synchronization is crucial; only when the response oscillator's chaotic waveforms are matched with the transmitter's can reliable data de-

tection be achieved.

The transmitted information bits are detected by calculating the Pearson correlation coefficient $\beta$ between the received information-carrying signal and the reconstructed $X'$ and $Y'$ signals from the response oscillator. The bit decision rule is as follows: a bit '1' is detected if $\beta_{X'} > \beta_{Y'}$, and bit '0' otherwise. This detection process relies on the similarity between the received and the response oscillator chaotic signals, emphasizing the importance of high-quality synchronization.

It is essential to note that the effectiveness of information detection in chaos-based communication systems is fundamentally linked to the quality of chaotic synchronization. As demonstrated in the previous section, different synchronization configurations can exhibit varying degrees of noise immunity, resulting in an imbalance where one state variable achieves stronger synchronization under noisy channel conditions than the other. Since the detection procedure is based on comparing correlation coefficients, such synchronization imbalances can introduce bias into the detection process, leading to increased bit errors for one symbol over the other. In these cases, precise threshold calculation and possible compensation techniques become necessary to ensure balanced and reliable data detection.

## 3.2 Chaos Shift Keying Implementation

CSK is the modulation scheme employed in the proposed communication system, enabling digital information transmission by selecting between two chaotic signals according to the instantaneous state of the binary data stream. As illustrated in Fig. 3.1, the CSK block receives three inputs—the digital data stream and two distinct chaotic signals, denoted as $X$ and $Y$—and produces an information-carrying signal as output. The CSK block operates as a digitally controlled switch or multiplexer, outputting either $X$ or $Y$ depending on the current value of the input data bit.

*Simulation Implementation*

In simulation, the implementation of CSK is straightforward due to the flexibility of numerical signal processing. The chaotic signals $X$ and $Y$ have subtracted their mean values to remove any DC offset. Subsequently, the amplitude of the $Y$ signal is adjusted to match that of $X$, ensuring uniform signal levels for both bit conditions. Once pre-processed, the CSK operation is realized through a logical switching function, in which the output follows either $X$ or $Y$ based on the state of the binary information signal. This approach simplifies processing signals and allows for quick performance evaluation in various operating conditions.

*Prototype Implementation*

In the hardware prototype, the CSK implementation requires analog circuitry for signal processing and switching. The removal of the DC offset is accomplished by passing the $X$ and $Y$ signals

through high-pass filter (HPF) with low cutoff frequencies, typically realized as simple RC filters. Each signal is then fed into a non-inverting amplifier with adjustable gain to equalize their amplitudes. The switching operation is performed using an analog electronic switch (ADG419), which is controlled by the digital data stream. The data stream itself is generated by an ADP3450 module, with control provided via Python code, enabling flexible and precise modulation of the transmitted information.

## 3.3 Detection and Threshold Determination under Imperfect Synchronization

At the detector input, the received information-carrying signal is evaluated together with the two reference signals generated by the synchronized response chaotic oscillator. These reference signals correspond to the oscillator's state variables and are the basis for correlation-based detection. Within each bit interval, the received signal is correlated with both reference signals using a sliding-window approach, yielding two correlation coefficients. A digital comparator then evaluates these coefficients to determine the transmitted bit value, and the resulting sequence is compared with the original bitstream to estimate the BER.

Accurate bit detection in chaos-based communication systems relies on comparing the similarity between the received information-carrying signal and the reconstructed chaotic signals from the response oscillator. Ideally, when both state variables achieve perfect and balanced synchronization, the correlation coefficients between the received signal and each candidate chaotic signal can be directly compared using a simple maximum correlation. However, as demonstrated in Section 2, under noisy conditions, the different state variables of the response oscillator may synchronize at different levels. This imbalance in synchronization leads to unequal correlation coefficients, even for equally likely transmitted symbols, and introduces bias into the detection process. Furthermore, nonzero cross-correlation between the chaotic signals and additional noise can further reduce the reliability of straightforward decision rules. Therefore, a nonzero and adaptively calculated threshold must be introduced into the bit decision process to compensate for these effects, ensuring reliable and balanced data recovery across varying channel conditions.

The threshold for bit detection can be derived using the likelihood ratio approach. Given that AWGN is added to the signal, the likelihood that the received information-carrying signal $s(t)$ was induced by the signal $X$ can be expressed in the form:

$$\Lambda[X|s(t)] = \frac{1}{(\sigma\sqrt{2\pi})^K} \exp\left(-\frac{1}{2}\sum_{k=1}^{K}\frac{(s_k - x_k)^2}{\sigma^2}\right), \tag{3.1}$$

where $\sigma$ denotes the AWGN standard deviation and $s_k$ and $x_k$ denote $k$th sample of CSK signal $s(t)$

and chaotic signal $X$, respectively. Then, the logarithm of the likelihood ratio can be expressed as:

$$\ln \Lambda[s(t)] = \frac{\Lambda[X|s(t)]}{\Lambda[Y|s(t)]} = \sum_{k=1}^{K} \frac{s_k}{\sigma^2}(x_k - y_k) - \frac{1}{2}\sum_{k=1}^{K} \frac{(x_k^2 - y_k^2)}{\sigma^2}. \tag{3.2}$$

In this case, the decision-making regions are split by the point where the likelihood ratio changes sign, which is given by:

$$\sum_{k=1}^{K} s_k(x_k - y_k) - \frac{1}{2}\sum_{k=1}^{K}(x_k^2 - y_k^2) \geqslant 0. \tag{3.3}$$

Assuming that the information-carrying signal $s(t)$ is a sum of $X$ state variable and noise signal $n(t)$, one can express the mathematical expectation $E[]$ of the first sum as:

$$E\left[(x_k + n_k)(x_k - y_k)\right] = \sum_{k=1}^{K} x_k^2 - \sum_{k=1}^{K} x_k y_k, \tag{3.4}$$

where $n_k$ is the $k$th sample of the noise signal. By substituting the calculated mathematical expectation in Equation (3.3), one can conclude that a high cross-correlation between the response oscillator's state variables $X'$ and $Y'$ decreases correct detection probability.

Rewriting Equation (3.3) gives the following criterion for decision making:

$$\sum_{k=1}^{K} s_k x_k \geqslant \sum_{k=1}^{K} s_k y_k + \frac{1}{2}\left[\sum_{k=1}^{K} x_k^2 - \sum_{k=1}^{K} y_k^2\right]. \tag{3.5}$$

Alternatively, the sums can be replaced by a priori ($\beta_X$ and $\beta_Y$) and a posteriori ($\beta_{X'}$ and $\beta_{Y'}$) correlation coefficients, resulting in the criterion in the form $\beta_{X'} \geqslant \beta_{Y'} + \frac{1}{2}(\beta_X - \beta_Y)$. If inequality is valid, the system detects a '1' bit; otherwise, a '0' bit is received.

This approach allows for the calculation of an adaptive threshold that accounts for synchronization imbalances, nonzero cross-correlation, and practical noise conditions, thereby improving the reliability and balance of bit detection in chaos-based communication systems.

## 3.4 Impact of Threshold Selection on BER

The previous discussion established that under AWGN channel conditions, imperfect synchronization between the drive and response chaotic oscillators leads to an imbalance in the correlation coefficients associated with each state variable. This imbalance can introduce bias into the bit detection process, causing one symbol ('1' or '0') to be favored over the other and increasing detection errors. To mitigate this effect and improve the reliability of the system, the use of a nonzero detection threshold in the correlation-based decision algorithm was proposed.

To demonstrate the practical benefits of this approach, the performance of the baseband chaos-based communication system was evaluated under various SNR conditions. Table 3.1 summarizes the BER and the number of misdetected '0' and '1' bits obtained both without and with the application of the detection threshold. The results are shown for a representative synchronization configuration using a specific state variable as the synchronization signal, tested in an AWGN channel.

Table 3.1.
Error count without and with the detection threshold in a system based on the Vilnius chaos oscillator using $v_{R1}$ as the synchronization signal

| SNR, dB | Without threshold | | | With threshold | | |
|---|---|---|---|---|---|---|
| | BER | False '0' count | False '1' count | BER | False '0' count | False '1' count |
| −20 | 0.4835 | 2414 | 2421 | 0.4810 | 2416 | 2394 |
| −15 | 0.4407 | 2287 | 2120 | 0.4370 | 2168 | 2202 |
| −10 | 0.3249 | 1761 | 1488 | 0.3195 | 1598 | 1597 |
| −5 | 0.1134 | 702 | 432 | 0.1053 | 519 | 534 |
| 0 | 0.0121 | 79 | 42 | 0.0107 | 57 | 50 |
| 2 | 0.0048 | 34 | 14 | 0.0043 | 21 | 22 |
| 4 | 0.0019 | 12 | 7 | 0.0014 | 7 | 7 |

As seen in Table 3.1, the application of a nonzero detection threshold significantly improves system performance across all SNR levels. Without the threshold, an imbalance in the number of false detections is observed, particularly at higher SNR, where the correlation levels become more separated due to imperfect synchronization. This results in an increased bit error rate and uneven distribution of detection errors between '0' and '1' bits. When the threshold is applied, the detection process is balanced, the number of errors for each symbol becomes more uniform, and the overall BER is reduced. These findings confirm the effectiveness of threshold compensation for mitigating the impact of synchronization imbalance in chaos-based communication systems.

## 3.5 Discussion

This section provided a structured overview of the development and signal processing strategies for chaos-based communication systems. Beginning with the conceptual design, the principal system components—including the drive and response chaos oscillators, the CSK modulation block, the communication channel, and the detection process—were outlined to establish a clear understanding of the signal flow and functional roles within the architecture. The practical realization of the CSK block was then addressed, with a comparative perspective on implementation in both simulation and hardware prototype environments. This highlights the flexibility of numerical signal processing and the additional considerations required for analog circuit design.

A detailed examination of synchronization imbalances revealed that direct correlation-based de-

tection can introduce systematic bias and increased error probability due to non-equal correlation levels among different chaotic state variables. To address this effect, an adaptive detection threshold was introduced and its analytical justification provided. The proposed threshold explicitly accounts for unequal correlation levels in the synchronized chaotic signals and defines the condition for minimizing the error probability in symbol detection. The results demonstrate that applying this threshold during the bit detection process significantly reduces the bit error rate and yields a more balanced distribution of symbol errors. These findings directly validate the central thesis of this section, confirming that optimal detection in chaos shift keying systems with non-equal correlation levels is achieved by appropriately compensating for synchronization asymmetry through the derived threshold condition. Collectively, the results highlight the need for adaptive detection strategies to ensure reliable data transmission in practical chaos-based communication systems.

# 4 ADVANCED MODULATION TECHNIQUES FOR CHAOS-BASED COMMUNICATION

Chaos-based communication systems inherently generate wideband baseband signals as a result of the underlying chaotic dynamics and chaos shift keying. While these baseband chaotic waveforms contain the information and synchronization components required for secure transmission, they cannot be propagated efficiently in practical wireless environments without further processing. WSN and IoT systems typically operate within regulated RF bands, where spectral placement, bandwidth control, and compatibility with existing radio hardware are essential. Therefore, an additional modulation stage is required to translate the chaotic baseband signals to the desired carrier frequency while preserving their information content and synchronization properties. This RF-stage modulation also determines how the chaotic spectrum is positioned within the channel, ultimately affecting the system's immunity to noise, interference, and multipath distortion.

In this section, advanced modulation techniques are introduced to perform RF translation and to shape the transmitted chaotic waveform according to the application requirements. Two representative approaches are examined: QAM, a linear modulation technique in which chaotic synchronization and information signals are mapped onto orthogonal amplitude components, and FM, a nonlinear technique in which information is embedded in the instantaneous frequency deviation. These modulation schemes are integrated with the previously developed CSK framework, implemented in both simulation and hardware prototypes, and evaluated in terms of noise immunity, synchronization sensitivity, and performance under selective fading. Together, these studies provide a comprehensive assessment of how the choice of advanced modulation schemes influences the overall performance and practicality of chaos-based communication systems.

Accordingly, the thesis of this section is that integrating advanced RF modulation techniques with chaos shift keying, specifically quadrature- and frequency-modulated chaos-based architectures implemented using the Vilnius chaotic oscillator, can yield improved resilience to frequency-selective multipath propagation compared to conventional modulation schemes. This thesis examines QCSK and FM-CSK systems through a comparative evaluation with corresponding 4-QAM and 2-FSK implementations under a two-ray channel model with a controlled spectral notch at the carrier frequency.

This section is organized as follows. Section 4.1 introduces the two RF modulation techniques used in this work, QAM and FM, and outlines how they map the synchronization and information-carrying chaotic signals to a carrier. Section 4.2 then presents the QAM-based chaos communication architecture (QCSK) and evaluates its noise immunity in simulation and prototype implementations. Section 4.3 introduces the FM-based chaos communication architecture (FM-CSK) and analyzes its noise immunity in the same manner. The influence of synchronization signal selection on QCSK performance is examined in Section 4.4. Section 4.5 evaluates QCSK and FM-CSK under two-ray

frequency-selective fading and compares them against 4-QAM and 2-FSK, respectively. Finally, Section 4.6 summarizes the main findings and relates them to the section thesis.

## 4.1 Modulation Schemes

*Quadrature Amplitude Modulation*

QAM is a linear modulation technique that combines two orthogonal carrier signals, enabling simultaneous transmission of two baseband components over the same frequency band. In the proposed system, the information-carrying chaotic signal is assigned to the quadrature component $Q(t)$, while the synchronization signal is assigned to the in-phase component $I(t)$.

Figure 4.1 presents the block diagram of the QAM transmitter and receiver. The structure consists of two mixers, operating with orthogonal carriers $\cos(\omega_c \cdot t)$ and $\sin(\omega_c \cdot t)$. The modulated signal is transmitted through a communication channel that may include AWGN or multipath propagation effects. At the receiver, coherent demodulation is performed using the same orthogonal carriers, followed by low-pass filtering to recover the baseband components $I'(t)$ and $Q'(t)$.

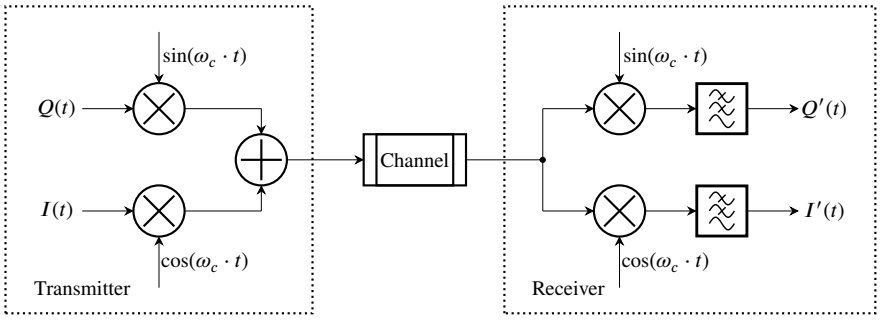


Fig. 4.1. Block diagram of the QAM transmitter and receiver used for chaos-based signal transmission.

At the transmitter, the QAM-modulated signal is formed as:

$$s(t) = I(t)\cos(\omega_c \cdot t) - Q(t)\sin(\omega_c \cdot t), \tag{4.1}$$

where $\omega_c$ is the carrier frequency, $I(t)$ is the synchronization signal, and $Q(t)$ is the information-carrying chaotic signal. Because QAM is a linear modulation technique, it does not introduce nonlinear distortions, thereby preserving the spectral characteristics of chaotic signals.

The received signal after transmission through the communication channel is expressed as:

$$r(t) = s(t) + n(t), \tag{4.2}$$

where $n(t)$ denotes the additive noise component.

At the receiver, the received signal is multiplied by the same orthogonal carrier functions used for modulation. The resulting signals can be expressed as:

$$s_{\text{mod}}(t)\cos(\omega_c \cdot t) = \frac{I(t)}{2} - \frac{I(t)}{2}\cos(2\omega_c \cdot t) + \frac{Q(t)}{2}\sin(2\omega_c \cdot t), \tag{4.3}$$

$$-s_{\text{mod}}(t)\sin(\omega_c \cdot t) = \frac{Q(t)}{2} - \frac{I(t)}{2}\sin(2\omega_c \cdot t) - \frac{Q(t)}{2}\cos(2\omega_c \cdot t). \tag{4.4}$$

The high-frequency components at $2\omega_c$ are suppressed using LPF, resulting in the recovered baseband signals. The filters are designed to remove spectral components above the baseband bandwidth while maintaining the main frequency content of the chaotic signals.

The recovered components $I'(t)$ and $Q'(t)$ correspond to the synchronization and information-carrying chaotic signals, respectively. These signals are further processed for chaos synchronization and data recovery.

*Frequency Modulation*

In the designed chaos-based communication systems, FM is employed to provide a reliable transmission of chaotic signals over various communication channels. Figure 4.2 illustrates the block diagram of the FM-based communication system used in this work. The transmitter consists of two branches that process the information-carrying and synchronization signals. Each signal first passes through a pre-emphasis filter that enhances high-frequency components before frequency modulation. The modulated signals are then transmitted through the communication channel, which may include additive noise or multipath propagation effects. At the receiver side, the incoming FM signals are filtered by a band-pass filter (BPF), demodulated, and finally passed through a de-emphasis filter to restore the original signal characteristics.

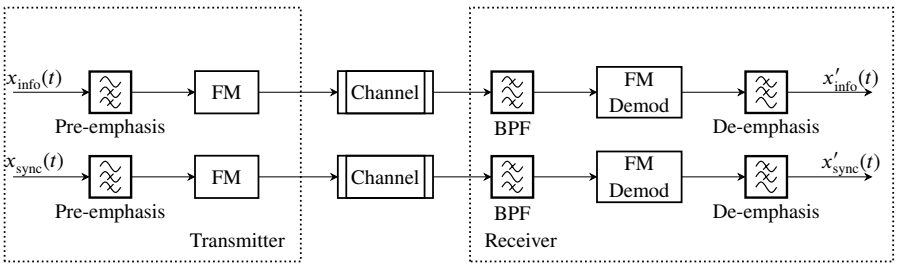


Fig. 4.2. Block diagram of the FM transmitter and receiver used for chaos-based signal transmission.

The pre-emphasis and de-emphasis filters form an essential part of the FM communication chain. Their primary purpose is to reduce the nonlinear distortions introduced during modulation and de-

modulation by compensating for frequency-dependent noise and system response. The pre-emphasis filter increases the amplitude of higher-frequency components, while the de-emphasis filter performs the inverse operation at the receiver, restoring the original spectral balance of the signal. The combined frequency responses of the filters ensure that the system transfer function remains flat across the operating bandwidth.

The pre-emphasis filter is implemented as a high-pass RC circuit, defined by the cutoff frequencies $f_1$ and $f_2$, as shown in Fig. 4.3(a). The component values are related to these cutoff frequencies as follows:

$$f_1 = \frac{1}{2\pi R_1 C}, \tag{4.5}$$

$$f_2 = \frac{R_1 + R_2}{2\pi R_1 R_2 C}. \tag{4.6}$$

The de-emphasis filter, shown in Fig. 4.3(b), is realized as a low-pass RC network, defined by a single cutoff frequency $f_1$, expressed as:

$$f_1 = \frac{1}{2\pi R_1 C}. \tag{4.7}$$

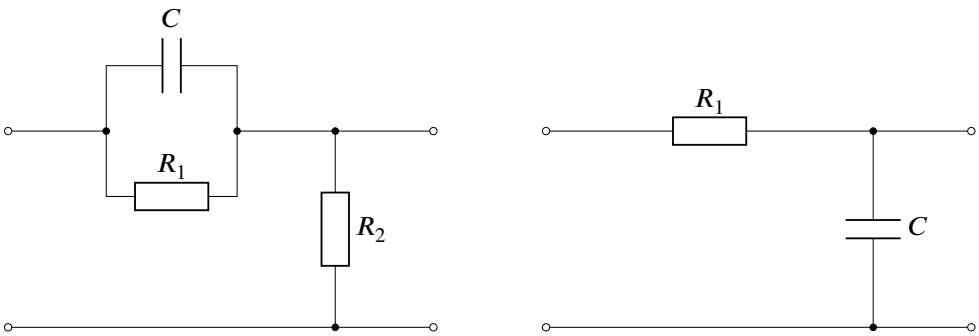


Fig. 4.3. (a) Pre-emphasis and (b) de-emphasis filter configurations used in the FM system.

The AFR of the pre-emphasis and de-emphasis filters is presented in Fig. 4.4. The pre-emphasis filter exhibits an increasing gain with frequency, enhancing high-frequency components before modulation. In contrast, the de-emphasis filter exhibits the opposite response, attenuating high frequencies after demodulation. This complementary design ensures minimal distortion of the transmitted signal's spectral characteristics while effectively reducing noise after demodulation.

The frequency deviation for modulation is selected based on the bandwidth of the modulating signals, defined at the $-20$ dB level of their spectra. This ensures consistent spectral occupancy across different types of chaotic signals, enabling a fair comparison of their performance under identical FM transmission parameters. The filter bandwidths are chosen such that the MSE between the

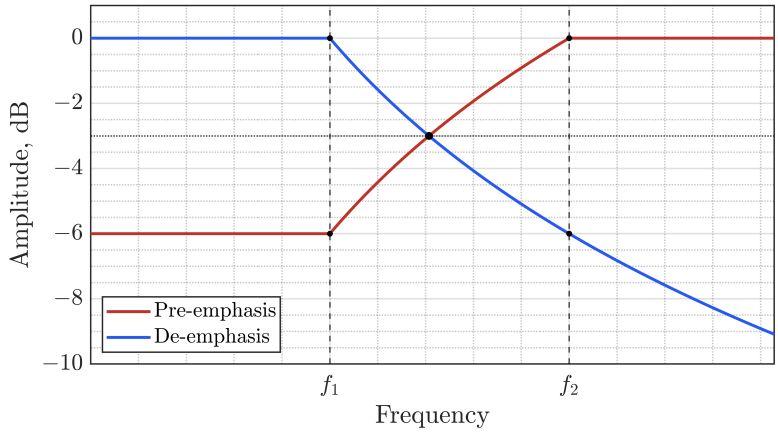


Fig. 4.4. AFR of the pre-emphasis (red) and de-emphasis (blue) filters.

original and demodulated signals remains below $-40$ dB, ensuring accurate reconstruction of the chaotic waveform.

Overall, the FM transmission structure, together with the pre-emphasis and de-emphasis filtering stages, forms a linear and spectrally balanced communication chain. This configuration allows the transmission of wideband chaotic signals with high fidelity while maintaining strong noise resistance, making it suitable for secure analog communication systems.

## 4.2 Quadrature Amplitude Modulation-based Communication System

*Quadrature Chaos Shift Keying Communication System*

The QCSK communication system represents an integration of CSK and QAM principles. The concept combines the security and nonlinear dynamics of chaotic modulation with the spectral efficiency of linear quadrature transmission. In this system, two orthogonal carrier components are used: one carries the synchronization signal, while the other carries the information-carrying chaotic signal. This configuration enables both signals to be transmitted simultaneously through the same frequency channel, allowing for coherent reception and improved utilization of the available bandwidth.

Figure 4.5 presents the block diagram of the QCSK communication system. At the transmitter, the drive chaos oscillator generates state variables that are used to form the synchronization and information-carrying signals. The synchronization signal is applied to the in-phase $I$ branch, while the information-carrying chaotic signal is applied to the quadrature $Q$ branch. Both branches are modulated using orthogonal carriers and combined into a single transmission signal. The resulting quadrature-modulated chaotic waveform is then transmitted through a communication channel.

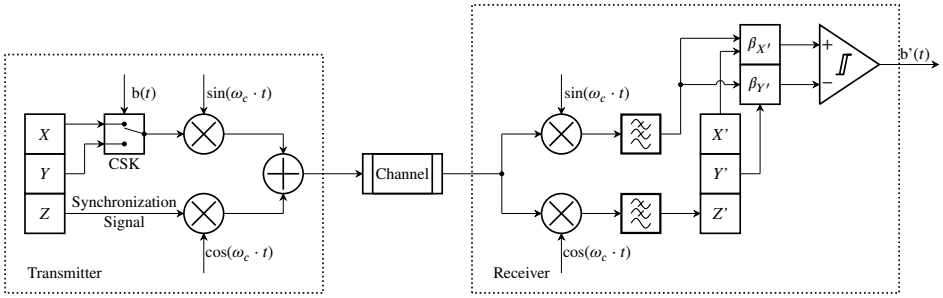


Fig. 4.5. Block diagram of the QCSK communication system combining chaos shift keying and quadrature modulation.

At the receiver, the incoming signal is demodulated using synchronized orthogonal carriers. The demodulated $I(t)$ and $Q(t)$ components are filtered by low-pass filters to extract the baseband chaotic signals. The synchronization signal, recovered from the in-phase branch, is used to drive the response chaos oscillator, enabling chaotic synchronization between the transmitter and receiver. The response oscillator outputs are then compared with the received quadrature signals through a correlation-based detection process, allowing data recovery from the chaotic waveform.

*Communication System Noise Immunity*

This section presents the noise-immunity analysis of the QCSK data transmission system based on both simulations and an experimental prototype. The goal is to assess the reliability of QCSK under varying noise conditions and to compare the behavior of the idealized model with that of a practical hardware implementation.

In the simulation environment, the drive and response chaotic oscillators were modeled in LTspice, while the CSK, QAM modulation, demodulation, and BER evaluation were performed in MATLAB. This approach enables direct adjustment of the channel noise level. Since all signal processing beyond the chaotic oscillators is performed digitally, parasitic coupling, analog noise sources, and component tolerances are absent. As a result, the simulation reflects the performance of the QCSK scheme under idealized noiseless circuit conditions. For experimental evaluation, chaotic oscillators and CSK switching were implemented on a custom PCB. The QCSK system employs an analog quadrature modulation chain based on commercially available Analog Devices development boards. The AD8346 was used for QAM modulation, while the AD8347 served as the corresponding demodulator. The received signal level was adjusted using a variable attenuator, and the received waveforms were captured with the ADP3450. The subsequent symbol detection and BER calculation were carried out offline in MATLAB. This setup captures practical impairments, such as mixer imbalance, finite switching speed, thermal noise contributions, and parasitic behavior, which are inherent to discrete components.

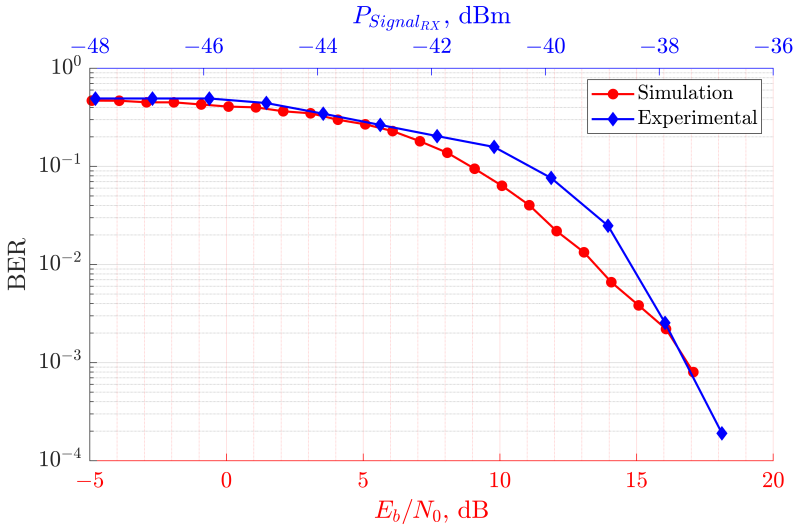


Fig. 4.6. BER performance of the QCSK communication system obtained from simulation (red) and experimental measurements (blue).

The simulation and measurement results are presented in Fig. 4.6, where the simulated BER (red curve) is plotted against $E_b/N_0$, and the experimental BER (blue curve) is plotted against the corresponding received signal power. In the simulation, the BER decreases steadily toward the $10^{-3}$ region as $E_b/N_0$ increases from approximately 0 dB to 17 dB. The slope in this region is close to linear on the logarithmic scale, reflecting stable synchronization and an absence of hardware non-idealities.

The experimental curve exhibits a smoother decrease in BER compared to the simulation, particularly in the region corresponding to the received powers between approximately $-48$ dBm and $-42$ dBm. In this interval, the measured performance improves only slightly, indicating that the system operates close to the sensitivity limit of the analog front end. A more noticeable decrease in BER is observed once the received power exceeds $-40$ dBm, crossing the $10^{-3}$ threshold near $-37$ dBm.

Although the simulation and experimental results are expressed in different domains—$E_b/N_0$ for the simulation and received power for the prototype—their BER characteristics follow similar trends. In both cases, the BER remains relatively high at higher noise and begins to decrease noticeably once $E_b/N_0$ exceeds approximately 8 dB or when the received power increases above about $-41$ dBm. The transition region is well-aligned: both curves cross the $10^{-3}$ level at comparable operating points, around $E_b/N_0 \approx 16$ dB for the simulation and $P_{RX} \approx -38$ dBm in the measurements.

The difference in slope between the two curves is primarily due to practical hardware limitations. The simulated system does not include analog impairments such as mixer noise, quadrature imbalance, or nonlinearities in the AD8346/AD8347 signal path. In the prototype, these effects introduce

additional noise and distortions, resulting in a slower BER decrease. Despite these non-idealities, the overall behavior of the measured curve closely follows the simulated trend, confirming the accuracy of the modeling framework and supporting the reliability of the implemented QCSK system.

## 4.3 Frequency Modulation-based Communication System

*Frequency-Modulated Chaos Shift Keying Communication System*

The FM-CSK communication system integrates CSK with FM to achieve reliable transmission of chaotic waveforms in noisy environments. In this architecture, the drive chaotic oscillator provides three state variables: one is designated as the synchronization signal, while the remaining two are used to form the information-carrying signal via CSK (i.e., data-dependent switching between the two chaotic state variables). This way preserves the nonlinear security properties of chaotic modulation while leveraging the noise immunity of FM.

Figure 4.7 shows the block diagram of the FM-CSK communication system. At the transmitter, the synchronization signal and the CSK-formed information-carrying signal are processed in two branches. Each branch applies pre-emphasis and then frequency modulation, after which the resulting waveforms are transmitted through the communication channel. Because the information is conveyed through instantaneous frequency rather than amplitude, the transmitted waveform exhibits improved resilience to additive noise and amplitude-related distortions while maintaining the essential chaotic dynamics.

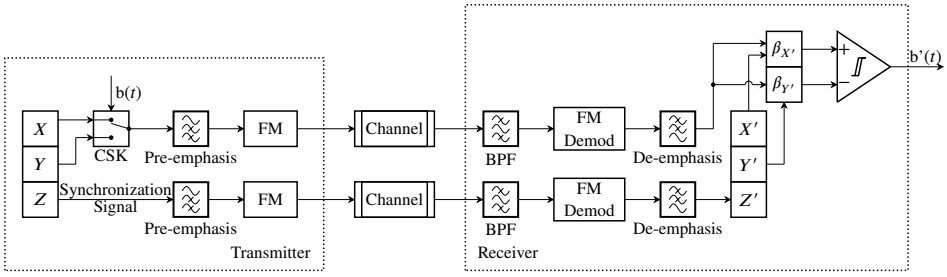


Fig. 4.7. Block diagram of the FM-CSK communication system combining CSK with frequency modulation.

At the receiver, the incoming composite signal is filtered and demodulated to recover the baseband synchronization and information-carrying signals, followed by de-emphasis to restore their spectral balance. The recovered synchronization signal drives the response chaos oscillator to establish chaotic synchronization. Once synchronized, correlation-based detection is performed between the response oscillator outputs and the received information-carrying signal to reconstruct the transmitted data.

*Communication System Noise Immunity*

This section presents the noise immunity study of the FM-CSK data transmission system. Two approaches were employed: a simulation study and an evaluation of an experimental prototype. In the simulation environment, the drive and response chaotic oscillators were modeled in LTspice, while the CSK modulation, frequency modulation, demodulation, and BER computation were performed in MATLAB. This workflow enabled precise control of the channel noise level, allowing the desired $E_b/N_0$ values to be set directly. The simulated signals were processed digitally, eliminating parasitic component effects and internal noise sources that would otherwise be present in physical hardware.

In the prototype implementation, the drive and response chaotic oscillators, as well as the CSK switching circuit, were realized on a custom PCB. Commercially available FM transmitter and receiver modules were used for the frequency modulation and demodulation stages. The transmitted signal was attenuated to vary the received power, and the received waveforms were captured using the ADP3450. Data detection and BER calculation were then carried out in MATLAB. This setup captures the practical limitations of a real hardware system, including amplifier noise, switching artifacts, and parasitic behavior of discrete components.

The BER curves resulting from the simulation and experimental measurements are shown in Fig. 4.8. In the simulation results (red curve), the BER is presented as a function of $E_b/N_0$. A BER of 10% is achieved at approximately 22 dB. As $E_b/N_0$ increases toward 27 dB, the BER decreases nearly linearly on the logarithmic scale, with a slope of about 14.2 orders of magnitude per decade.

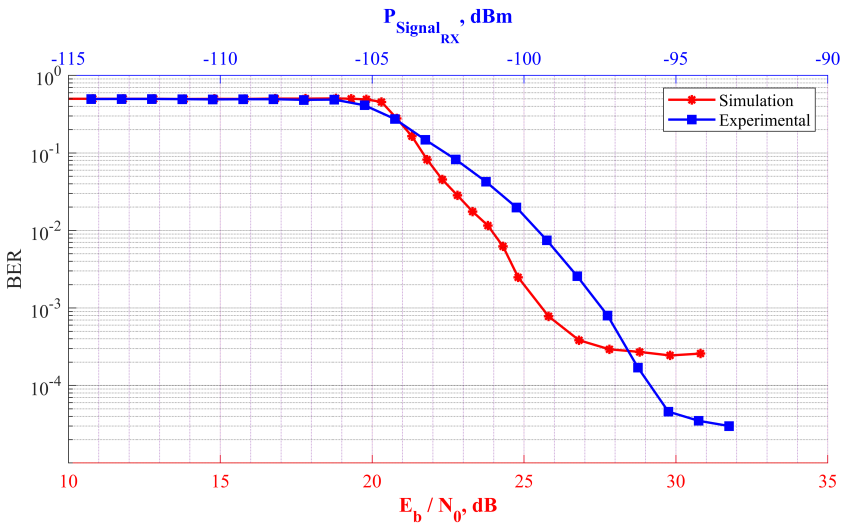


Fig. 4.8. BER performance of the FM-CSK communication system obtained from simulation (red) and experimental measurements (blue) [46].

The experimental results (blue curve) show the BER as a function of the received signal power. A nearly linear reduction in BER is observed for received power levels between $-105$ dBm and $-95$ dBm, with a slope of approximately 6.1 orders of magnitude per decade. For the selected carrier frequency, these received power values correspond to an operational distance of nearly 50 km, estimated using the Friis transmission equation (transmit power 5.75 dBm; transmit and receive antenna gains equal to 0 dB).

Although the simulation and experimental methods differ—one varying the noise level directly, the other varying the received signal power—the results are consistent and collectively characterize the noise immunity of the FM-CSK system. In both cases, further increasing the $E_b/N_0$ or received power beyond a certain point does not lead to additional BER reduction. This saturation is primarily due to the behavior of the synchronization subsystem.

The steeper BER slope observed in simulation reflects the idealized nature of the simulated system, where parasitic parameters and internal noise sources are absent. In contrast, the prototype includes several unavoidable noise contributors, such as broadband noise from operational amplifiers, switching noise from the CSK circuitry, imperfections in the FM modulation and demodulation modules, and parasitic effects of passive components. These practical limitations account for the shallower BER slope in the experimental measurements.

## 4.4 Performance Analysis of the QCSK System under Different Synchronization Signal Configurations

The performance of the QCSK communication system strongly depends on the selection of the synchronization signal used for coupling the chaotic oscillators. As demonstrated in Section 2, the synchronization quality varies significantly across different circuit nodes of a given chaotic oscillator, and different synchronization levels within the circuit introduce imbalance into the communication system. Since the receiver's ability to accurately reproduce the chaotic dynamics directly influences data detection accuracy and overall noise immunity, the choice of synchronization signal becomes a critical design factor.

In this section, the impact of synchronization signal selection on the QCSK communication system is investigated. For the Vilnius chaotic oscillator, all three signals, as in the Section 2, were evaluated as potential synchronization signals, enabling a direct comparison of system performance under different synchronization configurations. For the Colpitts chaotic oscillator, however, reliable synchronization was achieved only when using the $v_{C1}$ node, as shown previously in Section 2. The remaining nodes exhibited substantially lower synchronization quality; therefore, only the $v_{C1}$ configuration is included in the present performance comparison. The noise immunity study results for all four configurations are presented in Fig. 4.9, where the y-axis represents the BER, and the x-axis shows bit energy and noise power spectral density ratio ($E_b/N_0$).

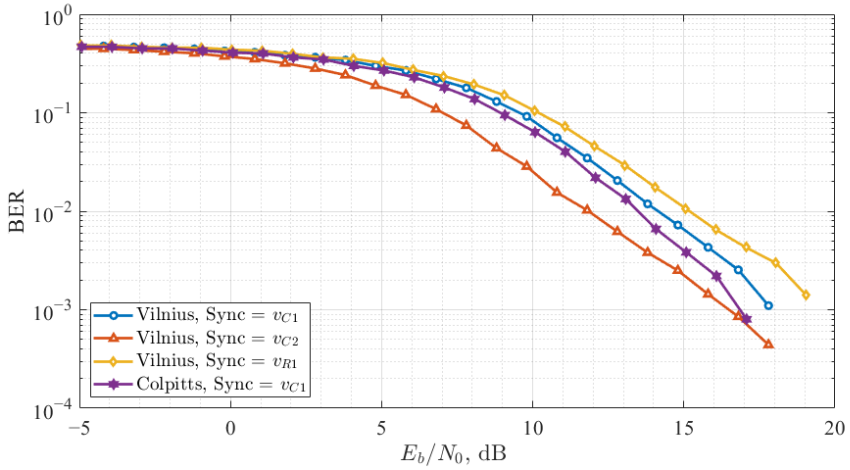


Fig. 4.9. BER versus $E_b/N_0$ curves of QCSK data transmission system.

The best performance among the tested QCSK configurations was observed in the Vilnius chaos oscillator-based system when $v_{C2}$ was used as the synchronization signal. In the chaotic synchronization noise immunity study, this configuration demonstrated the highest correlation values under noisy conditions, ensuring that $X$ and $Y$ correlations are of the same level. Additionally, the cross-correlation between chaotic signals forming the information-carrying signals was minimal, and it remained relatively unaffected by added noise, further enhancing the system's resilience.

The QCSK system, based on the Colpitts chaos oscillator, achieved the second-best performance using $v_{C1}$ for synchronization. In the previous study, this configuration displayed similar synchronization characteristics to the $v_{C2}$ synchronized Vilnius chaos oscillator. However, in the Colpitts oscillator, $X'$ and $Y'$ exhibited different correlation coefficient values, leading to a system imbalance, which required compensation during detection.

The remaining two configurations of the Vilnius chaos oscillator exhibited similar performance trends, aligning with findings from the synchronization noise immunity study. However, the worst BER performance was observed in the Vilnius chaos oscillator-based QCSK system when $v_{R1}$ was used as the synchronization signal. This configuration was more noise-sensitive since spectral components of the information-carrying signal occupied a wider band [48].

## 4.5 QAM- and FM-Based Communication System Performance in Selective Fading Conditions

This section presents a comparative analysis of the QCSK and FM-CSK communication systems to evaluate their suitability for WSN applications. Such applications require communication schemes that remain reliable under the typical impairments encountered in wireless environments. Among

these impairments, multipath propagation is particularly critical because it introduces inter-symbol interference, making resilience to selective fading a key requirement for reliable system performance. To investigate these effects, this section focuses on system behavior in a two-ray propagation channel. The analysis builds upon the AWGN results presented in the previous section, extending the performance evaluation to selective fading conditions. The section concludes with a comparison of the noise immunity of QCSK and FM-CSK in the presence of multipath-induced fading.

*Study Setup*

The system performance in selective fading conditions is evaluated using a simulation environment developed in MATLAB. The same general framework is applied to both chaos-based communication schemes—QCSK and FM-CSK—ensuring a consistent basis for comparison.

A two-ray multipath channel is used to emulate frequency-selective fading. The model consists of a line-of-sight component and a delayed reflected component, producing a spectral notch at a frequency determined by the path delay. For this study, the delay is chosen such that the notch appears at the intermediate frequency (IF) of 140 MHz. The channel structure is shown in Fig. 4.10. While the notch frequency remains fixed, its depth is varied to assess system resilience under different multipath conditions.

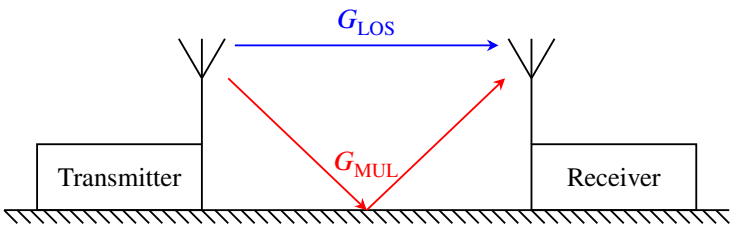


Fig. 4.10. The model of the emulated multipath channel.

To provide fair performance benchmarks, QCSK is compared with 4-QAM, and FM-CSK with binary FSK. The conventional systems are configured to match the bandwidths of their corresponding chaos-based counterparts. Fig. 4.11 (a) and (b) illustrate the effect of the two-ray channel on 4-QAM and QCSK spectra, along with the channel's estimated amplitude transfer function $|K(f)|$. Although the signals occupy the same bandwidth, their spectral structures differ, so the channel attenuation parameters are adjusted to ensure that both experience an equivalent notch depth at 140 MHz. A similar comparison is shown for FSK and FM-CSK in Fig. 4.12 (a) and (b).

After propagation through the multipath channel, additive white Gaussian noise is introduced at controlled SNR levels. The received signals are demodulated using the algorithms defined earlier in the Thesis, and the BER is estimated for multiple combinations of SNR and channel parameters.

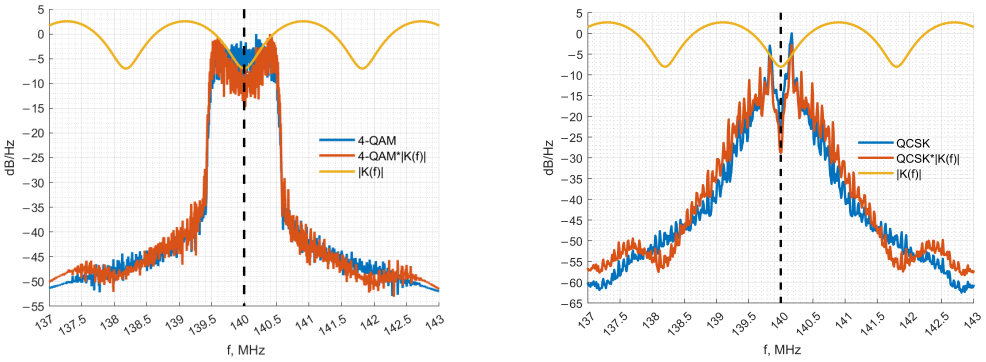


(a) (b)

Fig. 4.11. The effect of a two-ray channel on 4-QAM (a) and QCSK (b).

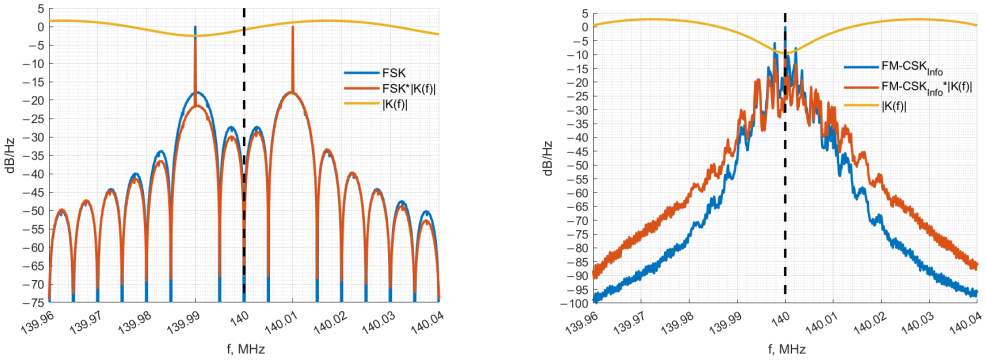


(a) (b)

Fig. 4.12. The effect of a two-ray channel on FSK (a) and FM-CSK (b).

*Performance Analysis in the Selective Fading Conditions*

The BER performance of the QCSK, 4-QAM, FM-CSK, and FSK systems under two-ray selective fading is presented in Fig. 4.13, 4.14, 4.15, and 4.16, respectively. Each figure shows the BER as a function of the normalized SNR for several spectral notch depths of the multipath channel. To ensure direct comparability, the SNR is normalized such that the reference point corresponds to a 0 dB notch at a BER of $10^{-3}$.

The results show that QCSK and 4-QAM exhibit similar behavior under shallow spectral notches. For notch depths of 0.10 dB and 0.48 dB, 4-QAM achieves BER values of $1.45 \times 10^{-3}$ and $3.42 \times 10^{-3}$, respectively, compared with $1.06 \times 10^{-3}$ and $1.68 \times 10^{-3}$ for QCSK. When the notch becomes deeper, 4-QAM degrades significantly: at 3.25 dB and 7.64 dB, its BER increases to $9.63 \times 10^{-2}$ and $3.29 \times 10^{-1}$. In contrast, QCSK maintains lower BER values of $3.29 \times 10^{-3}$ and $6.18 \times 10^{-3}$ at the same notch depths. Thus, although 4-QAM performs slightly better under mild fading, QCSK is more resilient to severe frequency-selective fading.

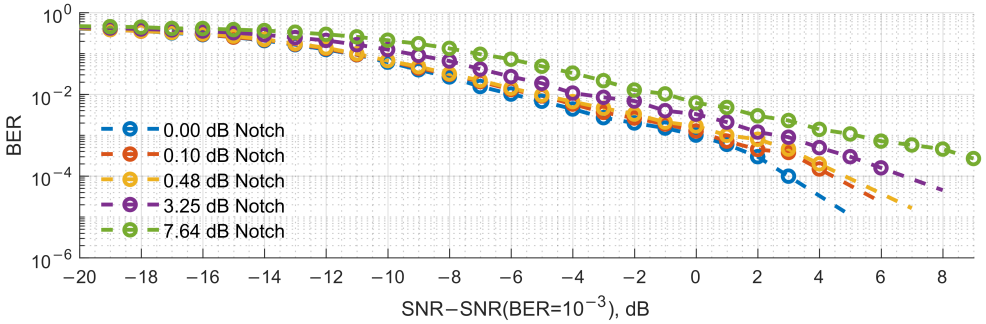


Fig. 4.13. QCSK communication system's performance for the two-ray channel.

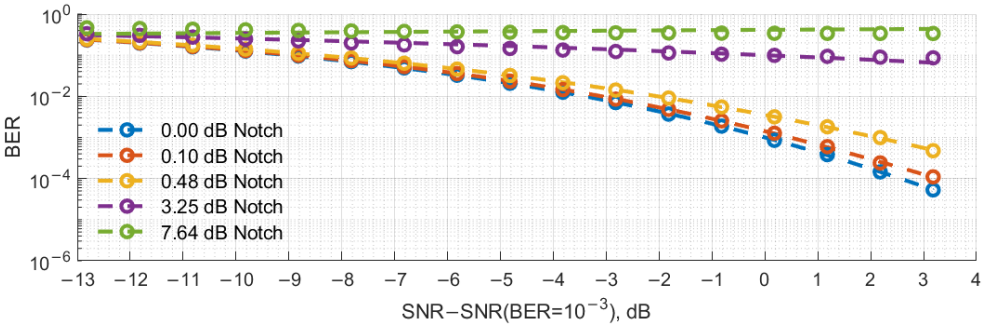


Fig. 4.14. QAM communication system's performance for the two-ray channel.

For FM-CSK and FSK, the results in Fig. 4.15 and 4.16 show a similar trend. At a 3.25 dB notch, FM-CSK achieves a slightly lower BER ($1.52 \times 10^{-3}$) than FSK ($1.79 \times 10^{-3}$). At a 5.00 dB notch, both systems perform almost identically, with BER values around $4 \times 10^{-3}$. At deeper notches, however, FSK maintains an advantage. For notch depths of 7.64 dB and 9.08 dB, FSK achieves BER values of $6.82 \times 10^{-3}$ and $1.18 \times 10^{-2}$, whereas FM-CSK yields $1.47 \times 10^{-2}$ and $2.55 \times 10^{-2}$. These results indicate that FM-CSK offers a slight benefit at moderate fading levels but becomes more sensitive at stronger notches.

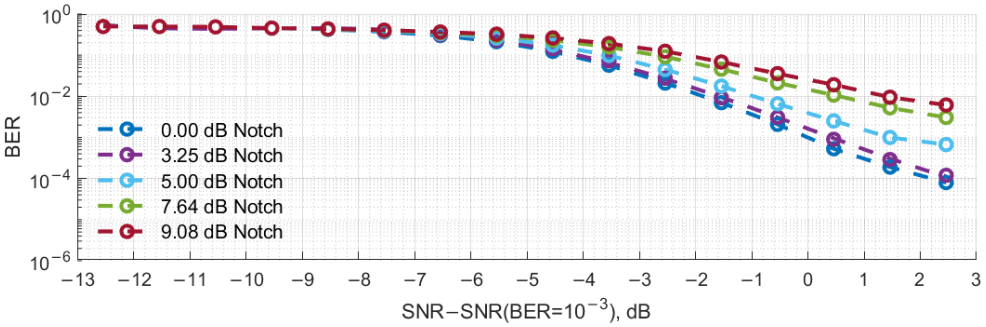


Fig. 4.15. FM-CSK communication system's performance for the two-ray channel.

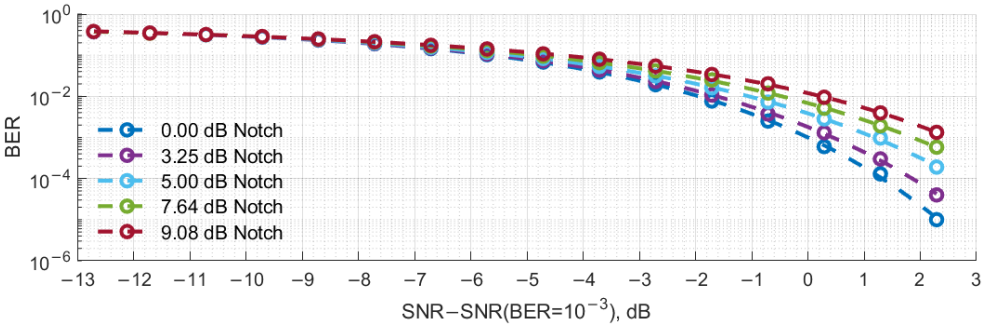


Fig. 4.16. FSK communication system's performance for the two-ray channel.

A comparison between the two chaos-based systems further highlights these differences. At a 3.25 dB notch, FM-CSK exhibits significantly lower BER than QCSK ($1.52\times10^{-3}$ vs. $3.29\times10^{-3}$). At a notch depth of 7.64 dB, the QCSK system achieves a lower BER than FM-CSK ($6.18\times10^{-3}$ vs. $1.47\times10^{-2}$), representing the only tested fading condition where QCSK outperforms FM-CSK. Overall, FM-CSK shows higher resilience to strong notch-type fading, while QCSK remains more resilient than its conventional counterpart (4-QAM) but less resilient than FM-CSK under severe two-ray fading.

## 4.6 Discussion

This section examined two chaos-based communication architectures—QCSK, which uses quadrature modulation, and FM-CSK, which uses frequency modulation—as representative implementations of advanced modulation techniques applied to chaotic baseband signals. The study covered system modeling, prototype development, noise-immunity evaluation, synchronization signal selection, and the effects of selective fading. The combined results provide a clear understanding of how each modulation approach influences the behavior of a chaos-based communication system.

The QCSK system, implemented using a quadrature modulator/demodulator pair, demonstrated reliable operation once the received signal quality exceeded the sensitivity threshold of the analog front end. The system's performance was strongly dependent on the choice of synchronization signal, with certain signals enabling noticeably better synchronization and lower BER values. In selective fading conditions, QCSK consistently outperformed its linear benchmark 4-QAM, especially at deeper spectral notches, indicating that the combined CSK-QAM structure preserves sufficient chaotic diversity to maintain data recovery even when multipath-induced distortion increases.

The FM-CSK architecture exhibited different performance characteristics. Because the information is carried by instantaneous frequency deviation, the prototype exhibited a more gradual yet steady BER improvement in the presence of increased received power, maintaining resilience across a broader range of noise levels. Under two-ray selective fading, the FM-CSK system achieved lower

BER values than QCSK as the notch depth increased, demonstrating stronger resilience to amplitude-related distortions and frequency-selective fading. The simulation and prototype results were consistent across noise levels, supporting the reliability of the FM-CSK design.

Beyond the qualitative performance trends, the results of this section provide direct quantitative validation of the thesis. In a two-ray multipath channel characterized by a 3.25 dB spectral notch at the carrier frequency, both chaos-based modulation schemes demonstrated superior performance compared to their conventional linear counterparts. Specifically, the QCSK system based on the Vilnius chaotic oscillator achieved a bit error probability of $3.29 \times 10^{-3}$, outperforming the corresponding 4-QAM benchmark under identical channel conditions. Similarly, the FM-CSK architecture attained a lower error probability of $1.52 \times 10^{-3}$, exceeding the performance of the reference 2-FSK system in the same two-ray fading scenario. These results confirm that incorporating chaotic dynamics provides a measurable resilience advantage in frequency-selective multipath environments.

In summary, the two chaos-based systems exhibit complementary strengths depending on the operating conditions. The QCSK architecture performs effectively in scenarios with moderate noise and shallow to moderate fading, particularly when an appropriate synchronization signal is employed. In contrast, the FM-CSK system demonstrates increased resilience under stronger fading and wider variations in signal quality, owing to its inherent resilience against amplitude-related distortions. Collectively, these findings establish that chaos-based modulation schemes can outperform conventional linear modulation techniques within RF bands relevant to IoT and WSN applications, provided that channel characteristics and system constraints are carefully considered in the modulation selection process.

# CONCLUSIONS

This Doctoral Thesis is devoted to the analysis, design, and experimental evaluation of chaos-based communication systems operating under noise and multipath propagation conditions. The research focused on the influence of the fundamental frequency of the chaotic oscillator, synchronization stability, detection optimality, and advanced modulation techniques on the achievable performance of such systems. The proposed methods and system architectures were verified through circuit-level simulations and experimental measurements, demonstrating their practical feasibility and consistency with the theoretical considerations.

The main objective of the Thesis—to investigate and demonstrate how chaotic oscillator characteristics, synchronization strategies, and modulation techniques affect the performance of chaos-based communication systems—has been achieved. All research tasks formulated in the Introduction have been completed. The principal results obtained within the framework of this Doctoral Thesis are summarized as follows:

- It has been demonstrated that variation of the fundamental frequency of analog chaotic oscillators provides a practical mechanism for adjusting the achievable data rate of chaos-based communication systems. A lag-based analysis of cross-correlation functions was established as a consistent method for selecting the bit duration, ensuring that consecutive symbols are transmitted using sufficiently decorrelated chaotic waveforms. This relationship was experimentally validated for two structurally different chaotic oscillators.
- A comprehensive study of chaotic synchronization under additive noise conditions showed that the synchronization quality strongly depends on the selected circuit node used for coupling the drive and response oscillators. Based on these findings, a systematic methodology for selecting synchronization signals was developed, enabling the identification of synchronization configurations that ensure higher stability in noisy environments.
- It was shown that different state variables of the same chaotic oscillator may show unequal correlation level under identical synchronization conditions. This effect leads to an imbalance in correlation-based detection when CSK is applied. To address this issue, a compensation threshold for correlation-based detection was proposed, restoring balanced symbol decision-making and improving detection reliability.
- The impact of synchronization signal selection on the overall performance of chaos-based communication systems was evaluated. The results demonstrated that inappropriate synchronization choices can degrade BER performance.
- Advanced modulation techniques were successfully integrated with chaos-based communication systems. QAM and FM were combined with CSK to enable transmission in RF bands while preserving chaotic synchronization feasibility. The resulting systems were evaluated in AWGN channels and two-ray propagation channels.
- Comparative performance analysis revealed that chaos-based communication systems ex-

hibit increased resilience to frequency-selective fading compared to conventional modulation schemes operating under identical bandwidth constraints, particularly in severe two-ray propagation conditions.

All investigated systems were implemented using a combined simulation and experimental framework, where chaotic oscillators were modeled at the circuit level and signal processing, detection, and performance evaluation were performed in MATLAB. Experimental prototypes based on discrete analog circuits and commercial modulation modules confirmed the validity of the proposed approaches.

Beyond theoretical validation, the obtained results provide experimentally validated insight into the feasibility and operational characteristics of chaos-based communication. In particular, the demonstrated relationship between the chaotic oscillator fundamental frequency and achievable data rate establishes a clear connection between oscillator parameters and transmission speed, which is relevant for low-rate wireless communication scenarios such as sensor-to-base-station links. The achieved data rates were shown to fall within the same order of magnitude as those employed by existing IoT communication technologies, indicating that chaos-based systems can be parameterized to operate within practically relevant transmission regimes. Furthermore, the conducted analysis of synchronization signal selection yields qualitative and quantitative observations that can inform circuit- and system-level design choices aimed at improving resilience in noisy and multipath environments.

In conclusion, the results of this Doctoral Thesis confirm that chaos-based communication systems can be systematically designed and optimized through the appropriate selection of oscillator parameters, synchronization signals, detection strategies, and modulation techniques. The obtained results demonstrate the feasibility and adaptability of chaos-based communication for operation in noisy and multipath environments. Therefore, the objective of the Thesis has been successfully achieved, the stated research tasks have been completed, and the formulated theses have been defended.

Future research may further extend the presented results by investigating the behavior of chaos-based communication systems under more complex and time-varying channel conditions, including mobility-induced fading and nonstationary interference. The development of adaptive synchronization and detection strategies that dynamically adjust system parameters in response to changing noise and propagation conditions represents another important direction. In addition, integrated, low-power implementations of chaotic oscillators and synchronization circuits should be explored to evaluate the practical feasibility of deployment in compact wireless devices. Finally, the combination of chaos-based signaling with more spectrally efficient modulation and multi-user access techniques may enable broader applicability of the proposed concepts in next-generation secure and low-rate wireless communication systems.

# BIBLIOGRAPHY


[1] P. Jonsson et al. *Ericsson Mobility Report November 2025*. en. Tech. rep. Nov. 2025. URL: https://www.ericsson.com/4aca6f/assets/local/reports-papers/mobility-report/documents/2025/ericsson-mobility-report-november-2025.pdf (visited on 11/28/2025).

[2] P. Sun et al. "A Survey of IoT Privacy Security: Architecture, Technology, Challenges, and Trends." en. In: *IEEE Internet of Things Journal* 11.21 (Nov. 2024), pp. 34567–34591. ISSN: 2327-4662, 2372-2541. DOI: 10.1109/JIOT.2024.3372518.

[3] N. M. Karie et al. "A Review of Security Standards and Frameworks for IoT-Based Smart Environments." en. In: *IEEE Access* 9 (2021), pp. 121975–121995. ISSN: 2169-3536. DOI: 10.1109/ACCESS.2021.3109886.

[4] K. K. S. Gautam et al. "Investigation of the Internet of Things (IoT) Security and Privacy Issues." en. In: *2023 5th International Conference on Inventive Research in Computing Applications (ICIRCA)*. Coimbatore, India: IEEE, Aug. 2023, pp. 1489–1494. ISBN: 9798350321425. DOI: 10.1109/ICIRCA57980.2023.10220814.

[5] M. S. Sharbaf. "IoT Driving New Business Model, and IoT Security, Privacy, and Awareness Challenges." en. In: *2022 IEEE 8th World Forum on Internet of Things (WF-IoT)*. Yokohama, Japan: IEEE, Oct. 2022, pp. 1–4. ISBN: 978-1-66549-153-2. DOI: 10.1109/WF-IoT54382.2022.10152044.

[6] T. Sauter and A. Treytl. "IoT-Enabled Sensors in Automation Systems and Their Security Challenges." en. In: *IEEE Sensors Letters* 7.12 (Dec. 2023), pp. 1–4. ISSN: 2475-1472. DOI: 10.1109/LSENS.2023.3332404.

[7] B. Omoniwa et al. "Fog/Edge Computing-Based IoT (FECIoT): Architecture, Applications, and Research Issues." In: *IEEE Internet of Things Journal* 6.3 (June 2019), pp. 4118–4149. ISSN: 2327-4662. DOI: 10.1109/JIOT.2018.2875544.

[8] J. M. Hamamreh, H. M. Furqan, and H. Arslan. "Classifications and Applications of Physical Layer Security Techniques for Confidentiality: A Comprehensive Survey." en. In: *IEEE Communications Surveys & Tutorials* 21.2 (2019), pp. 1773–1828. ISSN: 1553-877X, 2373-745X. DOI: 10.1109/COMST.2018.2878035.

[9] P. Rojas, S. Alahmadi, and M. Bayoumi. "Physical Layer Security for IoT Communications - A Survey." en. In: *2021 IEEE 7th World Forum on Internet of Things (WF-IoT)*. New Orleans, LA, USA: IEEE, June 2021, pp. 95–100. ISBN: 978-1-66544-431-6. DOI: 10.1109/WF-IoT51360.2021.9595025.

[10] E. Illi et al. “Physical Layer Security for Authentication, Confidentiality, and Malicious Node Detection: A Paradigm Shift in Securing IoT Networks.” en. In: *IEEE Communications Surveys & Tutorials* 26.1 (2024), pp. 347–388. ISSN: 1553-877X, 2373-745X. DOI: 10.1109/COMST.2023.3327327.

[11] Z. A. Traynor et al. “Physical-layer security solutions for IoT devices using Radio Frequency Fingerprints.” en. In: *2024 International Conference on Computing, Internet of Things and Microwave Systems (ICCIMS)*. Gatineau, QC, Canada: IEEE, July 2024, pp. 1–4. ISBN: 9798350351736. DOI: 10.1109/ICCIMS61672.2024.10690481.

[12] V. Mohan and A. Mathur. “Secrecy Analysis of DCSK-Based PLC Systems With Multiple Eavesdroppers.” en. In: *IEEE Systems Journal* 17.3 (Sept. 2023), pp. 3646–3657. ISSN: 1932-8184, 1937-9234, 2373-7816. DOI: 10.1109/JSYST.2022.3224982.

[13] F. Capligins et al. “FPGA Implementation and Study of Synchronization of Modified Chua’s Circuit-Based Chaotic Oscillator for High-Speed Secure Communications.” In: 2021. ISBN: 978-1-66542-538-4. DOI: 10.1109/AIEEE51419.2021.9435783.

[14] F. Yu et al. “CCII and FPGA Realization: A Multistable Modified Fourth-Order Autonomous Chua’s Chaotic System with Coexisting Multiple Attractors.” In: *Complexity* 2020 (2020), pp. 1–17. ISSN: 10990526. DOI: 10.1155/2020/5212601.

[15] J. Sun et al. “A Memristive Fully Connect Neural Network and Application of Medical Image Encryption Based on Central Diffusion Algorithm.” en. In: *IEEE Transactions on Industrial Informatics* 20.3 (Mar. 2024), pp. 3778–3788. ISSN: 1551-3203, 1941-0050. DOI: 10.1109/TII.2023.3312405.

[16] P. Sanprang et al. “Realization of image cryptography using FPAA-based two chaotic systems.” en. In: *2023 20th International Conference on Electrical Engineering/Electronics, Computer, Telecommunications and Information Technology (ECTI-CON)*. Nakhon Phanom, Thailand: IEEE, May 2023, pp. 1–4. ISBN: 9798350310467. DOI: 10.1109/ECTI-CON58255.2023.10153159.

[17] A. E. George et al. “Real-World Secure Communication based on Synchronised Lorenz Chaotic Circuits.” en. In: *2024 13th International Conference on Modern Circuits and Systems Technologies (MOCAST)*. Sofia, Bulgaria: IEEE, June 2024, pp. 1–6. ISBN: 979-8-3503-8542-7. DOI: 10.1109/MOCAST61810.2024.10615733.

[18] A. J. Michaels and C. Lau. “Generalized Multi-carrier Chaotic Shift Keying.” en. In: *2014 IEEE Military Communications Conference*. Baltimore, MD, USA: IEEE, Oct. 2014, pp. 657–662. ISBN: 978-1-4799-6770-4. DOI: 10.1109/MILCOM.2014.115.

[19] C. Bai et al. “Double-Stream Differential Chaos Shift Keying Communications Exploiting Chaotic Shape Forming Filter and Sequence Mapping.” In: *IEEE Transactions on Wireless Communications* 21.7 (July 2022), pp. 4954–4972. ISSN: 1536-1276, 1558-2248. DOI: 10.1109/TWC.2021.3135043.

[20] V. Mohan and A. Mathur. “Performance Evaluation of DCSK-Based PLC Systems Under Pulse Jamming Attacks.” en. In: *2024 IEEE 99th Vehicular Technology Conference (VTC2024-Spring)*. Singapore, Singapore: IEEE, June 2024, pp. 1–6. ISBN: 9798350387414. DOI: 10.1109/VTC2024-Spring62846.2024.10683280.

[21] T. Bonny and W. Al Nassan. “Optimizing Security and Cost Efficiency in N-Level Cascaded Chaotic-Based Secure Communication System.” en. In: *Applied System Innovation* 7.6 (Oct. 2024), p. 107. ISSN: 2571-5577. DOI: 10.3390/asi7060107.

[22] Z. Hua and Y. Zhou. “Exponential Chaotic Model for Generating Robust Chaos.” en. In: *IEEE Transactions on Systems, Man, and Cybernetics: Systems* 51.6 (June 2021), pp. 3713–3724. ISSN: 2168-2216, 2168-2232. DOI: 10.1109/TSMC.2019.2932616.

[23] T. I. Karimov et al. “The Study on Multiparametric Sensitivity of Chaotic Oscillators.” en. In: *2020 IEEE Conference of Russian Young Researchers in Electrical and Electronic Engineering (EIConRus)*. St. Petersburg and Moscow, Russia: IEEE, Jan. 2020, pp. 134–137. ISBN: 978-1-72815-761-0. DOI: 10.1109/EIConRus49466.2020.9039312.

[24] M. Sadia et al. “Robust Chaos With Novel 4-Transistor Maps.” en. In: *IEEE Transactions on Circuits and Systems II: Express Briefs* 70.3 (Mar. 2023), pp. 914–918. ISSN: 1549-7747, 1558-3791. DOI: 10.1109/TCSII.2022.3217416.

[25] S. Ergun and S. Tanriseven. “Random Number Generator Based on Skew-tent Map and Chaotic Sampling.” en. In: *2020 IEEE Asia Pacific Conference on Circuits and Systems (APCCAS)*. Ha Long, Vietnam: IEEE, Dec. 2020, pp. 224–227. ISBN: 978-1-7281-9396-0. DOI: 10.1109/APCCAS50809.2020.9301661.

[26] S. Araki, J.-H. Wu, and J.-J. Yan. “A Novel Design of Random Number Generators Using Chaos-Based Extremum Coding.” In: *IEEE Access* 12 (2024), pp. 24039–24047. ISSN: 2169-3536. DOI: 10.1109/ACCESS.2024.3365638.

[27] C.-C. Liu et al. “Design of a Multiple Pseudorandom Number Generator Combined Chaotic System With RNS and Its Application to Secure Image Processing.” en. In: *IEEE Access* 12 (2024), pp. 155246–155258. ISSN: 2169-3536. DOI: 10.1109/ACCESS.2024.3482012.

[28] J. Arif et al. “A Novel Chaotic Permutation-Substitution Image Encryption Scheme Based on Logistic Map and Random Substitution.” en. In: *IEEE Access* 10 (2022), pp. 12966–12982. ISSN: 2169-3536. DOI: 10.1109/ACCESS.2022.3146792.

[29] M.-A. Estudillo-Valdez, V.-A. Adeyemi, and J.-C. Nuñez-Perez. “FPGA realization of an image encryption system using the DCSK-CDMA technique.” en. In: *Integration* 96 (May 2024), p. 102157. ISSN: 01679260. DOI: 10.1016/j.vlsi.2024.102157.

[30] H. Lu et al. “Chip-Scale Random Number Generator Based On Self-Chaotic Dynamics Of Broad-Area VCSELs.” en. In: *2024 IEEE 29th International Semiconductor Laser Conference (ISLC)*. Orlando, FL, USA: IEEE, Sept. 2024, pp. 1–2. ISBN: 9798350372991. DOI: 10.1109/ISLC57752.2024.10717369.

[31] X. Hu et al. “Color Image Encryption Algorithm Based on Dynamic Chaos and Matrix Convolution.” en. In: *IEEE Access* 8 (2020), pp. 12452–12466. ISSN: 2169-3536. DOI: 10.1109/ACCESS.2020.2965740.

[32] R. Kiliç and F. Yildirim. “A survey of Wien bridge-based chaotic oscillators: Design and experimental issues.” en. In: *Chaos, Solitons & Fractals* 38.5 (Dec. 2008), pp. 1394–1410. ISSN: 09600779. DOI: 10.1016/j.chaos.2008.02.016.

[33] A. Elwakil and M. Kennedy. “A family of Colpitts-like chaotic oscillators.” en. In: *Journal of the Franklin Institute* 336.4 (May 1999), pp. 687–700. ISSN: 00160032. DOI: 10.1016/S0016-0032(98)00046-5.

[34] E. V. Efremova. “Generation of Dynamic Chaos in a Range of 10–30 GHz.” en. In: *Journal of Communications Technology and Electronics* 63.4 (Apr. 2018), pp. 367–373. ISSN: 1064-2269, 1555-6557. DOI: 10.1134/S1064226918040046.

[35] K. Maezawa et al. “Direct Observation of High-Frequency Chaos Signals from the Resonant Tunneling Chaos Generator.” en. In: *Japanese Journal of Applied Physics* 43.8R (Aug. 2004), p. 5235. ISSN: 0021-4922, 1347-4065. DOI: 10.1143/JJAP.43.5235.

[36] K. Maezawa. “A new generation of negative-resistance devices—New developments in ultrahigh-frequency applications based on resonant tunneling elements.” en. In: *Electronics and Communications in Japan (Part II: Electronics)* 89.4 (Apr. 2006), pp. 29–38. ISSN: 8756-663X, 1520-6432. DOI: 10.1002/ecjb.20202.

[37] L. M. Pecora and T. L. Carroll. “Synchronization of chaotic systems.” In: *Understanding Complex Systems* 48 (2009), pp. 101–133. ISSN: 18600832. DOI: 10.1007/978-3-642-00937-2_6.

[38] A. A. Kekha Javan et al. “Design of adaptive-robust controller for multi-state synchronization of chaotic systems with unknown and time-varying delays and its application in secure communication.” In: *Sensors (Switzerland)* 21.1 (2021), pp. 1–21. ISSN: 14248220. DOI: 10.3390/s21010254.

[39] A. Karimov et al. “Adaptive Generalized Synchronization between Circuit and Computer Implementations of the Rössler System.” en. In: *Applied Sciences* 11.1 (Dec. 2020), p. 81. ISSN: 2076-3417. DOI: 10.3390/app11010081.

[40] H. Xie et al. “A Secure Communication Framework Based on Chaotic Synchronization via Approximate Nonlinear Model Predictive Control.” en. In: *IEEE Control Systems Letters* 8 (2024), pp. 1559–1564. ISSN: 2475-1456. DOI: 10.1109/LCSYS.2024.3410151.

[41] E. Ozpolat, V. Celik, and A. Gulten. “A Novel Four-Dimensional Hyperchaotic System: Design, Dynamic Analysis, Synchronization, and Image Encryption.” en. In: *IEEE Access* 12 (2024), pp. 126063–126073. ISSN: 2169-3536. DOI: 10.1109/ACCESS.2024.3454820.

[42] X. Cui et al. “A Chaotic Synchronization Method Based on Time-Synchronized Control.” en. In: *2024 43rd Chinese Control Conference (CCC)*. Kunming, China: IEEE, July 2024, pp. 335–340. ISBN: 978-988-758-158-1. DOI: 10.23919/CCC63176.2024.10662335.

[43] D. Cirjulina et al. “Experimental Study of the Impact of Component Nominal Deviations on the Stability of Vilnius Chaotic Oscillator.” In: *2020 IEEE Microwave Theory and Techniques in Wireless Communications (MTTW)*. Riga, Latvia: IEEE, Oct. 2020, pp. 231–236. ISBN: 978-1-72819-398-4. DOI: 10.1109/MTTW51045.2020.9245054.

[44] V. Rybin et al. “Estimating Optimal Synchronization Parameters for Coherent Chaotic Communication Systems in Noisy Conditions.” In: *Chaos Theory and Applications* 5 (July 2023). DOI: 10.51537/chaos.1314803.

[45] R. Babajans et al. “Impact of the Chaotic Synchronization’s Stability on the Performance of QCPSK Communication System.” In: *Electronics* 10.6 (2021), p. 640. ISSN: 2079-9292. DOI: 10.3390/electronics10060640.

[46] D. Cirjulina et al. “Experimental Study on Frequency Modulated Chaos Shift Keying Communication System.” In: *2022 Workshop on Microwave Theory and Techniques in Wireless Communications (MTTW)*. Riga, Latvia: IEEE, Oct. 2022, pp. 1–4. ISBN: 978-1-6654-6439-0. DOI: 10.1109/MTTW56973.2022.9942593.

[47] D. Cirjulina, R. Babajans, and D. Kolosovs. “Design Particularities of Quadrature Chaos Shift Keying Communication System with Enhanced Noise Immunity for IoT Applications.” en. In: *Entropy* 27.3 (Mar. 2025), p. 296. ISSN: 1099-4300. DOI: 10.3390/e27030296.

[48] R. Babajans et al. “Performance Analysis of Vilnius Chaos Oscillator-Based Digital Data Transmission Systems for IoT.” en. In: *Electronics* 12.3 (Jan. 2023), p. 709. ISSN: 2079-9292. DOI: 10.3390/electronics12030709.

[49] D. Cirjulina et al. “Fundamental Frequency Impact on Colpitts Chaos Oscillator Dynamics.” In: *2023 Workshop on Microwave Theory and Technology in Wireless Communications (MTTW)*. Riga, Latvia: IEEE, Oct. 2023, pp. 19–23. ISBN: 9798350393491. DOI: 10.1109/MTTW59774.2023.10320021.

[50] D. Cirjulina et al. “Experimental Study on Colpitts Chaotic Oscillator-Based Communication System Application for the Internet of Things.” en. In: *Applied Sciences* 14.3 (Jan. 2024), p. 1180. ISSN: 2076-3417. DOI: 10.3390/app14031180.

[51] D. Cirjulina, R. Babajans, and D. Kolosovs. “Experimental Study on Quadrature Chaos Shift Keying Communication System.” In: *2024 IEEE Workshop on Microwave Theory and Technology in Wireless Communications (MTTW)*. Riga, Latvia: IEEE, Oct. 2024, pp. 29–32. ISBN: 979-8-3315-3317-5. DOI: 10.1109/MTTW64344.2024.10742187.

[52] D. Cirjulina et al. “Fundamental Frequency Impact on Vilnius Chaos Oscillator Dynamics.” en. In: *16th Chaotic Modeling and Simulation International Conference*. Ed. by C. H. Skiadas and Y. Dimotikalis. Cham: Springer Nature Switzerland, 2024, pp. 87–101. ISBN: 978-3-031-60906-0 978-3-031-60907-7. DOI: 10.1007/978-3-031-60907-7_8.

[53] F. Corinto, A. Ascoli, and M. Gilli. “Nonlinear Dynamics of Memristor Oscillators.” In: *IEEE Transactions on Circuits and Systems I: Regular Papers* 58.6 (June 2011), pp. 1323–1336. ISSN: 1549-8328, 1558-0806. DOI: 10.1109/TCSI.2010.2097731.

[54] L. Fu et al. “A Memristive Hénon Map Based on the State Variable Difference and Its Analog Circuit Implementation.” en. In: *IEEE Transactions on Industrial Electronics* 71.8 (Aug. 2024), pp. 9668–9676. ISSN: 0278-0046, 1557-9948. DOI: 10.1109/TIE.2023.3292857.

[55] X. Chen et al. “Memristor-based chaotic synchronization control and circuit experiments via single-input controller.” en. In: *2024 36th Chinese Control and Decision Conference (CCDC)*. Xi’an, China: IEEE, May 2024, pp. 5431–5436. ISBN: 9798350387780. DOI: 10.1109/CCDC62350.2024.10587435.

[56] A. Ascoli et al. “Edge of Chaos Induces a Hopf Bifurcation in a Bio-Inspired Thermally-Activated Memristor Oscillator.” In: *2025 IEEE International Symposium on Circuits and Systems (ISCAS)*. London, United Kingdom: IEEE, May 2025, pp. 1–5. ISBN: 979-8-3503-5683-0. DOI: 10.1109/ISCAS56072.2025.11043813.

[57] L. O. Chua et al. “A Universal Circuit for Studying and Generating Chaos—Part II: Strange Attractors.” In: *IEEE Transactions on Circuits and Systems I: Fundamental Theory and Applications* 40.10 (1993), pp. 745–761. ISSN: 10577122. DOI: 10.1109/81.246150.

[58] M. Kennedy. “Chaos in the Colpitts oscillator.” en. In: *IEEE Transactions on Circuits and Systems I: Fundamental Theory and Applications* 41.11 (Nov. 1994), pp. 771–774. ISSN: 10577122. DOI: 10.1109/81.331536.

[59] G. A. Gottwald and I. Melbourne. “On the Implementation of the 0-1 Test for Chaos.” In: (2009). DOI: 10.48550/ARXIV.0906.1418.

[60] A. Tamaševičius et al. “A simple chaotic oscillator for educational purposes.” In: *European Journal of Physics* 26.1 (Nov. 2004), p. 61. DOI: 10.1088/0143-0807/26/1/007.

[61] A. Ipatovs et al. “Complete Bifurcation Analysis of the Vilnius Chaotic Oscillator.” en. In: *Electronics* 12.13 (June 2023), p. 2861. ISSN: 2079-9292. DOI: 10.3390/electronics12132861.

[62] D. Pikulins et al. “Study of Nonlinear Dynamics of Vilnius Oscillator.” en. In: *Nonlinear Dynamics and Applications*. Ed. by S. Banerjee and A. Saha. Cham: Springer International Publishing, 2022, pp. 1219–1228. ISBN: 978-3-030-99791-5 978-3-030-99792-2. DOI: 10.1007/978-3-030-99792-2_103.

[63] *LoRaWAN™ 1.1 Specification*. Nov. 2017. URL: https://resources.lora-alliance.org/technical-specifications/lorawan-specification-v1-1 (visited on 03/26/2024).

[64] *IEEE Standard for Low-Rate Wireless Networks*. ISBN: 9798855713152. DOI: 10.1109/IEEESTD.2024.10794632. URL: https://ieeexplore.ieee.org/document/10794632/ (visited on 01/15/2025).

[65] *3GPP TR 21.917, ”Release 17 Description; Summary of Rel-17 Work Items,”* Technical TR 21.917. 3GPP (produced by ETSI). URL: https://www.etsi.org/deliver/etsi_tr/121900_121999/121917/17.00.01_60/tr_121917v170001p.pdf (visited on 11/24/2024).

[66] *ETSI EN 300 220-2*. Mar. 2025. URL: https://www.etsi.org/deliver/etsi_en/300200_300299/30022002/03.03.01_60/en_30022002v030301p.pdf (visited on 09/19/2025).

[67] L. M. Pecora and T. L. Carroll. “Synchronization in chaotic systems.” en. In: *Physical Review Letters* 64.8 (Feb. 1990), pp. 821–824. ISSN: 0031-9007. DOI: 10.1103/PhysRevLett.64.821.

[68] R. Babajans, D. Cirjulina, and D. Kolosovs. “Field-Programmable Gate Array-Based Chaos Oscillator Implementation for Analog–Discrete and Discrete–Analog Chaotic Synchronization Applications.” en. In: *Entropy* 27.4 (Apr. 2025), p. 334. ISSN: 1099-4300. DOI: 10.3390/e27040334.

[69] B. Bilgehan and O. Sabuncu. “Synchronization and Analysis of Chaotic Circuit with Application to Communication in the internet of things (IoT) Services.” In: *2022 International Conference on Artificial Intelligence in Everything (AIE)*. Lefkosa, Cyprus: IEEE, Aug. 2022, pp. 674–678. ISBN: 978-1-6654-7400-9. DOI: 10.1109/AIE57029.2022.00132.

[70] L. M. Pecora et al. “Fundamentals of synchronization in chaotic systems, concepts, and applications.” eng. In: *Chaos (Woodbury, N.Y.)* 7.4 (Dec. 1997), pp. 520–543. ISSN: 1089-7682. DOI: 10.1063/1.166278.

[71] Z. Yu et al. “Compounding and Synchronization of Fractional Order Chaotic Systems With Prescribed Performance for Secure Communication.” In: *IEEE Transactions on Circuits and Systems I: Regular Papers* 71.3 (Mar. 2024), pp. 1335–1345. ISSN: 1549-8328, 1558-0806. DOI: 10.1109/TCSI.2023.3334036.

[72] C. Zhao, N. Wang, and M. Ji. “Research on an Improved Driver-response Chaotic Synchronization Voice Encryption Technology.” en. In: *2021 International Conference on Electronic Communications, Internet of Things and Big Data (ICEIB)*. Yilan County, Taiwan: IEEE, Dec. 2021, pp. 330–334. ISBN: 978-1-6654-3755-4. DOI: 10.1109/ICEIB53692.2021.9686450.

[73] Z. Liu et al. “Stabilization and complete synchronization of a new time-reversed system.” In: *2023 IEEE International Conference on Memristive Computing and Applications (ICMCA)*. Jinan, China: IEEE, Dec. 2023, pp. 1–5. ISBN: 9798350316230. DOI: 10.1109/ICMCA59770.2023.10481469.

# A CHAOTIC OSCILLATORS

## A.1 Autocorrelation Function in Colpitts Chaotic Oscillator

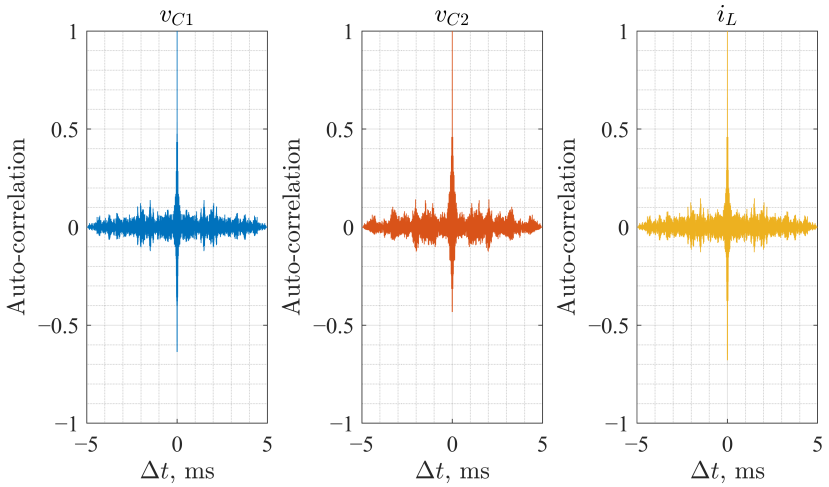


Fig. A.1. Autocorrelation functions of $v_{C1}$, $v_{C2}$, and $i_L$ obtained from LTspice simulations of the Colpitts chaotic oscillator at $f_0 = 96.86\,\text{kHz}$.

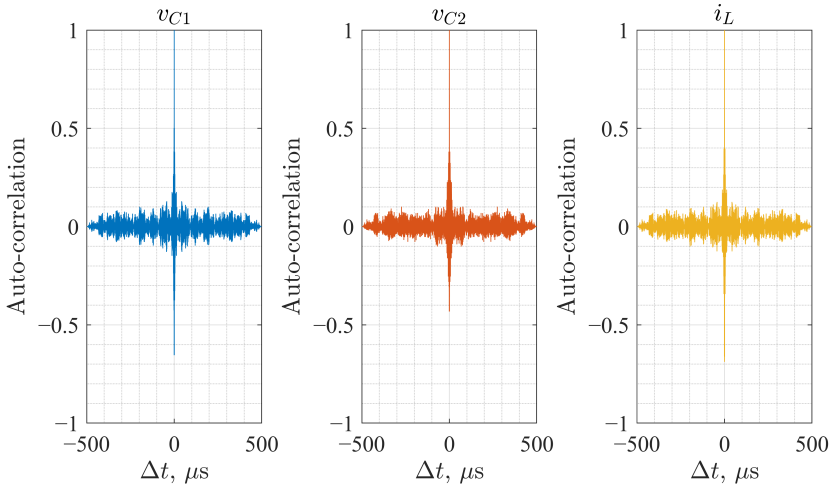


Fig. A.2. Autocorrelation functions of $v_{C1}$, $v_{C2}$, and $i_L$ obtained from LTspice simulations of the Colpitts chaotic oscillator at $f_0 = 968.59\,\text{kHz}$.

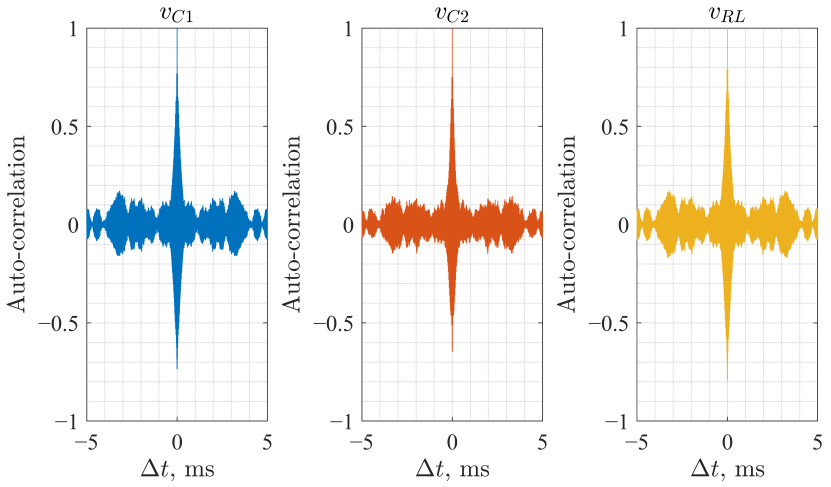


Fig. A.3. Autocorrelation functions of $v_{C1}$, $v_{C2}$, and $v_{RL}$ obtained from prototype measurements of the Colpitts chaotic oscillator at $f_0 = 96.86\,\text{kHz}$.

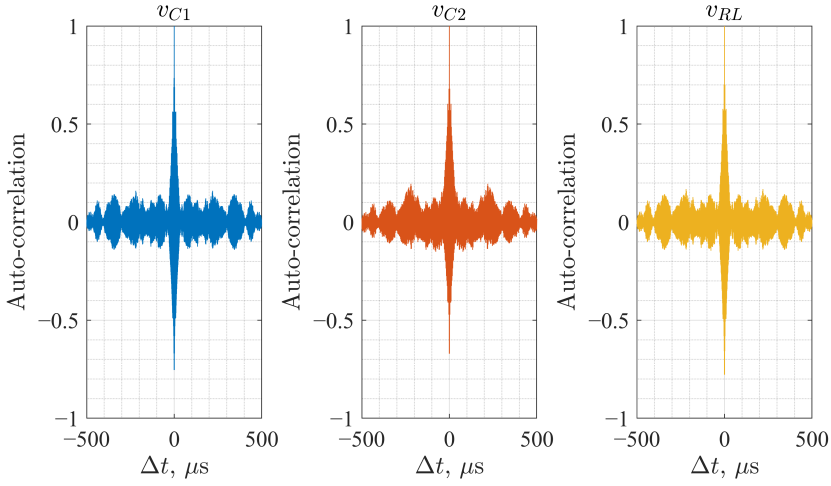


Fig. A.4. Autocorrelation functions of $v_{C1}$, $v_{C2}$, and $v_{RL}$ obtained from prototype measurements of the Colpitts chaotic oscillator at $f_0 = 968.59\,\text{kHz}$.

## A.2 Autocorrelation Function in Vilnius Chaotic Oscillator

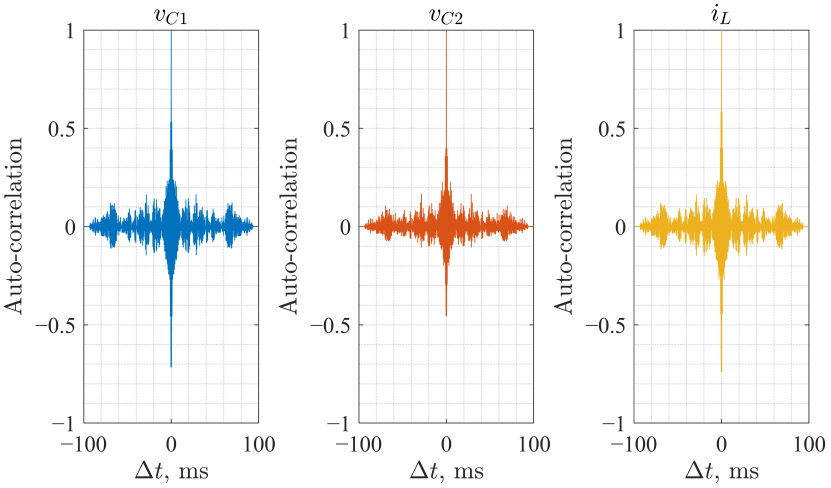


Fig. A.5. Autocorrelation functions of $v_{C1}$, $v_{C2}$, and $i_L$ obtained from LTspice simulations of the Vilnius chaotic oscillator at $f_0 = 1.6\,\text{kHz}$.

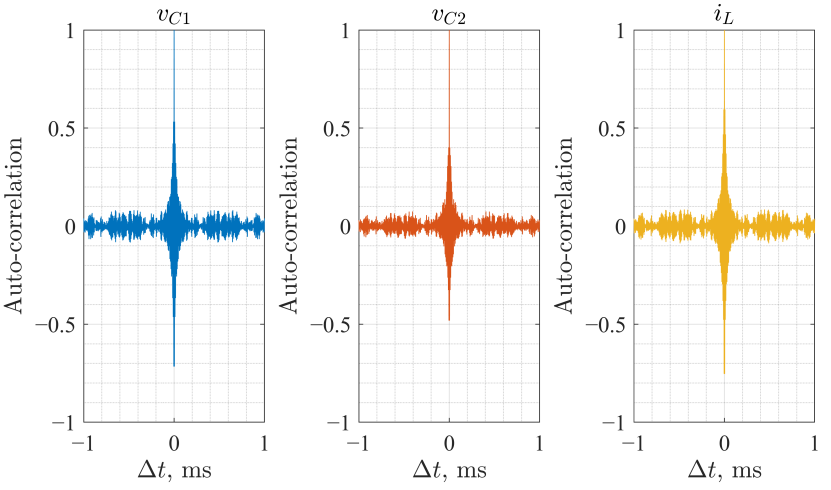


Fig. A.6. Autocorrelation functions of $v_{C1}$, $v_{C2}$, and $i_L$ obtained from LTspice simulations of the Vilnius chaotic oscillator at $f_0 = 160\,\text{kHz}$.

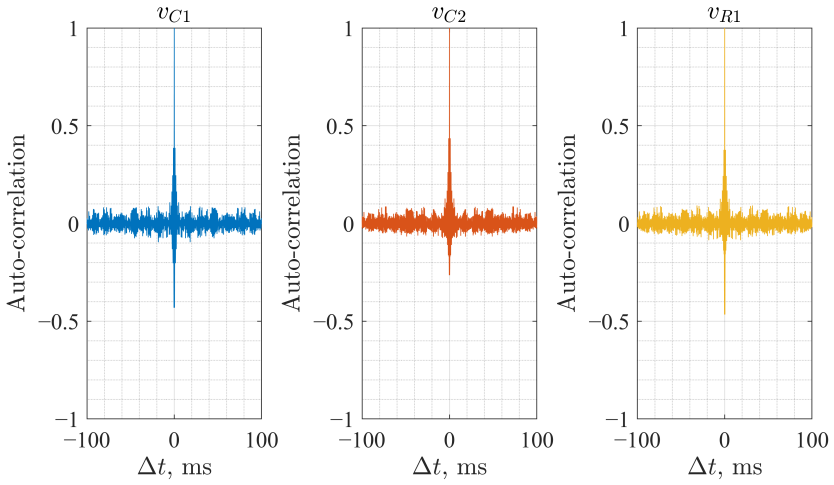


Fig. A.7. Autocorrelation functions of $v_{C1}$, $v_{C2}$, and $v_{R1}$ obtained from prototype measurements of the Vilnius chaotic oscillator at $f_0 = 1.6\,\text{kHz}$.

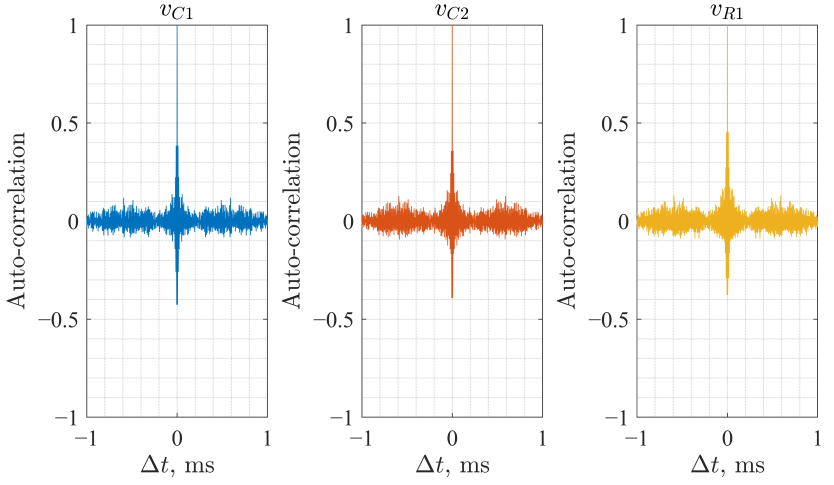


Fig. A.8. Autocorrelation functions of $v_{C1}$, $v_{C2}$, and $v_{R1}$ obtained from prototype measurements of the Vilnius chaotic oscillator at $f_0 = 160\,\text{kHz}$.

**Darja Čirjuļina** was born in 1999 in Riga, Latvia. She received an Academic Bachelor's degree in Electrical Engineering (2020) and a Professional Master's degree in Electronics and the qualification of Lead Electronics Engineer (2022) from Riga Technical University (RTU). Since 1 March 2019, she has been working at RTU, initially as a Research Assistant and since September 2022, as a Researcher at the Institute of Photonics, Electronics and Telecommunications, where she participates in research projects and teaches students.

During her doctoral studies, she has participated in several international mobilities and professional visits, including KTH Royal Institute of Technology (Sweden), Infineon Technologies Austria, Cracow University of Technology (Poland), Keysight Technologies GmbH (Germany), Politecnico di Torino (Italy), and Aristotle University of Thessaloniki (Greece). Her scientific and academic achievements during doctoral studies have been recognised with several awards, including the IEEE Student and Young Professional travel grant (2025) and the Best Student Presentation Award at the Days of Applied Nonlinearity and Complexity (DANOC'24) conference.

Her research interests focus on chaos-based data transmission systems for IoT applications. During her doctoral studies, she has also expanded her research activities in photonics, particularly high-speed IM/DD transmission systems, enabling her to participate in major international conferences such as OFC, ECOC, and IPC.